MULTI WAVELENGTH ANALYSIS OF MORPHOLOGY AND EVOLUTION OF GALAXIES

A thesis submitted to the

University of Calicut, Kerala for the award of the Degree of

DOCTOR OF PHILOSOPHY

in **PHYSICS**

under the Faculty of Science

by

Vinod. K. T

Department of Physics

University of Calicut

Kerala, India

March 2024

"However difficult life may seem, there is always something you can do, and succeed at. It matters that you don't just give up."

—Stephen Hawking

Dedicated to my beloved wife

CERTIFICATE

This is to certify that the thesis entitled "**Multi Wavelength Analysis of Morphology and Evolution of Galaxies**" submitted to the Department of Physics, University of Calicut by **Mr. Vinod. K. T** in partial fulfilment of the requirements for the award of the degree of **Doctor of Philosophy** is the original work carried out by her under my supervision and guidance at the Department of Physics, University of Calicut. No part of this thesis has been included previously for the award of any other degree, either in this university or any other institution. The thesis has been checked for plagiarism, using the *OURIGINAL* software, at the CHMK library, University of Calicut and the similarity index is found within the permissible limit. Also, no changes were suggested by the thesis referees after evaluation, and therefore, there are no further corrections to be made in this thesis.
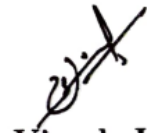
Supervisor:
Dr. C. D. Ravikumar
Professor
Department of Physics
University of Calicut

DECLARATION

*I hereby declare that the thesis titled "**Multi Wavelength Analysis of Morphology and Evolution of Galaxies**" is an authentic record of research work carried out by me at the Department of Physics, University of Calicut under the supervision of Dr. C. D. Ravikumar. No part of this thesis has been included previously for the award of any other degree, either in this university or any other institution. The thesis has been checked for plagiarism, using the OURIGINAL software, at the CHMK library, University of Calicut and the similarity index is found within the permissible limit.*

Date: 25-03-2024

Vinod. K. T
Research scholar
Department of Physics
University of Calicut

Contents

List of Tables

List of Figures

Acknowledgement

Throughout my Ph.D. study, many people have supported and encouraged me in different ways and I am grateful for the chance to thank them all. I would like to begin by expressing my gratitude to my supervisor, Dr. C. D. Ravikumar, for all of his guidance and support throughout my research work. He was the first person who ever taught me the fundamentals of astronomy and motivated me to explore it. As a guide, he is exceptional as he always gives all of his students unrestricted freedom. I could never have finished my Ph.D. work without his constant encouragement and precise advice.

I am grateful to Dr. Aswathy, who helped me in the learning process of various photometric software programs and analysis techniques. Outside of our discussions on the research, she was always an inspiration to me and a source of encouragement when I needed it. I want to express a special thanks to my junior Baheeja because we used to talk about and collaborate on research topics. Apart from the academic discussions, she was like a sister to me and she never failed to cheer me up whenever I was down. I thank Baheeja for her constant support and care for me. I also remember my senior Dr. Sitha at this moment for all the help and nice company she gave me in our department. My colleagues Dr. Sruthi, Habeeb, and Amina were always there to help whenever I required. I am happy for each one of my friends, especially for Nicemon, Rijin, Dr. Divya, Dr. Sebastian, Arjun, Nabeela, Anju, Midhun, Farha, and all the other research scholars in our department. I would like to extend my sincere thanks to all of the former HODs, faculty, and non-teaching staff of our department for their support over the entire Ph.D. period. I am so thankful to CSIR for the financial support during the research period.

To express my gratitude to my family for their unwavering love and support

would be beyond the scope of words. My parents are my greatest encouragement to continue in difficult circumstances and without them, I would not be where I am now. I am also blessed with two sisters who will always be there for me. I thank my brother-in-law Sumesh for giving me the laptop which served as my constant companion throughout the research period. I thank all the other family members for their sincere prayers and support.

Last but not least, I would like to thank my wife Suneesha for being my pillar of support and strength. She has been extremely patient and tolerant with me, and I appreciate everything she has done. Our lovely children Sivanya, Sriyaan, and Srived, whose innocent smiles was sufficient to temporarily relieve all my anxieties, make me very pleased. Once again, I thank everyone who helped me directly or indirectly to accomplish this work.

List of Publications

1. **K. T. Vinod**, C. Baheeja, S. Aswathy and C. D. Ravikumar
   "Study of Central Intensity Ratio of Seyfert Galaxies in Nearby Universe",
   Research in Astronomy and Astrophysics , 23, 045008 (2023).

2. **K. T. Vinod**, C. Baheeja, and C. D. Ravikumar
   "Connections between Central Intensity Ratio and hot gas properties of early-type galaxies",
   Monthly Notices of the Royal Astronomical Society , 528, 2040-2045 (2024).

List of conference presentations

1. "Evolution connection of Central Intensity Ratio with host galaxy properties of Seyfert Galaxies", Vinod. K. T and C. D. Ravikumar, 40th Annual Meeting of the Astronomical Society of India (ASI), 25-29 March 2022, IIT Roorkee and ARIES Nainital.

2. "The relationship between Central Intensity Ratio and host galaxy properties in nearby Seyfert galaxies", Vinod. K. T and C. D. Ravikumar, 38th Annual Meeting of the Astronomical Society of India (ASI), 13-17 February 2020, IISER, Tirupati.

3. "Study of Central Intensity Ratio in Seyfert galaxies", Vinod. K. T and C. D. Ravikumar, 37th Annual Meeting of the Astronomical Society of India (ASI), 18-22 February 2019, CHRIST (Deemed to be University), Bengaluru.

4. "Central Intensity Ratio and star formation in nearby active galaxies", Vinod. K. T and C. D. Ravikumar, National Seminar on Astronomy and Astrophysics, 21-22 November 2018, Post Graduate and Research Department of Physics, Farook College (Autonomous), Calicut.

Constants and Abbreviations

Physical Constants

Parsec	$pc = 3.086 \times 10^{18}$ cm
Solar Luminosity	$L_\odot = 3.826 \times 10^{33}$ erg/s
Solar Mass	$M_\odot = 1.989 \times 10^{33}$ g

Abbreviations

AGN	Active Galactic Nucleus
ACS	Advanced Camera for Surveys
CIR	Central Intensity Ratio
ETGs	Early-Type Galaxies
FUV	Far UltraViolet
GALEX	Galaxy Evolution Explorer
HST	Hubble Space Telescope
IR	Infrared
IRAC	Infrared Array Camera
IRAF	Image Reduction Analysis Facility
ISM	Inter Stellar Medium
LTGs	Late-Type Galaxies
$\mathbf{L_{X,GAS}}$	X-ray Gas Luminosity
MAST	Mikulski Archive for Space Telescopes
$\mathbf{M_{BH}}$	Black Hole Mass
NED	NASA/IPAC Extragalactic Database
NGC	New General Catalogue
NUV	Near UltraViolet

RL	Radio-Loud
RQ	Radio-Quiet
SExtractor	Source Extractor
SFR	Star Formation Rate
SMBH	Supermassive Black Hole
Sy	Seyfert
T$_{\mathbf{GAS}}$	X-ray Gas Temperature
WFPC2	Wide-Field Planetary Camera 2

Chapter 1

Introduction

Astronomy and astrophysics deals with the study of heavenly bodies in the Universe and the investigation of their physical properties. The goal of astronomy is to investigate and explain everything we observe in the Universe. The Universe has always attracted human curiosity and observational astronomy has developed into a well-known branch of astronomy. Focusing and imaging of the sky are highly crucial for investigating the nature and physics of celestial objects, which leads to the development of efficient telescopes. In 1608, Galileo improved the first telescope discovered by Hans Lippershey and utilized it for astronomy. By 1655, astronomers developed telescopes which were more efficient than Galileo's instrument for observing the apparent motion of celestial objects. Light gathering and resolving power of a telescope plays a significant role in observational astronomy. The aperture size of a telescope determines how much light it can gather. The ability of a telescope to distinguish two point sources into distinct images is known as its resolution. Compared to the ancient era, we now have a wide range of ground- and space-based telescopes that enable us to observe the Universe at different wavelengths with excellent resolution. So, astrophysics broadens its reach far beyond the horizon of the Universe that is not accessible by human beings with bare eyes to study the physical mechanism behind the evolution of celestial objects.

Galaxies are believed to be the largest and the most fundamental components of our Universe. A galaxy is a large system of stars, interstellar gas, dust, and dark matter that is bound together by gravity. Nearly 200 billion galaxies of different

sizes and shapes have been found by astronomers in the observable Universe (Lauer et al., 2021). The high-resolution images taken by the space observatories provide an understanding of the nature and morphology of galaxies. Galaxies can be classified based on their morphology as well as the activity of the host galaxy. The renowned astronomer, Edwin Hubble, made significant findings on galaxy evolution and proposed the first and most important morphological classification of galaxies (Hubble, 1936). The classification scheme of galaxies is discussed in the next section.

1.1 Classification of galaxies

In 1936, Edwin Hubble proposed the classification of galaxies according to their morphology. This classification is well-known and occasionally referred to as Hubble's tuning fork diagram since the arrangement of galaxies resembles a tuning fork. All types of galaxies, including elliptical, lenticular, spiral, and irregular galaxies, are part of Hubble's classification as shown in Figure 1.1. Elliptical galaxies are displayed at the handle of the tuning fork based on their ellipticity (E0 to E7). Spiral galaxies are categorized into Barred and Unbarred classes and positioned them on the fork's arms. Between elliptical and spiral galaxies are lenticular galaxies (S0s). All other galaxies with unusual structures are classified as irregular galaxies. Moreover, galaxies can be categorized based on whether they are active or normal galaxies. In general, elliptical and lenticular galaxies are referred to as early-type galaxies, while spiral galaxies are considered late-type galaxies (Thomas et al., 2010). Since early-type and late-type galaxies exhibit a range of evolutionary paths, this classification may not always be appropriate (Baldry, 2008; Masters et al., 2019). In this thesis, we focus on morphological studies of normal and active galaxies using photometry with multi-wavelength data to understand the formation and evolution of early-type galaxies (ETGs) and late-type galaxies (LTGs).

1.1.1 Normal galaxies

In a normal galaxy, there may be billions or trillions of stars and the sum of the luminosity of these stars constitutes the galaxy's total luminosity. Normal galaxies have total luminosity up to about $10^{11} L_\odot$ and most of the energy can be emitted
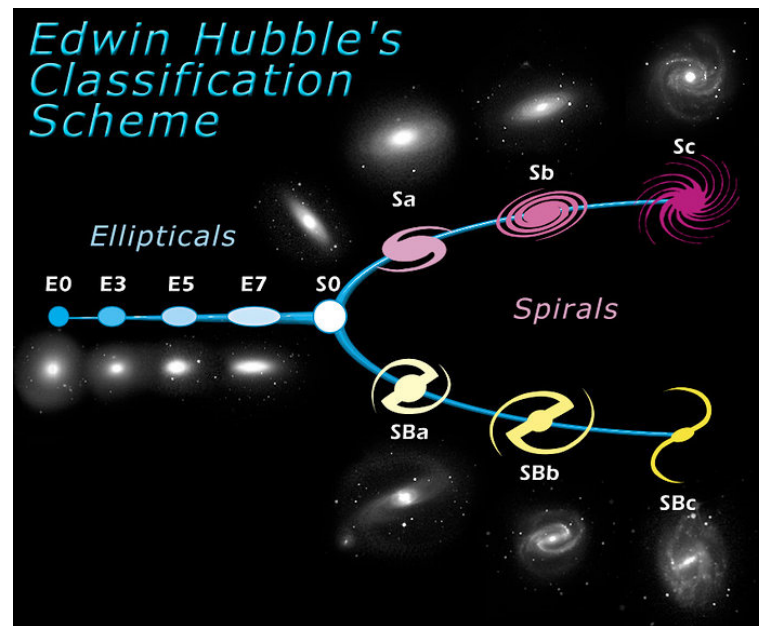
Figure 1.1: Hubble's morphological classification of galaxies. Image Courtesy: **www.spacetelescope.org**

Figure 1.2: Difference in the intensity of light emitted by normal (left:NGC4414) and active (right:NGC7742) galaxies. Image Courtesy: **AURA/STScI/NASA**

near the visible portion of the electromagnetic spectrum. Normal galaxies constitute nearly 90% of the Universe and they are categorized by astronomers into three distinct groups (de Vaucouleurs, 1959; Sandage, 1961).

Elliptical galaxies

Elliptical galaxies are believed to be quiescent systems. Elliptical galaxies appear in ellipsoidal shapes with little features like disks, spiral arms, bars, and dust lanes. Massive elliptical galaxies are typically assumed to be the outcome of galaxy mergers and found in galaxy clusters (Dressler, 1980). Elliptical galaxies are divided into eight types, from E0 to E7, with the integer indicating the ellipticity of the galaxies. The size of elliptical galaxies varies, ranging from dwarf ellipticals with a few million stars to supergiants having a hundred trillions of stars. Elliptical galaxies possess an old stellar population and less amount of fuel such as gas and dust compared to other types of galaxies (De Lucia et al., 2006), which prevents star formation in host galaxies. Due to their low star formation rate and the populations of old, red stars, elliptical galaxies are usually referred to as 'red and dead' systems.

Lenticular galaxies

Lenticular galaxies are the intermediate class between elliptical and spiral galaxies. The peculiarity of lenticular galaxies is that they have a disk with a central bulge, but no spiral arms. The galaxies which possess prominent disks are referred to as disk galaxies. Lenticular galaxies are similar to spiral and elliptical galaxies in terms of kinematics due to their bulge and disk features (Moran et al., 2007). S0 galaxies resemble E0 galaxies when the disk is extremely faint. Apart from spiral galaxies, the disks of lenticular galaxies are primarily composed of stars. It has also been suggested that lenticular galaxies grew their disks through accretion events that involved gas and minor mergers (Graham et al., 2015). Bar structures also can be found in some of the lenticular galaxies as well. A lenticular galaxy is more like an elliptical galaxy in terms of its stellar population and gas content and they are together called ETGs.

Spiral galaxies

Spiral galaxies are the late-type galaxies in the galaxy classification. The typical structure of a spiral galaxy is a rotating disk with spiral arms that extend outward from a compact central region, the bulge, which is composed of mainly older stars. Spiral arms are the extended regions of stars from the centre of galaxies that exhibit intense star formation. It is probable to detect new stars in the disk because of its abundance of gas and dust. Also, bar structure can be seen at the centre of nearly 60% of spiral galaxies (de Vaucouleurs et al., 1991). Spiral galaxies are typically classified as Sa/SBa, Sb/SBb, and Sc/SBc (unbarred/barred) based on the tightness of their spiral arms and the presence of the bar structure. For instance, Sc/SBc galaxies have loose arms whereas Sa/SBa galaxies possess tightly wounded arms.

1.1.2 Active galaxies

The core region of a galaxy that emits a vast amount of energy than a normal galaxy is called Active Galactic Nucleus or AGN. AGN-hosting galaxies are commonly referred to as active galaxies. AGNs are the most luminous persistent sources in the Universe and they emit radiation over the entire electromagnetic spectrum (Fabian, 1999). Active galaxies are typically more luminous than normal galaxies and possess luminosity ranging from $10^{11}L_\odot$ to $10^{15}L_\odot$. Figure 1.2 displays the difference in the intensity of light emitted by normal and active galaxies. The accretion of matter onto the supermassive black hole (SMBH) having mass, $M_{BH} \geq 10^6 M_\odot$, residing at the center of the galaxy is believed to be the origin of the AGN's extraordinary emission (Lynden-Bell, 1969).

It is convenient to divide AGN into two classes, conventionally, radio-loud (RL) and radio-quiet (RQ, see Figure 1.3). This classification is based on the radio (5 GHz) to optical (B-band) flux ratio (F_5/F_B). The sources with a ratio greater than 10 are known as RL, whereas those with a ratio less than 10 are known as RQ (Kellermann et al., 1989). Radio-loud AGNs have emission contributions from both jets and lobes. These emission contributions dominate the luminosity of the AGN at radio wavelengths and possibly at some or all other wavelengths. Blazars, Radio galaxies, BL Lac objects, etc. are examples of radio-loud objects. A brief description
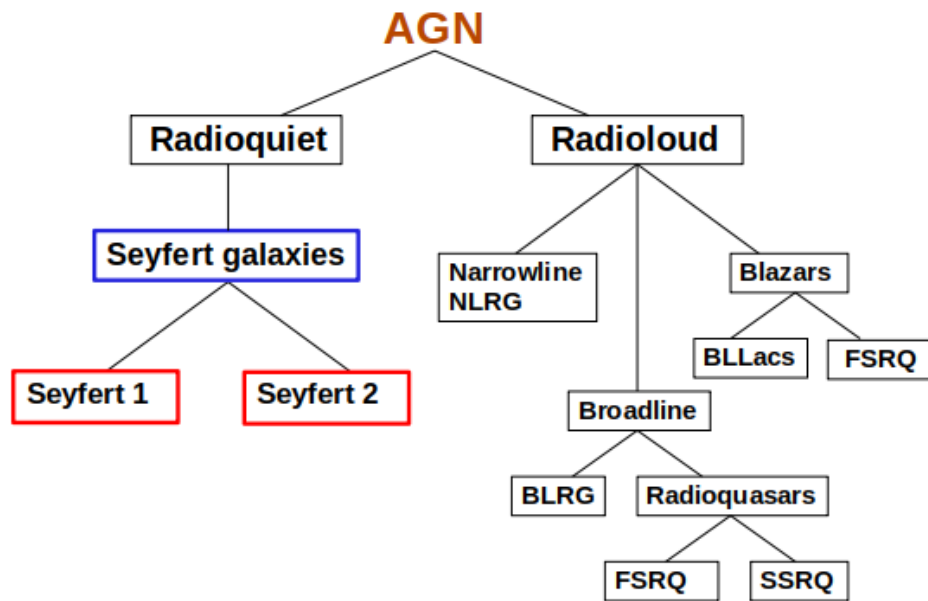
Figure 1.3: Classification of Active Galactic Nucleus.

of these sub-classes is given below.

Blazars are a special class of RL sources with a relativistic jet of ionized matter that is pointed towards the observer (Urry & Padovani, 1995). High variability and polarization are seen in the observed emission of blazars and they can be further divided into BL Lacertae objects (BLLacs) and flat spectrum radio quasars (FSRQs). Blazars show weak emission lines in their optical spectra and are referred to as BLLacs while FSRQs have strong emission lines.

A radio galaxy is a giant elliptical galaxy that emits more light at radio wavelengths than at optical wavelengths. The salient feature of a radio galaxy is its extended lobe structure of strong radio emission which is driven by the jet emitted from its AGN. Radio galaxies can be further classified into Narrow Line Radio Galaxies (NLRG) and Broad Line Radio Galaxies (BLRG) based on the optical/UV emission lines. Additionally, radio galaxies are categorized into two groups, FR I and FR II (Fanaroff & Riley, 1974), which are together known as NLRG. FR I galaxies have the peculiarity of decreasing jet luminosity from the nucleus towards their

lobes whereas FR II galaxies exhibit an opposite pattern of gradual increase in jet luminosity towards the lobes.

Radio-quiet objects are simpler systems since jet and any jet-related emission can not be observed in any wavelength. Seyfert galaxies and radio-quiet quasars are examples of this category. Seyfert galaxies were the earliest distinct class of AGN to be identified (Seyfert, 1943) and unlike quasars, their host galaxies are detectable. We started our study by using Seyfert galaxies as the nearby AGN sources using simple photometry.

1.2   Surface Photometry

Surface photometry is the oldest method used in astronomy to measure the surface brightness of spatially extended celestial objects like galaxies. Surface photometry was introduced by Reynolds (1913) and it is used to investigate the formation and evolution of galaxies by quantifying the light distribution with their two-dimensional images (de Vaucouleurs, 1948; Fish, 1964; Milvang-Jensen & Jørgensen, 1999). Initially, photographic plate detectors were used for surface photometry, but the low detection efficiency of such instruments reduced the accuracy of this method. The advent of Charge Coupled Devices (CCDs) changed this difficulty because of their improved efficiency in detecting relatively faint sources. Using surface photometry, the two-dimensional image data can be converted into a one-dimensional surface brightness profile which describes how the intensity and ellipticity vary with radius. We can determine the colors of the galaxies from surface photometry using several passbands. These colors reveal information regarding the stellar populations of the galaxies, such as their ages and metallicity.

1.2.1   Light Concentration Indices

The parameterization of galaxies heavily depends on the estimation of their central light concentration. The concentration indices C_{21} and C_{32} were introduced by Fraser (1972) and can be expressed as $C_{21} = r_e/r_1$ and $C_{32} = r_3/r_e$, where r_e is the half-light radius (the effective radius that contains 50% of the total flux from the model light profile) of the galaxy. The radii r_1 and r_3 contain 25% and 75%

of the total galaxy luminosity, respectively. The ratio of flux luminosity enclosed within some inner and outer radii is another measure called the "mean concentration index" (Okamura et al., 1984). By utilizing the concentration index and the mean surface brightness of galaxies, Doi et al. (1993) proposed a simple method for the morphological classification of galaxies. Based on these studies, Abraham et al. (1994) suggested another parameter the "central concentration of light" which can be used as a key parameter for the classification system. The concentration index was defined by Graham et al. (2001) as the ratio of flux inside the designated fraction of the half-light radius to that inside the half-light radius and reported the first-ever correlation between light concentration and the velocity dispersion of elliptical galaxies. The central concentration of galaxies can be a key factor in the formation of supermassive black holes since more massive galaxies are likely to be more centrally concentrated (Graham et al., 2001). Conselice (2003) defined the concentration index as $C = 5 \times \log\left(r_{80}/r_{20}\right)$ by using a curve of growth radii (r_{80}, r_{20}) that enclosed 80% and 20% of the total flux. The concentration index displays how concentrated/distributed the galaxy's light is and can be a measure of the size, luminosity, and mass of the galaxy (Conselice, 2003).

The entire study presented in this thesis utilized photometric images from the Hubble Space Telescope (HST), Galaxy Evolution Explorer (GALEX), and Spitzer Space Telescope missions. Hence, we provide a short description of these space-based observatories and their associated instruments in the following sections.

1.3   Hubble Space Telescope

Hubble Space Telescope (HST) was built by the National Aeronautics and Space Administration (NASA) of the United States and launched into space in April 1990. It was named in honor of renowned astronomer Edwin Powell Hubble. Later, the European Space Agency (ESA) joined in this project and HST is currently operated by NASA and ESA. The scientific operation of HST and delivery of observed data are controlled by the Space Telescope Science Institute (STScI). Figure 1.4 shows the photograph of HST which was captured during its fifth servicing mission in 2009. At the time of launching HST carried five instruments viz. High-Speed Photometer, Faint Object Camera, Faint Object Spectrograph, Goddard High-Resolution Spec-
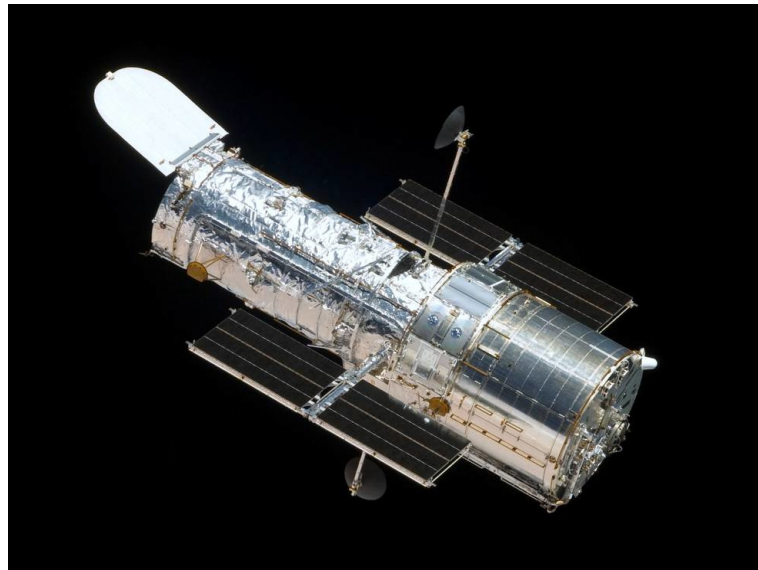
Figure 1.4: The photograph of HST captured from space shuttle during its last servicing mission in 2009. Image Courtesy: **www.nasa.gov**

trograph, and Wide Field and Planetary Camera (WF/PC), which is eventually replaced by Wide Field Planetary Camera 2. All of these are replaced by advanced instruments during different servicing missions. Currently, there are six instruments onboard HST: Advanced Camera for Surveys (ACS), Wide Field Camera 3 (WFC3), Near Infrared Camera and Multi-Object Spectrometer (NICMOS), Space Telescope Imaging Spectrograph (STIS), Cosmic Origins Spectrograph (COS), and Fine Guidance Sensors (FGS).

We used photometric images captured by the two HST instruments, WFPC2 and ACS for our study. The following sections contain a brief description of each instrument.

1.3.1 Wide Field Planetary Camera 2 (WFPC2)

Wide Field Planetary Camera 2 was built by Jet Propulsion Laboratory and installed by replacing the original Wide Field and Planetary Camera (WF/PC) in the first servicing mission in 1993. It captured images using a range of 48 colour filters that covered the visible, near-infrared, and far-ultraviolet spectral bands. It contained four CCD detectors, three of them were assembled into an L-shaped unit known as the Wide Field Camera (WFC), and the fourth one operated as the Planetary
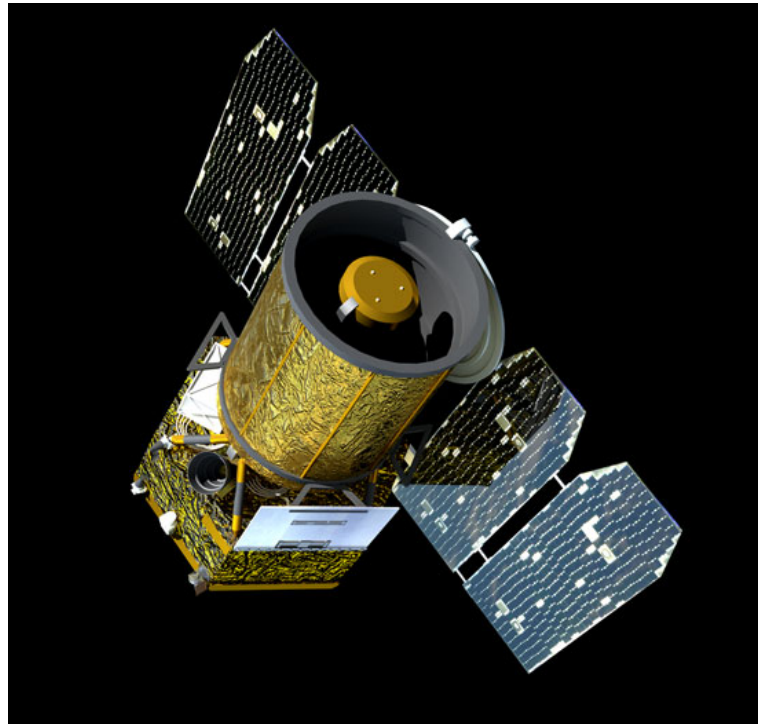
Figure 1.5: Artist's impression of GALEX spacecraft. Image Courtesy: **www.nasa.gov**

Camera (PC). WFPC2 served as the primary instrument until ACS was installed in 2002 and it was replaced by WFC3 in the fourth servicing mission in 2009.

1.3.2 Advanced Camera for Surveys (ACS)

ACS is the third generation instrument onboard HST which replaced the Faint Object Camera during servicing mission 3B in 2002. The main purpose of ACS is to explore a wide area of the sky at multiple wavelengths with excellent resolution. The observational range of ACS spans the ultraviolet, visible, and near-infrared bandwidths and it is 10 times more efficient than the past instrument WFPC2. ACS has three sub-instruments: the Wide Field Channel (WFC), designed to look for galaxies, High Resolution Channel (HRC), designed to capture high-resolution images of the light from the centre of the galaxies possess massive black holes, and the Solar Blind Channel (SBC), obstructs visible light and enable the detection of weak UV radiation.

1.4 Galaxy Evolution Explorer

The Galaxy Evolution Explorer (GALEX) was a NASA mission led by the California Institute of Technology, launched into orbit in 2003. GALEX was a space-based telescope designed to observe celestial objects in ultraviolet wavelength exclusively to study the star formation history of the Universe. In order to capture direct images in the near-UV (NUV, $1750 - 2800$ Å) and far-UV (FUV, $1350 - 1750$ Å) bands, GALEX utilized microchannel plate detectors. After completing 10 years of survey, it was decommissioned in 2013. In our study, we used FUV images to estimate the star formation rate (SFR) of sample galaxies, since FUV data is a reliable tracer of SFR of young stellar populations in galaxies. Figure 1.5 shows an artist's impression of the GALEX spacecraft.

1.5 Spitzer Space Telescope

Spitzer Space Telescope, formerly known as the Space Infrared Telescope Facility (SIRTF), was NASA's Infrared Great Observatory launched in 2003. The satellite was equipped with three instruments: Infrared Array Camera (IRAC), Infrared Spectrograph (IRS), and Multiband Imaging Photometer for Spitzer (MIPS), which enable astronomical imaging and photometry in the wavelengths from 3.6 to 160 μm, spectroscopy from 5.2 to 38 μm, and spectrophotometry from 55 to 95 μm (Werner et al., 2004). The Infrared Science Archive (IRSA) serves as the main repository for infrared data including the Spitzer mission. An artistic rendering of the Spitzer Space Telescope is shown in Figure 1.6.

In this study, we used photometric images taken by IRAC in the 3.6 μm waveband, and a short description of IRAC is provided in the following section.

1.5.1 Infrared Array Camera (IRAC)

The Infrared Array Camera was developed by the NASA Goddard Space Flight Center (GSFC). IRAC was an infrared camera that simultaneously operated at four different wavelengths (3.6 μm, 4.5 μm, 5.8 μm, and 8 μm). The IRAC pixel scale was almost identical in all channels ($\sim$ 1.2 arcseconds per pixel) and provided a
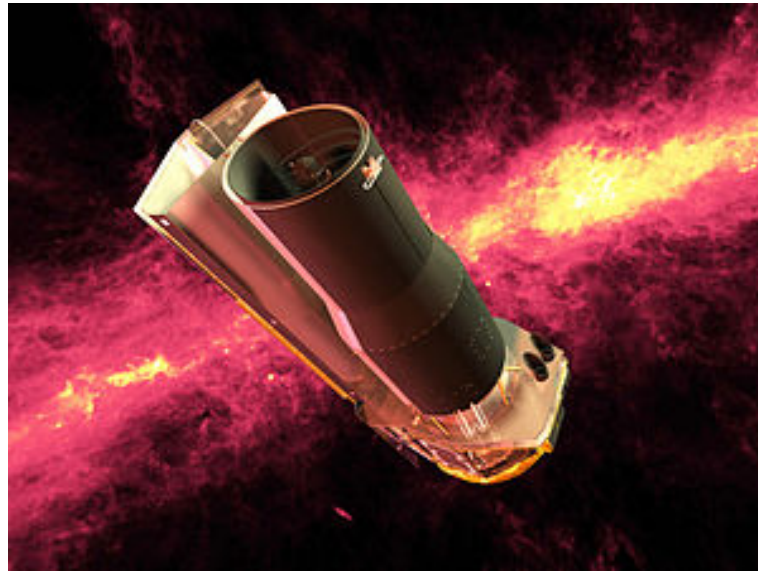
Figure 1.6: Artist's impression of Spitzer Space Telescope. Image Courtesy: **www.nasa.gov**

field of view of 5.2 arcmin x 5.2 arcmins. IRAC was a powerful instrument because of its great sensitivity, wide field of view, mapping capabilities, and simultaneous four-channel imaging (Fazio et al., 2004).

We used publicly available photometric images observed by HST and GALEX from Mikulski Archive for Space Telescopes (MAST, `mast.stsci.edu`) and the images captured by SPITZER from NASA/IPAC Infrared Science Archive (IRSA, `irsa.ipac.caltech.edu`). Photometric analysis was performed on these images using different software. In this work, we primarily employed two software for data analysis which are described below.

1.6 Software used for data analysis

1.6.1 Source Extractor (SExtractor)

Sextractor is a program developed by Bertin & Arnouts (1996) for the extraction of catalogue for objects from an astronomical image. SExtractor was basically designed on UNIX platforms and supports large files in FITS format with excellent speed. The important features of SExtractor are the ability to function on large images

with minimum human intervention and to handle a wide range of object shapes and magnitudes. SExtractor can perform aperture photometry on CCD images and it can compute four types of magnitudes: isophotal, corrected-isophotal, fixed-aperture, and adaptive aperture. While performing photometry, the user can control both the input and output parameters.

All the research conducted for this thesis is associated with the central region of galaxies. We identified the central region of galaxy images and obtained the measurement of central light distribution within the pre-defined apertures by employing SExtractor.

1.6.2 Image Reduction and Analysis Facility (IRAF)

Image Reduction and Analysis Facility, *IRAF*, is a multipurpose software system developed for astronomical data analysis (Tody, 1986, 1993). Both photometric and spectroscopic data reduction are possible with *IRAF*. The software was created and developed by the National Optical Astronomy Observatories (NOAO), Arizona. *IRAF* was designed for UNIX-like operating systems, but with some modifications it may be used on Windows also. Nowadays, Linux and macOS are its main platforms of use.

IRAF commands also referred to as tasks, are arranged in package structures. The user has the option to add more packages to *IRAF*. Many packages are available from NOAO as well as outside developers. The *STSDAS* and *TABLES* packages offered by STScI are particularly helpful for photometry. The calibration of flux and position of a celestial object within a CCD image is one of the features offered by *IRAF*. By analyzing the spectral lines, it can also be used to determine redshifts of astronomical objects. We used *IRAF* for reducing the UV flux for the sample galaxies with the help of the '*apphot*' task and we analyzed the central region of galaxy images by utilizing the package '*ellipse*'.

We have used the cosmological parameters: $H_0 = 73.0\,\mathrm{km\,s^{-1}}Mpc^{-1}$; $\Omega_{\mathrm{matter}} = 0.27$; $\Omega_{\mathrm{vacuum}} = 0.73$ to calculate luminosity distance in this study.

The subsequent sections provide a literature review essential to the entire study.

1.7   Study of Central Intensity Ratio of Seyfert Galaxies in nearby Universe

In this work, we investigate variations between the central intensity ratio of nearby Seyfert galaxies and their galactic properties including the mass of the central supermassive black hole. It is necessary to have some previous knowledge about the co-evolution of SMBHs and their host galaxies to comprehend the importance of this study. Since Seyfert galaxies are AGN host galaxies, a short description of AGN classification and Seyfert types is also provided.

1.7.1   Seyfert galaxies

Seyfert galaxies are the prime and most studied objects in the RQ category along with quasars and they have high surface brightness and exhibit strong, high-ionization emission lines in their spectra (Weedman, 1977; Osterbrock & Martel, 1993; Rashed et al., 2015). Most Seyfert galaxies seem to be typical spiral galaxies when observed in visible light. But when explored at other wavelengths, it becomes evident that the majority of Seyfert galaxies have core luminosity comparable to that of an entire galaxy with sizes equivalent to the Milky Way. Bulges are thought to be formed in Seyfert galaxies via secular evolution, in contrast to other galaxies where merger events regulate this process. Consequently, the interconnections between the bulge characteristics of Seyfert galaxies and the evolution of SMBH are still unknown (Hopkins et al., 2006; Kormendy & Ho, 2013a; Heckman & Best, 2014).

According to the spectral characteristics, Khachikian & Weedman (1974) identified and classified Seyfert galaxies into two categories, Seyfert 1 (Sy1) and Seyfert 2 (Sy2). Sy1 galaxies are very strong sources of UV and X-ray energy, along with the visible light emanating from their cores. Sy2 galaxies also possess the typical bright core and are visible as luminous objects in infrared wavebands. The spectra of Sy1 galaxies exhibit broad lines, comprising both permitted lines such as H I, He I, or He II, and narrower forbidden lines such as O III, whereas the spectra of Sy2 galaxies exhibit only narrow lines that are both permitted and forbidden. Furthermore, four sub-classes are there, Sy1.2, Sy1.5, Sy1.8, and Sy1.9, in between Sy1 and Sy2 which are classified based on the emission line width shown by their spectra. The Hβ line

appears less broad in Sy1.2 galaxies compared to other Balmer lines, whereas in Sy1.5 objects, the intensities of Hα and Hβ lines are comparable. In Sy1.8, broad but weak Hβ and Hα lines are seen, but in Sy1.9, the broad line is only visible in Hα (Osterbrock, 1981; Osterbrock & Pogge, 1985).

AGN structure and characteristics especially in the central regions of all sources are thought to be very similar and obviously, Sy1 and Sy2 galaxies are intrinsically the same, which is explained by the Unification Model of AGN (Antonucci, 1993; Urry & Padovani, 1995). Even though, the observable properties of AGN differ from one another in terms of line of sight and observing angle with them. Independent of redshifts, AGNs are hosting at the centres of elliptical galaxies or bulge-dominating spheroids (Kauffmann et al., 2003; Pović et al., 2009), but the morphology of local Seyfert galaxies are considered to spiral (Ho et al., 1995; Ho, 2008). The gas flow towards the central region of galaxies forms a ring-like structure and the concentration of gas in the shape of a ring can boost star formation. This type of star-forming ring can be found in the central 1-2 kpc region of almost all barred spiral galaxies (Knapen et al., 1995a). Various studies suggest that intense circumnuclear star formation is vital in the evolution process of Seyfert galaxies, particularly for Sy2s (e.g., Terlevich & Melnick, 1985; Maiolino et al., 1998; Cid Fernandes & Terlevich, 1995; González Delgado et al., 2001; Cid Fernandes et al., 2001).

The co-evolution of SMBHs with their host galaxies and different correlations involving SMBH mass are briefly introduced in the next section.

1.7.2   Correlation between SMBH mass and host galaxy properties

Super massive black holes residing at the centre of elliptical galaxies and spiral bulges is a widely accepted phenomenon (e.g., Begelman & Rees, 1996; Magorrian et al., 1998; Richstone et al., 1998; Kormendy & Gebhardt, 2001) over decades, which squeezes matter towards the centre of the galaxy due to its strong gravity. Kormendy & Richstone (1995), reported that SMBH masses (M_{BH}) well correlate with the blue band luminosity of bulges of spirals and ellipticals. The most explored fundamental relation in observational studies is that the masses of supermassive black holes (SMBHs) well correlate with the stellar mass and central velocity dispersion

(σ) of the bulges of their host galaxies (see, e.g., Magorrian et al., 1998; Ferrarese & Merritt, 2000; Gebhardt et al., 2000; Marconi & Hunt, 2003; Häring & Rix, 2004; Kormendy & Ho, 2013b; McConnell & Ma, 2013; Savorgnan & Graham, 2015). At the same time, Kormendy & Kennicutt (2004) explored these relations and reported that spirals and ellipticals may not follow these relations simultaneously.

It is believed that accretion of matter onto the SMBH leads to the formation of a compact region at the centre of the host galaxy which exhibits an unusual luminosity with non-stellar emission and such compact region is termed as active galactic nuclei (AGN; Lynden-Bell, 1969; Rees, 1984; Edelson et al., 1996). An active galaxy is a galaxy that possesses an AGN at its centre. AGNs are classified mainly into two categories, Radio-quiet (RQ) and Radio-loud (RL) according to the luminosity of emission coming out in the radio waveband (de Bruyn & Wilson, 1978; Baum & Heckman, 1989; Miller et al., 1993). Most of the RL sources are ellipticals, they are a rare classification of AGN (e.g., Padovani, 1993), which produce radio jets and lobes with high energy, at the same time, RQ sources mainly comprise spiral galaxies with weak radio emission (Wilson & Colbert, 1995). AGNs are also obeying the $M_{BH} - \sigma$ relation but with significantly large scatter (Caglar et al., 2020).

Central light concentration is a fundamental parameter, which can be used as a tracer of star formation activity and galaxy evolution (Abraham et al., 1994; Conselice, 2003). The Central Intensity Ratio (CIR), a new photometric parameter, is well correlated with the SMBH mass and other structural properties of the spheroid of early-type galaxies in the nearby Universe (Aswathy & Ravikumar, 2018). Connections between SMBH and host galaxy properties are still an active research problem, especially in AGN host galaxies. Thus, we were motivated by the scaling relations involving SMBH mass and performed a photometric study in AGN host galaxies by using the new photometric tool CIR. This work is summarized in Chapter 2.

Apart from optical properties, X-ray properties like X-ray gas luminosity and gas temperature are also reported to be well correlated with the galaxy parameters such as M_{BH} and σ of the host galaxies. Hence, we extended our work to explore the connection of optical CIR with the hot gas properties of ETGs which is provided in the next section.

1.8 Connections between Central Intensity Ratio and hot gas properties of early-type galaxies

In this work, we explore correlations between the optical central intensity ratio and hot gas properties of nearby early-type galaxies. Most massive early-type galaxies emit X-rays and possess high gas temperature in their ISM. Prior studies (Boroson et al., 2011; Negri et al., 2014; Kim & Fabbiano, 2015; Gaspari et al., 2019) reported X-ray gas luminosity and gas temperature are well correlated, and this relation is fundamental to investigating the evolution process of early-type galaxies. The X-ray gas luminosity ($L_{X,GAS}$) and gas temperature (T_{GAS}) of the thermal ISM are the two fundamental parameters of X-ray-emitting ETGs. These observables are directly related to the gas mass and total entropy of the systems and describe the physics of the baryonic matter inside the system (Goulding et al., 2016). The following sections provide a short description of the hot gas properties of galaxies.

1.8.1 X-ary gas luminosity ($L_{X,GAS}$)

During their evolution, early-type galaxies have a significant amount of hot gas at their ISM. The source of this gas has been believed to mainly be the stellar mass loss caused by the evolved stars in the host galaxies (Forbes et al., 2017a). This hot, diffuse gas is one of the prime sources of X-ray emission from early-type galaxies (O'Sullivan et al., 2003; Fabbiano, 2006). According to cosmological simulations, the total mass of a galaxy is believed to be a key parameter in regulating the X-ray gas luminosity (Choi et al., 2015). Also, Kim & Fabbiano (2013) reported a strong correlation between measurements of $L_{X,GAS}$ and the dynamical mass (i.e. baryonic + dark matter) within 5Re, where Re is the effective radius of the galaxy optical light. These investigations suggested that the dynamical mass might actually be an important parameter in determining $L_{X,GAS}$ associated with ETGs.

The contribution from various sources (like hot gas, active galactic nuclei (AGNs), supermassive black hole (SMBH) and X-ray binaries) to the X-ray emission of ETGs has been a hot topic (Kim & Fabbiano, 2003; Pellegrini, 2010; Boroson et al., 2011). Hot gas that has been entrapped in the ISM of ETGs by the galaxy's gravitational potential may be the origin of X-ray emission (Canizares, 1999; Goulding et al.,

2016). In the case of AGN host galaxies, the synchrotron jet emission from the
nucleus might even contribute to and enhance the X-ray gas luminosity (Wilson &
Yang, 2002; Yuan et al., 2009).

1.8.2 Gas temperature (T_{GAS})

One of the most fundamental X-ray properties is the gas temperature, which is
also a measure of the gravitational potential of the systems. Older galaxies contain
a large amount of hot diffuse gas and the temperature of this gas is proportional
to the X-ray emission from the host galaxies (Kim & Fabbiano, 2015; Goulding
et al., 2016; Gaspari et al., 2019). Due to the gravitational potential of galaxies, hot
gas might be trapped in the ISM (Canizares, 1999; Goulding et al., 2016) and the
kinematics of stellar components in the core region might enhance the temperature of
the gas. Previous studies suggested that X-ray gas luminosity and gas temperature
are proportional to the total galaxy mass (Mathews & Brighenti, 2003; Boroson
et al., 2011; Kim & Fabbiano, 2013; Civano et al., 2014). It further supports the
hypothesis that the diffuse X-ray luminosity primarily depends on the depth of the
galaxy's potential well (Forbes et al., 2017a).

It is commonly known that X-ray luminosity and gas temperature are positively
correlated in massive galaxies (O'Sullivan et al., 2003; Mathews & Brighenti, 2003;
Boroson et al., 2011; Negri et al., 2014). Also, $L_{\mathrm{X,GAS}}$ and T_{GAS} reported to correlate
well with the SMBH mass (Gaspari & Sadowski, 2017; Gaspari et al., 2019). In this
light, we carried out simple photometry to establish new scaling relations using
optical CIR. Then, for the first time, we identified significant correlations between
CIR and X-ray properties of ETGs like $L_{\mathrm{X,GAS}}$ and T_{GAS} and we summarized this
work in Chapter 3.

As mid-infrared emission exhibits significant connections with galaxy parame-
ters, we were inspired to estimate CIR using mid-infrared data and investigate the
various relationships between mid-infrared CIR and galaxy parameters of ETGs.
The next section provides details about this investigation.

1.9 Central Intensity Ratio in Mid-Infrared for early-type galaxies

It is believed that most of the infrared radiation from galaxies is thermal emission by dust (Soifer & Neugebauer, 1991). Understanding the distribution of galaxy luminosities and stellar masses in the current Universe is crucial for studying the assembly of galaxies over cosmic time (Brinchmann & Ellis, 2000; Cole et al., 2000; Wolf et al., 2003). The stellar mass distribution in galaxies can be traced with great precision using the mid-infrared (3.6 and 4.5 µm) IRAC bands on Spitzer (Sheth et al., 2010). The contamination from old stellar population light is quite low in the 3.6 and 4.5 µm IRAC bands. Since the less dust extinction and no other substantial emission sources at these wavelengths, it is possible to investigate the distribution of stellar mass in galaxies in the nearby Universe in a unique and almost dust-free manner (Sheth et al., 2010). In this study, we determined the mid-infrared CIR of early-type galaxies using SPITZER/ IRAC 3.6 µm data, and in the following section, we described the galaxy properties which show a significant connection with mid-infrared CIR.

1.9.1 Mid-Infrared light and stellar mass of host galaxy

For any galaxy, total stellar mass is a vital parameter to understand its evolution process. The dark matter content of the galaxy can be traced through accurate measurement of stellar mass (Forbes et al., 2017b). The stellar masses of galaxies can be measured particularly well at 3.6 µm wavelength (Norris et al., 2014). In contrast to shorter wavelengths, the 3.6 µm light from galaxies is predominantly composed of light from old stars, which is less affected by variations in the star formation process. The mass-to-light ratio at this wavelength is relatively insensitive to metallicity and modestly sensitive to age for old stellar populations, making the 3.6 µm emission from early-type galaxies a perfect tracer of stellar mass (Forbes et al., 2017b).

1.9.2 Connections between stellar mass and galaxy properties

Stellar mass distribution in galaxies is considered essential for understanding several structural and evolutionary characteristics of galaxies (Kormendy & Kennicutt, 2004). Several cosmological studies reported the close correlation between star formation rate (SFR) and stellar mass of galaxies (e.g., Daddi et al., 2007; Noeske et al., 2007; González et al., 2011), which suggest that stellar mass governs the growth and evolution of galaxies. It is essential to consider the stellar mass distribution to assess the function of bars, spiral structures, and inner stellar components of galaxies in their evolution process (Knapen et al., 1995b; Regan & Elmegreen, 1997; Falcón-Barroso et al., 2006; Salo et al., 2010; Eliche-Moral et al., 2011). Moreover, understanding the stellar mass distribution in the galaxy is crucial in order to comprehend how gravitational potential influences the distribution of gas and its dynamics (Knapen et al., 1995b; García-Burillo et al., 2005; Jogee et al., 2005; Hunt et al., 2008; Haan et al., 2009).

Different studies explored the connection between stellar mass and other galaxy properties to explain the evolution mechanism of ETGs since stellar mass provides vital information about the galaxy mass as well as the dark matter content (Forbes et al., 2017b). In this context, we carried out photometric analysis using SPITZER/IRAC 3.6 μm image of ETGs and summarized this work in Chapter 4.

1.10 Motivation and outline of the thesis

Photometry is the study and measurement of light emitted by astronomical objects. Surface photometry is a method for determining the surface brightness distribution of extended objects, like galaxies. These photometric parameters are highly associated with morphology, star formation, and evolution of galaxies. Multi-wavelength observations (optical, IR, and UV) using space telescopes with high resolution (for instance resolution of HST, R ∼ 0.04 arcsec) provide good-quality images of galaxies. Photometric studies utilized these images to investigate the nature of galaxies and provided new insights into how galaxies evolve. Since the presence of a supermassive black hole is identified at the central region of galaxies, studies on the central region

of host galaxies are very important. Analyzing the central region of galaxies is crucial for understanding the physical mechanisms that contribute to the co-evolution of the central supermassive black hole and host galaxy, or vice versa. Exploring interconnections between galaxy features and their interpretation is quite exciting in order to understand the morphology and evolution of the galaxies using photometry. In this context, we employ photometric techniques to do an investigation on galaxies in the nearby Universe.

We carried out aperture photometry on multi-wavelength images of different groups of galaxies which are morphologically comparable including active and quiescent galaxies, and establish possible connections between various parameters related to the galaxies. We start by investigating the central properties of nearby Seyfert galaxies. We attempt to study the central region of these AGN host galaxies, the majority of which are spiral galaxies, using optical data to find new scaling relations for calculating the mass of the central supermassive black hole. A study of X-ray-emitting early-type galaxies and their characteristics, such as hot gas temperature and X-ray gas luminosity, is then presented. In the last part of the work, we perform photometric analysis utilizing infrared data on a sample of early-type galaxies, which also provides some insights into the evolution scenario of galaxies. In this chapter, we include a brief overview of all of these works, followed by a short description.

In Chapter 1, we describe the motivation behind the studies done for this thesis. The entire work has been divided into three main sections. The first section is an optical study using the central intensity ratio (CIR) of nearby AGN host galaxies, the second part deals with the connections between the optical central intensity ratio and hot gas properties of nearby X-ray emitting early-type galaxies, and the final part further elaborates the study of early-type galaxies with infrared central intensity ratio. This chapter includes a literature review of the complete work and discusses the present context in which the research was carried out. Also, we have included descriptions of telescopes used for data acquisition for the entire study along with a short explanation of different software that was used in the analysis.

In the first part of the study, we determined the optical central intensity ratio of 57 nearby Seyfert galaxies using aperture photometry by employing source extractor (SExtractor). We find a strong correlation between the CIR of Seyfert galaxies and

the mass of their central SMBH (M_{BH}). At the same time, the elliptical galaxies in the sample host systematically high black hole mass when compared to lenticulars and spirals. We find a positive correlation between CIR and OIV flux of the host galaxy. However, there is no significant correlation between CIR and central velocity dispersion (σ) of Seyfert galaxies. In addition, we noticed that the scatter in the relation between M_{BH} and central velocity dispersion is greater than that of the CIR – M_{BH} relation. Hence, we propose that CIR might be a better tracer of the M_{BH} than the central velocity dispersion. This work is summarized in Chapter 2.

In the second part of the study, we propose new scaling relations with gas properties of early-type galaxies using optical CIR. We find that CIR is well correlated with X-ray gas luminosity and gas temperature of the galaxies. We identified a difference between core and coreless galaxies in all the correlations involving CIR. Furthermore, CIR is found to be strongly correlated with the age of the central stellar population and the K-band magnitude of the galaxies. The correlations mentioned above strongly imply that older galaxies have more hot, diffuse gas trapped in their interstellar medium (ISM), which causes excessive X-ray emission and drives the evolution of galaxies. To measure X-ray gas luminosity from ISM with greater accuracy, it is necessary to subtract various contributors to the X-ray emission in galaxies using rigorous spectroscopic modeling. In this context, the simple photometric parameter CIR can be used instead of employing spectroscopy for determining the X-ray gas luminosity of ETGs. This work is summarized in Chapter 3.

The final part of the study, which is detailed in Chapter 4, includes a mid-infrared analysis of nearby ETGs. In this study, we estimated mid-infrared CIR of the sample galaxies using 3.6 µm data and we report significant correlations between mid-infrared CIR and various properties of galaxies. Mid-infrared CIR is found to be anti-correlated well with the total stellar mass and absolute B band magnitude of the galaxies. It also exhibits a negative correlation with central velocity dispersion and mass of the SMBH. Similar to the optical CIR, mid-infrared CIR shows the same trend with the fundamental parameters in early-type galaxies. Consequently, we propose that mid-infrared CIR can be used to trace SMBH mass and other galaxy properties in ETGs and CIR can be a key parameter for unfolding the evolution scenario of nearby galaxies. Chapter 5 of this thesis summarizes all the work done and discusses future scopes of the study.

Chapter 2

Study of Central Intensity Ratio of Seyfert Galaxies in nearby Universe

2.1   Introduction

The central supermassive black hole (SMBH) residing in massive galaxies is believed to play a key role in the evolution scenario of host galaxies. The evolution mechanism of the central engine of every galaxy is connected with the star formation process in the host galaxy. It is commonly accepted that the accretion mechanism is the prime reason for the origin and growth of active galactic nucleus (AGN) in the nuclear region of galaxies (Kawakatu et al., 2006; Ellison et al., 2011; Silverman et al., 2011; Villforth et al., 2012).

AGNs are hosted at the centre of elliptical galaxies or bulge dominating spheroids across all redshifts (Kauffmann et al., 2003; Pović et al., 2009), whereas the morphology of local Seyfert galaxies is generally spiral (Ho et al., 1995; Ho, 2008). Intense circumnuclear star formation plays a crucial role in the evolution and emission process of Seyfert galaxies, specifically, Sy2 galaxies. (e.g., Terlevich & Melnick, 1985; Maiolino et al., 1998; Cid Fernandes & Terlevich, 1995; González Delgado et al., 2001; Cid Fernandes et al., 2001).

Seyfert galaxies are among the most studied objects in the radio-quiet (RQ)

category, along with quasars (Weedman, 1977; Osterbrock & Martel, 1993; Rashed et al., 2015). The role of feedback by the central SMBH in the relationships between the mass of the SMBH and bulge properties of Seyfert galaxies is still unclear because the merger events govern the formation of bulges while Seyfert galaxies are believed to be evolving through secular evolution (Hopkins et al., 2006; Kormendy & Ho, 2013b; Heckman & Best, 2014). Recent studies revealed the existence of fast outflows of ionized gas in nearby Seyfert galaxies, but their influence on star formation is still under debate (Christensen et al., 2006; Krause et al., 2007; Wang et al., 2012; García-Burillo et al., 2014; Morganti et al., 2015; Querejeta et al., 2016). However, if the host galaxies possess such outflows, they could expel the gas from the central region and suppress the star formation (Alexander & Hickox, 2012; García-Burillo et al., 2014; Alatalo et al., 2015; Hopkins et al., 2016; Wylezalek & Zakamska, 2016).

The masses of central supermassive black holes (SMBHs) are reported to correlate well with the stellar mass and stellar velocity dispersion of the bulges of their host galaxies (see, e.g., Magorrian et al., 1998; Ferrarese & Merritt, 2000; Gebhardt et al., 2000; Marconi & Hunt, 2003; Häring & Rix, 2004; Kormendy & Ho, 2013a; McConnell & Ma, 2013; Savorgnan & Graham, 2015). The bulges and supermassive black holes seem to evolve together and regulate each other (Alonso-Herrero et al., 2013). The relations (between M_{BH}, bulge mass, and stellar velocity dispersion) propose a strong connection between the formation of black hole mass, emergence of AGNs, and the host galaxy evolution (Ferrarese & Merritt, 2000; Gültekin et al., 2009) as well.

Central light concentration is a vital parameter, which can be used as a tracer of the disk-to-bulge ratio, star formation activity, and galaxy evolution (Abraham et al., 1994; Conselice, 2003). The Central Intensity Ratio (CIR), a new photometric parameter, is well correlated with the masses of central SMBHs of the spheroid of early-type galaxies (Aswathy & Ravikumar, 2018). Furthermore, CIR is an efficient photometric tool to study the central and structural properties of spiral galaxies, especially barred systems, and also gives some important information regarding nuclear star formation and AGN formalism in the host galaxies (Aswathy & Ravikumar, 2020). In this light, we perform an optical analysis by utilizing the parameter, CIR, to study the central properties as well as the evolution of Seyfert galaxies.

2.2 The Data

For this work, we consider a complete sample of Seyfert galaxies drawn from the Revised Shapley-Ames catalog (RSA; Shapley & Ames, 1932; Sandage & Tammann, 1987) analyzed by Diamond-Stanic et al. (2009); Diamond-Stanic & Rieke (2012), which include 114 nearby ($z < 0.02$) Seyfert galaxies brighter than $B_T = 13.2$. We took archival images of the sample observed by the Hubble Space Telescope (HST) to estimate CIR. Among the 114 galaxies, 83 had HST observations in optical bands. From this, 13 galaxies consisting of bad pixels or defects on their images within the region of central 3 arcsecs are avoided from the sample. Also, we excluded 10 small galaxies, in which the size of their images is less than the 3 arcsecs aperture, and 3 highly inclined galaxies ($i > 70°$). The final sample consists of 57 Seyfert galaxies comprising 40 spiral, 9 lenticular, and 8 elliptical galaxies. We chose galaxy images observed with Wide Field Planetary Camera 2 (WFPC2). It is already reported that though there exist slight variations among values of CIR estimated from nearby filters, the variations are not strong enough to disrupt the observed correlations involving CIR (Sruthi & Ravikumar, 2021). Hence we included observations using all filters of WFPC2 from F606W to F814W, giving preference to the filter in the highest wavelength region available. Further, we added four observations using F814W with Advanced Camera for Surveys to improve the statistics for which no WFPC2 images were available. Since the sample galaxies possess AGN, we have checked the central region of the sample galaxies by constructing residual images using the *ellipse* task in IRAF (see A1). Many sub-structures like bar, ring, and spiral arms are visible in the residual image, however, no significant optical excess flux could be identified in these galaxies that could affect the determination of CIR.

2.2.1 Data Reduction

Following Aswathy & Ravikumar (2018), the CIR is determined for the sample galaxies by using the aperture photometry (MAG_APER) technique, which is provided in source extractor (SExtractor, Bertin & Arnouts, 1996).

$$CIR = \frac{I_1}{I_2 - I_1} = \frac{10^{0.4(m_2 - m_1)}}{1 - 10^{0.4(m_2 - m_1)}}. \tag{2.1}$$

where I_1 and I_2 are the intensities and m_1 and m_2 are the corresponding magnitudes of the light within the inner and outer apertures of radii R_1 and R_2, respectively. The inner radius is chosen such that it's a few times the PSF. The outer radius (conventionally $2R_1$) is chosen such that the aperture is lying fairly within the galaxy image. For the sample, we chose the inner and outer radii as 1.5 and 3 arcsecs, respectively.

Ultraviolet (UV) observations are vital in providing recent star formation activity in galaxies (e.g., Gil de Paz et al., 2005, 2007; Thilker et al., 2005; Koribalski & López-Sánchez, 2009). For the estimation of circumnuclear star formation rate (SFR), we took far-UV (FUV, 1350-1750 Å) data of the sample galaxies observed by the GALaxy Evolution eXplorer (GALEX) mission. We used an aperture size of 10 arcsecs at the centre of the image to estimate the circumnuclear SFR which is provided in Table 4.1.

According to the calibration of López-Sánchez (2010),

$$f_{FUV} = 1.40 \times 10^{-15} \times 10^{0.4(18.82 - m_{FUV}^0)} \tag{2.2}$$

where $m_{FUV}^0 = m_{FUV} - A_{FUV}$, is the extinction corrected magnitude and $A_{FUV} = 7.9E(B-V)$ is the extinction correction parameter. The value of $E(B-V)$ adopted from NED and f_{FUV} is obtained in units of $erg\,s^{-1}\,cm^{-2}\,\mathring{A}^{-1}$. When the FUV luminosity is computed using the calculated flux ($L_{FUV} = 4\Pi D_L^2 f_{FUV}$), the FUV-based SFR can be derived by applying the calibration provided by Salim et al. (2007),

$$SFR_{FUV} = 8.1 \times 10^{-41} L_{FUV} \tag{2.3}$$

Table 2.1: Properties of Seyfert galaxies. Name of the galaxy (column 1), Distance (2), Seyfert type (3), Morphology (4), HST observation (5), CIR computed in the corresponding filter (6), uncertainty of CIR (7), estimated circumnuclear SFR (8), uncertainty of SFR (9), OIV flux taken from Diamond-Stanic et al. (2009) (10), stellar velocity dispersion adopted from Hyperleda (11), SMBH mass (12), and corresponding references (13).

Galaxy	Distance (Mpc)	Seyfert type	Morphology	HST filter	CIR	ΔCIR	log SFR ($M_\odot\,yr^{-1}$)	ΔSFR	OIV flux ($erg\,cm^{-2}\,s^{-1}$)	σ ($km\,s^{-1}$)	$\log M_{\mathrm{BH}}$ ($M_\odot$)	Ref
(1)	(2)	(3)	(4)	(5)	(6)	(7)	(8)	(9)	(10)	(11)	(12)	(13)
IC2560	40.7	S2	(R')SB(r)b	WFPC2_F814	1.44	0.03	0.67	0.013	5.43E-13	136.5	6.64	1
IC3639	35.3	S2	SB(rs)bc	WFPC2_F606	1.27	0.02	1.64	0.040	3.55E-13	97.1	6.83	2
NGC0613	20.7	S?	SB(rs)bc	WFPC2_F814	0.86	0.02	0.91	0.007	–	122.1	7.60	3
NGC0788	54.1	S2	SA(s)0/a	WFPC2_F606	1.16	0.03	1.01	0.021	1.80E-13	134.4	7.51	2
NGC1275	70.1	S2	E-cD	WFPC2_F606	1.07	0.03	2.22	0.170	1.85E-13	244.6	8.58	2
NGC1358	53.6	S2	SAB(r)0/a	WFPC2_F606	1.17	0.02	–	–	7.61E-14	215.1	7.88	2
NGC1365	21.5	S1.8	SB(s)b	WFPC2_F814	1.78	0.03	1.06	0.009	1.58E-12	141.1	6.05	4
NGC1386	10.6	S2	SB0+(s)	WFPC2_F814	1.10	0.02	-0.11	0.001	8.70E-13	133.1	7.23	2
NGC1399	19.4	S2	E1 pec	WFPC2_F814	0.58	0.01	–	–	–	332.2	8.94	3
NGC1433	13.3	S2	(R')SB(r)ab	WFPC2_F814	0.91	0.02	0.38	0.002	6.07E-14	107.0	7.24	5
NGC1566	19.4	S1.5	SAB(s)bc	WFPC2_F814	1.03	0.03	0.67	0.005	8.88E-14	97.7	7.11	4
NGC1667	61.2	S2	SAB(r)c	WFPC2_F606	1.09	0.03	1.51	0.049	9.28E-14	169.4	7.88	2
NGC1672	16.7	S2	SB(s)b	WFPC2_F814	0.77	0.02	1.35	0.010	–	109.5	7.70	6

Table 2.1 continued.

Galaxy	Distance (Mpc)	Seyfert type	Morphology	HST filter	CIR	ΔCIR	log SFR ($M_\odot\,yr^{-1}$)	ΔSFR	OIV flux ($\mathrm{erg\,cm^{-2}\,s^{-1}}$)	σ ($\mathrm{km\,s^{-1}}$)	log M_{BH} ($M_\odot$)	Ref
(1)	(2)	(3)	(4)	(5)	(6)	(7)	(8)	(9)	(10)	(11)	(12)	(13)
NGC1808	12.3	S2	(R)SAB(s)a	WFPC2_F814	0.90	0.02	-0.11	0.001	–	126.1	7.20	7
NGC2273	28.4	S2	SB(r)a	WFPC2_F791	1.15	0.03	0.14	0.004	1.47E-13	141.0	7.30	2
NGC2639	42.6	S1.9	(R)SA(r)a	WFPC2_F814	0.69	0.03	0.43	0.009	3.27E-14	175.3	7.94	2
NGC2782	37.0	S2	SAB(rs)a pec	WFPC2_F814	1.21	0.03	1.81	0.032	–	182.2	7.70	8
NGC2974	20.9	S2	E4	WFPC2_F814	1.20	0.02	–	–	–	232.2	8.23	9
NGC3081	34.2	S2	(R)SAB(r)0/a	WFPC2_F814	0.88	0.03	–	–	9.89E-13	118.8	7.20	3
NGC3169	17.4	S	SA(s)a pec	WFPC2_F814	0.74	0.02	-0.42	0.001	–	184.9	8.01	10
NGC3185	21.3	S2	(R)SB(r)a	WFPC2_F814	1.58	0.03	-0.44	0.001	4.70E-14	76.1	6.52	2
NGC3227	20.6	S1.5	SAB(s)a pec	ACS_F814	1.66	0.00	–	–	5.71E-13	126.8	6.75	11
NGC3281	44.7	S2	SA(s)ab pec	WFPC2_F606	0.86	0.04	–	–	1.39E-12	168.6	7.28	2
NGC3486	7.4	S2	SAB(r)c	WFPC2_F814	1.10	0.03	-0.41	0.001	3.30E-14	60.2	7.00	12
NGC3489	6.73	S2	SAB0+(rs)	WFPC2_F814	1.34	0.01	-0.41	0.001	–	104.2	6.78	13
NGC3516	38.9	S1.2	(R)SB(s)0	WFPC2_F791	1.45	0.02	1.83	0.037	5.60E-13	153.6	7.23	24
NGC3982	17.0	S1.9	SAB(r)b	WFPC2_F814	1.12	0.03	–	–	1.18E-13	71.8	7.20	14
NGC4168	16.8	S1.9	E2	WFPC2_F702	0.74	0.04	–	–	1.39E-14	182.0	9.01	15
NGC4235	35.1	S1.2	SA(s)a	WFPC2_F606	0.99	0.03	-0.17	0.003	4.33E-14	133.6	7.64	2

Table 2.1 continued.

Galaxy	Distance (Mpc)	Seyfert type	Morphology	HST filter	CIR	ΔCIR	log SFR ($M_\odot\,yr^{-1}$)	ΔSFR	OIV flux ($\mathrm{erg\,cm^{-2}\,s^{-1}}$)	σ ($\mathrm{km\,s^{-1}}$)	log M_{BH} ($M_\odot$)	Ref
(1)	(2)	(3)	(4)	(5)	(6)	(7)	(8)	(9)	(10)	(11)	(12)	(13)
NGC4258	8.0	S1.9	SAB(s)bc	ACS_F814	0.72	0.08	0.25	0.001	7.49E-14	132.8	7.58	2
NGC4303	13.6	S2	SAB(rs)bc	WFPC2_F814	1.69	0.01	–	–	–	95.1	6.58	16
NGC4374	18.5	S2	E1	WFPC2_F814	0.60	0.01	–	–	–	277.6	8.97	1
NGC4472	17.1	S2	E2	WFPC2_F814	0.53	0.02	–	–	6.64E-14	282.0	9.18	17
NGC4477	16.8	S2	SB0(s)	WFPC2_F606	0.79	0.02	0.08	0.002	1.69E-14	172.5	7.91	2
NGC4501	16.8	S2	SA(rs)b	WFPC2_F606	1.22	0.02	0.02	0.004	3.98E-14	166.2	7.30	3
NGC4507	59.6	S2	(R')SAB(rs)b	WFPC2_F814	1.34	0.02	–	–	3.31E-13	149.0	7.58	2
NGC4552	15.4	S2	E0-1	WFPC2_F814	0.91	0.01	–	–	–	250.3	8.63	18
NGC4579	16.8	S1.9	SAB(rs)b	WFPC2_F791	1.13	0.02	0.22	0.044	2.83E-14	165.8	7.70	19
NGC4594	20.0	S1.9	SA(s)a	WFPC2_F814	0.91	0.01	0.38	0.003	2.62E-14	225.7	8.76	2
NGC4698	16.8	S2	SA(s)ab	WFPC2_F814	1.03	0.02	-0.53	0.001	2.03E-14	137.4	7.61	2
NGC4725	12.4	S2	SAB(r)ab pec	WFPC2_F606	0.87	0.01	-0.01	0.002	1.24E-14	131.5	7.51	2
NGC5005	21.3	S2	SAB(rs)bc	ACS_F814	0.60	0.00	1.91	0.013	1.99E-14	171.5	7.84	20
NGC5033	18.7	S1.9	SA(s)c	WFPC2_F814	0.96	0.02	-0.28	0.001	1.59E-13	133.9	7.64	2
NGC5135	57.7	S2	SB(s)ab	WFPC2_F606	1.11	0.02	1.95	0.069	5.83E-13	125.5	7.34	2
NGC5194	8.4	S2	SA(s)bc pec	WFPC2_F814	1.27	0.02	-0.62	0.000	2.46E-13	87.9	6.95	2

Table 2.1 continued.

Galaxy	Distance (Mpc)	Seyfert type	Morphology	HST filter	CIR	ΔCIR	log SFR ($M_\odot\,yr^{-1}$)	ΔSFR	OIV flux ($erg\,cm^{-2}\,s^{-1}$)	σ ($km\,s^{-1}$)	$\log M_{\rm BH}$ ($M_\odot$)	Ref
(1)	(2)	(3)	(4)	(5)	(6)	(7)	(8)	(9)	(10)	(11)	(12)	(13)
NGC5273	21.3	S1.5	SA0(s)	WFPC2_F791	1.47	0.03	-0.10	0.001	3.72E-14	65.9	6.61	3
NGC5322	24.3	S	E3-4	WFPC2_F814	0.96	0.02	–	–	–	230.0	8.51	21
NGC5427	40.4	S2	SA(s)c pec	WFPC2_F606	1.16	0.03	1.00	0.013	2.68E-14	69.9	7.58	3
NGC5643	14.4	S2	SAB(rs)c	WFPC2_F814	1.45	0.02	–	–	8.16E-13	–	6.44	22
NGC5806	27.4	S2	SAB(s)b	WFPC2_F814	1.10	0.03	–	–	–	124.3	7.07	23
NGC6814	25.6	S1.5	SAB(rs)bc	WFPC2_F606	1.29	0.03	1.55	0.025	2.13E-13	108.1	7.26	2
NGC6951	24.1	S2	SAB(rs)bc	WFPC2_F814	0.73	0.02	0.60	0.014	8.37E-14	114.8	7.34	2
NGC7469	67.0	S1.2	(R')SAB(rs)a	ACS_F814	1.06	0.00	2.99	0.281	3.67E-13	132.9	7.08	2
NGC7479	32.4	S1.9	SB(s)c	WFPC2_F814	0.85	0.04	–	–	2.67E-13	151.3	7.68	2
NGC7582	22.0	S2	(R')SB(s)ab	WFPC2_F606	1.84	0.02	-0.10	0.002	2.22E-12	118.4	7.74	2
NGC7590	22.0	S2	SA(rs)bc	WFPC2_F606	1.09	0.02	0.52	0.005	6.88E-14	91.5	6.79	2
NGC7743	24.4	S2	(R)SB0+(s)	WFPC2_F606	1.49	0.02	–	–	3.30E-14	83.5	6.72	2

References: 1. Kormendy & Ho (2013b), 2. Diamond-Stanic & Rieke (2012), 3. van den Bosch (2016), 4. Davis et al. (2014), 5. Smajić et al. (2014), 6. Combes et al. (2019) (7)Busch et al. (2017), 8. Dong & De Robertis (2006), 9. Savorgnan & Graham (2016), 10. Dong & Wu (2015), 11. Onken et al. (2003), 12. Koliopanos et al. (2017), 13. Nowak et al. (2010), 14. Beifiori et al. (2012), 15. Magorrian et al. (1998), 16. Davis et al. (2018), 17. Graham & Soria (2019), 18. Pellegrini (2010), 19. Barth et al. (2001), 20. Izumi et al. (2016), 21. Dullo et al. (2018), 22. Goulding et al. (2010), 23. Dumas et al. (2007).

Table 2.2: Best-fitting parameters for the relation x $= \alpha$ CIR $+ \beta$ and linear correlation coefficient (r) for various relations. n denotes the number of galaxies.

x	subsample	n	α	β	r	s
log M_{BH}	(spiral+lenticular)	47	-1.25±0.16	8.67±0.19	-0.74	> 99.99%
log M_{BH}	(elliptical)	8	-1.16±0.15	9.67±0.13	-0.94	99.40%
log OIV flux		38	1.49±0.24	-14.60±0.28	0.70	> 99.99%

2.3 Results

Recently, the estimation and interpretation of correlations between galaxy properties have drawn much attention, since they are recognized as a crucial tool to understand the evolution scenario of galaxies. Scaling relations displayed by various structural and dynamical observables of galaxies can shed vital information on formation and evolution processes in galaxies. We have estimated the CIR at the optical centre of 57 Seyfert galaxies observed using HST. The sample properties, along with the estimated values of CIR, are tabulated in Table 4.1. We next explore various trends involving CIR.

2.3.1 Correlation between CIR and SMBH mass

This study shows a significant connection between CIR and mass of the central SMBH of the Seyfert galaxies. The scaling relations of black hole mass are generally determined and explored utilizing the bulge properties of the host galaxies, specifically in early-type galaxies (Kormendy & Richstone, 1995; Ferrarese & Merritt, 2000; McConnell & Ma, 2013). Structural properties of late-type galaxies, like the pitch angle of spiral arms, share intriguing scaling relation with the black hole mass (Davis et al., 2018, 2019).

Figure 2.1 shows the correlation of CIR with the mass of SMBH for the sample galaxies. Filled circles, triangles, and squares represent spiral, lenticular, and elliptical galaxies, respectively. We find a strong correlation between the CIR of the Seyfert galaxies and the mass of their central SMBH. However, the early-type

galaxies in the sample host systematically high black hole mass when compared to lenticulars and spirals, for the same value of CIR considered. The Pearson's linear correlation coefficient, r, for the correlation exhibited by spirals and lenticulars together is -0.74 with a significance, s, > 99.99 per cent (Press et al., 1992) while that for elliptical galaxies is -0.94 with a significance of 99.40 per cent.

Two galaxies, NGC4594 and NGC7582, show significant deviation from this correlation. NGC4594, the Sombrero galaxy, is reported to have an unusually large bulge mass and a very massive SMBH at the centre of the galaxy. It is usually classified as a normal spiral, Sa, galaxy (de Vaucouleurs et al., 1991) but following many scaling relations of ellipticals (Gadotti & Sánchez-Janssen, 2012). NGC7582 is reported to host a ring with active star formation within the pc scale radius ($\approx$ 190 pc) surrounding the nucleus of the galaxy, along with a high stellar velocity dispersion (Riffel et al., 2009). The intense nuclear starburst activity (Cid-Fernandes et al., 2001; Bianchi et al., 2007) can affect its CIR value.

We noticed that there is no apparent correlation between CIR and stellar velocity dispersion of Seyfert galaxies, even though the latter and the mass of SMBH are reported to share a strong correlation. In order to explore this discrepancy, we also employed a color code to distinguish the method adopted to estimate the masses of SMBH. Masses estimated using a dynamical method (e.g., reverberation mapping, stellar dynamics, maser dynamics, and gas dynamics) are shown in red while mass estimations based on stellar velocity dispersion are shown in gray in Figure 2.1. If we include only dynamically estimated masses, the correlation coefficient improves to -0.77 at a significance, $s = 99.97$ per cent, while it reduces drastically to -0.68 ($s = 99.98$ per cent) when these data points are excluded.

2.3.2 Variation between the CIR and σ

The variation of CIR with the stellar velocity dispersion of the sample galaxies is shown in Figure 2.2(a). As already mentioned, there is no significant correlation between CIR and stellar velocity dispersion (σ) of Seyfert galaxies. However, if we exclude the eight early-type galaxies in the sample, the velocity dispersion measurements of galaxies with the dynamical estimation of SMBH (red triangles and circles) show a larger scatter compared to their gray counterparts. Such a discrepancy is
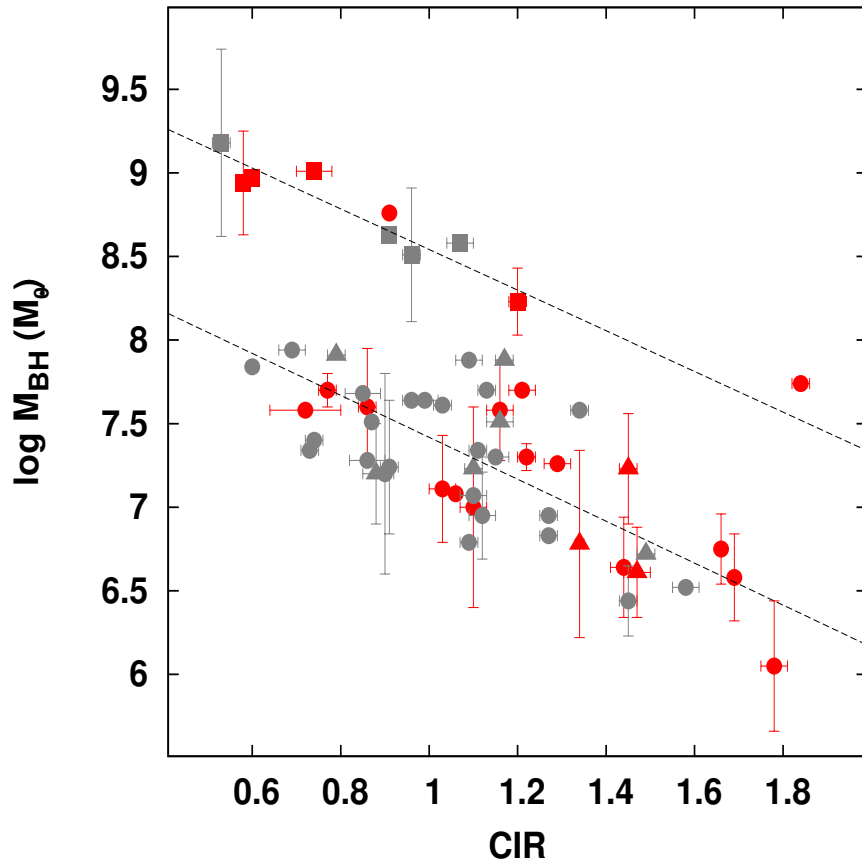
Figure 2.1: Correlation between the central intensity ratio and mass of the SMBH of the sample galaxies. Filled circles, triangles, and squares represent spiral, lenticular, and elliptical galaxies, respectively. Estimations of masses of SMBH using dynamical methods are denoted as red data points, while gray color is used to represent those from the stellar velocity dispersion measurements of host galaxies. The dashed line shows the best fit linear model to the data.

not clear in early-type galaxies. The measurement of σ in active galaxies is a difficult task due to the AGN activity. The extreme emission from AGN outshined and/or diluted the stellar spectral lines (Riffel et al., 2013) and thus the measurement of stellar velocity dispersion obtained with a significant discrepancy in AGNs, particularly in spiral galaxies.

Moreover, measurements of stellar velocity dispersion may be biased by the contribution of rotating stellar disks because of the rotational broadening of the stellar absorption lines and the velocity dispersion measurements could be noticeably increased by the rotational effect (Woo et al., 2015). The rotation effect is comparatively small for early-type galaxies because the velocity dispersion is usually greater than the rotation velocity (V). Due to higher velocity-to-dispersion (V/σ) ratios, the rotational effect is significantly more prominent in late-type galaxies (LTGs) than in ETGs. Thus, it is further confirmed that if a spectrum is used without correcting the rotational broadening effect, the velocity dispersion might be overestimated by up to $\sim 20\%$ for late-type galaxies (Kang et al., 2013; Woo et al., 2013).

2.3.3 Variation between the CIR and SFR

In Figure 2.2(b), we explore the connection between CIR and circumnuclear SFR traced by the UV luminosity (FUV) in an aperture of radius 10 arcsec at the galactic centre. We find that there is no correlation between CIR and circumnuclear SFR. The properties of sub-structures in the nuclear region of host galaxies may influence the star formation process, and thereby affecting CIR. The nuclear spiral structure is one of the sub-structures of Seyfert galaxies, which are caused by a turbulent process. In galaxies, turbulence may be caused by gas accretion. Pressure or gravitational-force-induced turbulence may produce structures that are eventually transformed into a spiral shape by differential rotation (Martini et al., 2003). The galaxies IC2560, NGC0788, NGC1667, NGC3516, NGC5427, and NGC6814, denoted by the numbers 1 to 6 respectively in the figure, possess nuclear dust spirals, which can regulate the nuclear SFR at the central region of the galaxies (Evans et al., 1996; Pérez-Ramírez et al., 2000; Martini et al., 2003; Muñoz Marín et al., 2007).

The star formation occurs at a rate that is far higher than what is generally observed and is referred to as starburst activity (Muñoz Marín et al., 2007; Bianchi
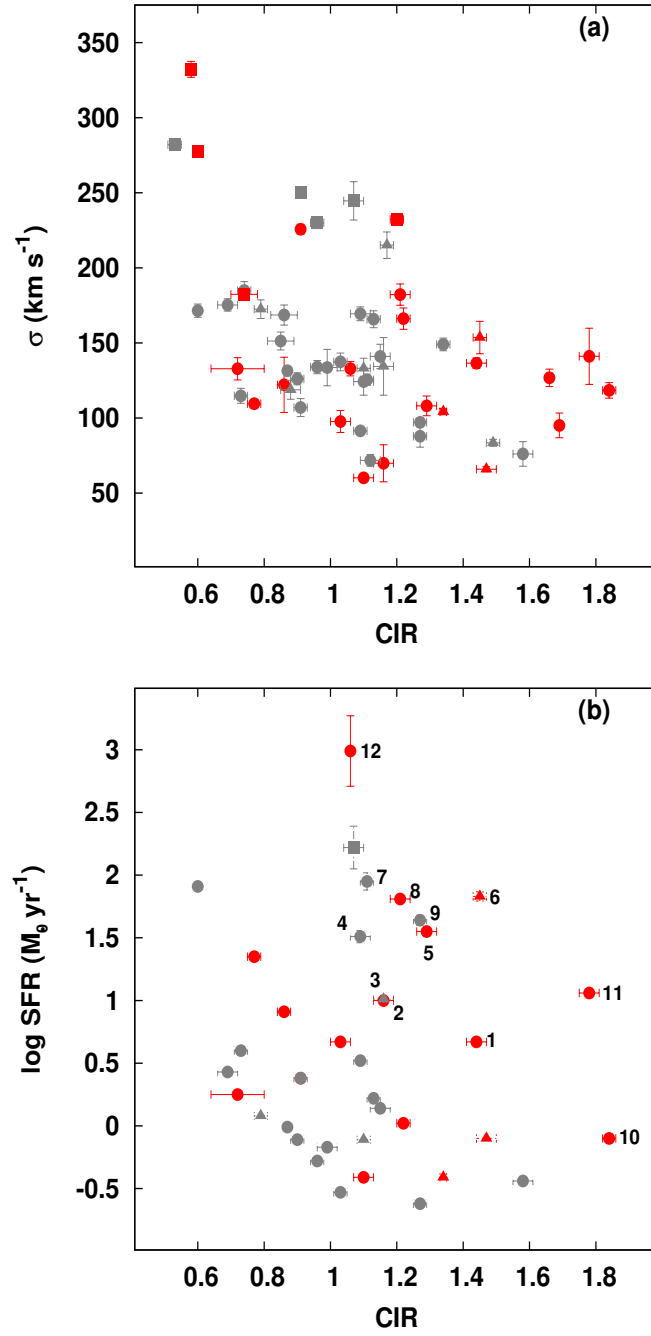
Figure 2.2: Variations between the central intensity ratio and (a) stellar velocity dispersion (σ) adopted from HyperLEDA database and (b) circumnuclear star formation rate. The symbols used to denote the galaxies are same as in Figure 2.1 .
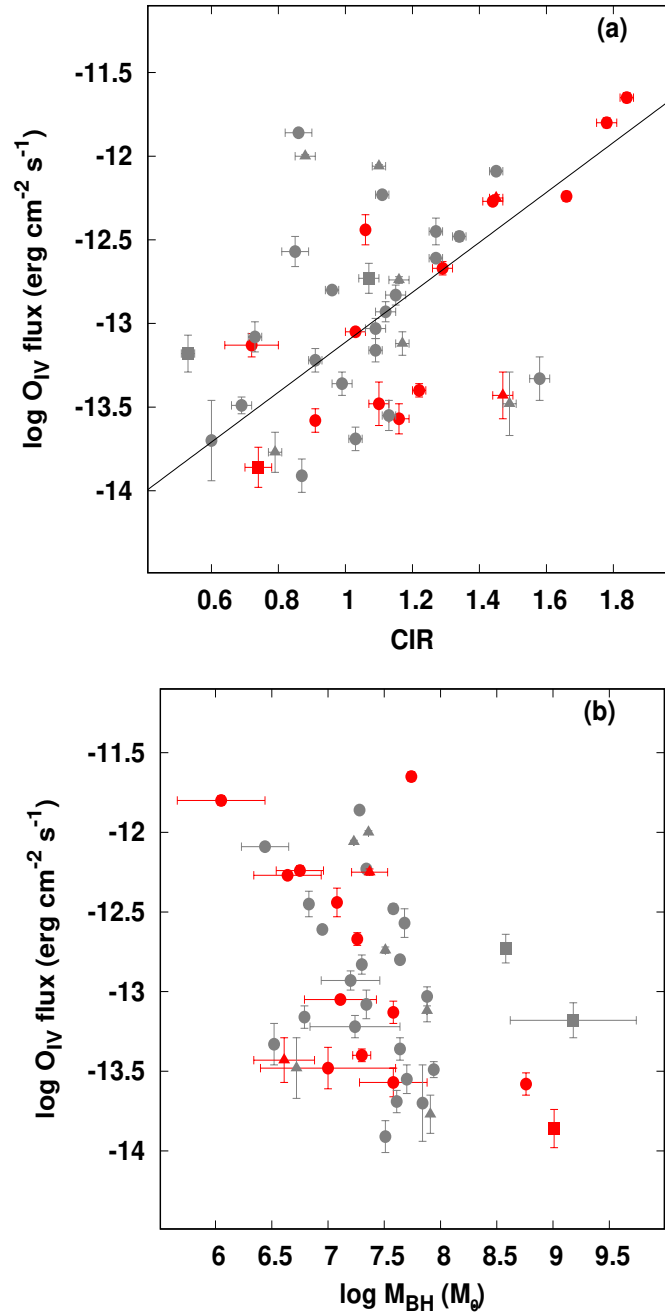
Figure 2.3: (a)Correlation between the central intensity ratio and OIV flux of AGN taken from (Diamond-Stanic et al., 2009) and (b) variation between M_{BH} and OIV flux of the sample galaxies. The symbols used to denote the galaxies are the same as in Figure 2.1

.
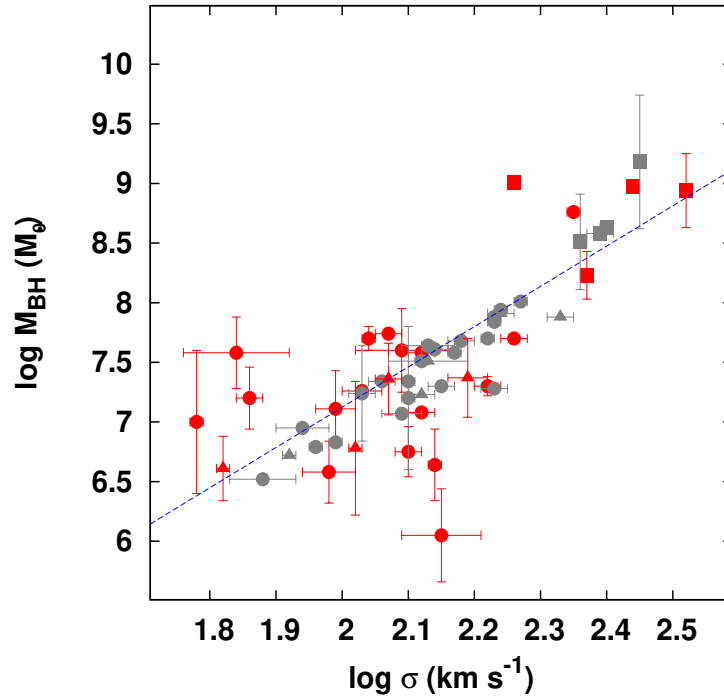
Figure 2.4: Variation between stellar velocity dispersion and mass of the SMBH of sample galaxies along with the best fit adopted from Caglar et al. (2020). The symbols used to denote the galaxies are the same as in Figure 2.1

et al., 2007). The interstellar gas supply will be consumed by this starburst activity over a period of time that is considerably shorter than the galaxy's lifetime. The galaxies IC3639, NGC2782, NGC5135, and NGC7582, numbered 7 to 10, with nuclear star burst activity (Boer et al., 1992; González Delgado et al., 2001; Muñoz Marín et al., 2007; Bianchi et al., 2007) are also apparent outliers in the figure. NGC1365 and NGC7469 are the galaxies showing intense nuclear SFR, with star-forming regions concentrated in hot spots around the nucleus (Ramos Almeida et al., 2009; Davies et al., 2007), which are shown in the figure by the numbers 11 and 12. By excluding these galaxies, we may see a negative trend in CIR and SFR. However, it is insufficient to confirm any connection between CIR and SFR, necessitating a thorough investigation with a larger sample size.

2.3.4   Correlation between the CIR and OIV flux

In Figure 2.3(a), we show the observed correlation between CIR and OIV flux of the host galaxy, which is taken from Diamond-Stanic et al. (2009). OIV emission is produced in the narrow line region (NLR) of an AGN, therefore it is unaffected by torus obscuration, and nuclear starburst activity of host galaxies does not contribute to this emission line significantly. So, OIV flux is considered to be an accurate measure of intrinsic AGN power (Meléndez et al., 2008; Rigby et al., 2009; Diamond-Stanic et al., 2009) and we find a positive correlation with CIR ($r = 0.70$ with $s > 99.99$ per cent).

OIV emission (25.9 μm) is a tracer of highly ionized gas of the order of 35-97 eV, and these types of mid-IR emission lines can be produced in the vicinity of hot stars in the central region of AGN host galaxies (Pottasch et al., 2001; Smith et al., 2004; Devost, 2007). AGN luminosity depends upon the fuel consumed by the SMBH at the nuclear region of the galaxy, and early-type galaxies have less fuel than late-type galaxies (Rieke, 2002). This suggests that AGN power is likely to decrease while SMBH grows in the host galaxy. However, NGC3081, NGC3185, NGC3281, NGC5273, and NGC7743 deviated from this correlation.

2.4   Discussion and conclusion

We report photometric analysis of Seyfert galaxies in the nearby Universe using the recently discovered parameter central intensity ratio. The CIR shows good correlations with many structural parameters of host galaxies, especially with the mass of the SMBHs residing at the centre of galaxies (Aswathy & Ravikumar, 2018, 2020). For Seyfert galaxies also, the CIR shows strong anti-correlation with the mass of SMBHs. However, the massive SMBHs hosted by ellipticals in the sample display a distinct trend from that displayed by lenticulars and spirals, in the sense that ellipticals host more massive SMBHs than that hosted by lenticulars and spirals. The disky systems (lenticular and spiral galaxies) are indistinguishable in this correlation. The morphological characteristics of spiral galaxies are similar to those of lenticular galaxies, except that lenticular galaxies are devoid of spiral structures. In light of the close analogies between lenticulars and spirals, it has been proposed that lenticulars

evolved from spirals through morphological transformation (Saha & Cortesi, 2018). Moreover, recent studies of bulge-disk decomposition on disk galaxies suggested that the structural properties of bulges of lenticular galaxies are similar to those in spiral galaxies and surface brightness of spiral bulges are same as that of lenticular bulges (Oohama et al., 2009; Laurikainen et al., 2010; Barway et al., 2016). It is possible that the more massive the central SMBH, the higher the suppression of star formation due to AGN feedback (Harrison, 2017). As a decrease in the light in the inner aperture reduces the value of CIR, we can expect the anti-correlation between CIR and the mass of SMBH.

AGN feedback is the process in which an AGN releases a large amount of energy to the surrounding gaseous medium of the host galaxies. The AGN feedback mechanism has a significant role in the evolution process of galaxies, in which the energy released by AGN to the surrounding galactic medium halts the cooling of gas in the central region of galaxies and also removes the gas in the form of massive outflows (Morganti, 2017). The AGN feedback process is considered a key factor of galaxy evolution and has been included in several simulations and analytical models for years (e.g., Kauffmann & Haehnelt, 2000; Di Matteo et al., 2005; Schaye et al., 2015; Sijacki et al., 2015). This feedback may suppress the star formation at the central part of the galaxy by preventing gas from cooling or by expelling gas from the central region of the galaxy and may decrease or stall completely the growth of the SMBH (e.g., Croton et al., 2006; Sijacki et al., 2007), thus setting up a co-evolution scenario for the galaxy and its SMBH (Aswathy & Ravikumar, 2018). Around 30 per cent of Seyfert galaxies are reported to possess outflow incidents (Crenshaw & Kraemer, 2007; Crenshaw et al., 2003, 2012). The pc scale AGN-driven outflows in the massive galaxies can expel the gas from the nuclear region, which may reduce the gas accretion towards the centre of the galaxy and leads to quenching of star formation at the central region (Morganti, 2017). This interesting phenomenon has been observed in optical, UV, and X-ray emissions and could be traced to such outflows using ionized gas and absorption lines (e.g., Veilleux et al., 2005; Bland-Hawthorn et al., 2007; Tadhunter, 2008; King & Pounds, 2015).

Different studies argued for the probability of AGN feedback by thermal process in the vicinity of the SMBH (e.g., Di Matteo et al., 2005; Springel et al., 2005; Johansson et al., 2009). Simulations of the AGN feedback mechanism suggest that

the Compton heating effect can raise the temperature of the gas at the nuclear region of about 10-35 pc, to $\sim 10^9$ K (e.g., Gan et al., 2014; Melioli & de Gouveia Dal Pino, 2015). This AGN heating may also reduce the star formation in the central region of the galaxy, thus the value of CIR.

Stellar velocity dispersion (σ) of the bulge component is strongly connected with the central SMBH (Ferrarese & Merritt, 2000; Gebhardt et al., 2000; Tremaine et al., 2002; Gültekin et al., 2009). Active galaxies are also obeying the $\sigma - M_{\rm BH}$ relation but with significant scatter (Caglar et al., 2020). It is also reported that the CIR of early-type galaxies is well correlated with the stellar velocity dispersion (Aswathy & Ravikumar, 2018). In the present study, however, Seyfert galaxies show a large scatter in the CIR $-\sigma$ relation, even though they exhibit a strong CIR $- M_{\rm BH}$ relation. The extreme AGN emission may lower the quality of stellar spectral lines. As a result, the measurement of stellar velocity dispersion in AGN host galaxies may become less accurate. (Riffel et al., 2013). Furthermore, stellar velocity dispersion measurements may be skewed due to the rotational effect of stellar disks (Woo et al., 2015). In order to explain further this, we have plotted the variation of $M_{\rm BH}$ with σ in Figure 2.4. The velocity dispersion measurements for galaxies with the dynamical estimation of the mass of SMBH available, shown in red, clearly display a larger scatter than that of galaxies without dynamical estimation of $M_{\rm BH}$ (gray points). For the $\sigma - M_{\rm BH}$ correlation in the combined sample of spirals and lenticulars, we obtained a linear correlation coefficient of $r = 0.65$ with significance, $s > 99.99$ per cent. At the same time, the correlation coefficient of CIR - $M_{\rm BH}$ (for spirals + lenticulars) relation is, $r = -0.74$ with significance, $s > 99.99$ per cent. The scatter of the correlations $\sigma - M_{\rm BH}$ and CIR $- M_{\rm BH}$ are 2.63 and 2.04 dex respectively, further establishing that the CIR is, in fact, a better tracer of the $M_{\rm BH}$ than the central velocity dispersion.

The observed correlation between CIR and OIV flux, shown in Figure 2.3(a), also displays the possibility of larger uncertainties present in measurement of emission lines in galaxies associated with AGN (e.g., Lutz et al., 2003; Armus et al., 2006, 2007; Veilleux et al., 2009; Diamond-Stanic et al., 2009). In this case also, the correlation coefficient increases to 0.76 with a significance, $s = 99.38$ per cent if we consider galaxies with dynamically estimated SMBH masses, but it drops to 0.62 ($s = 99.74$ per cent) when these data points are excluded. Seyfert galaxies with

high OIV flux emission possess enhanced nuclear star formation (Diamond-Stanic & Rieke, 2012), and an increase in CIR is expected in galaxies with increased OIV emission. However, the OIV flux of the sample galaxies shows only a very weak anti-correlation ($r = -0.58$ with $s = 99.95$ per cent) with the mass of SMBH shown in Figure 2.3(b), possibly due to the increased uncertainties involved in both the quantities.

Generally, Seyfert galaxies can be observed and located through the UV emission coming out from the sources (Rieke, 2002). Apart from age and morphological classification, the common feature of Seyfert galaxies is their intense star formation (Cid Fernandes et al., 2004; Sarzi et al., 2007; Davies et al., 2007; Kauffmann & Heckman, 2009). The process of star formation that takes place in hot spots like rings or spirals within the nuclear region (1-2 kpc) of galaxies is referred to as circumnuclear star formation (Storchi-Bergmann et al., 1996; Allard et al., 2006). We explore the variation of the estimated circumnuclear SFR by the excess UV with CIR, as shown in Figure 2.2(b). We notice that the galaxies harbouring central structures such as pc scale nuclear dust spiral, nuclear starburst, and the galaxies possessing high SFR are showing large deviations in the observed CIR−SFR relation. The measure of nuclear SFR has been shown to increase from the central region to the outskirts of galaxies (Diamond-Stanic & Rieke, 2012; Esquej et al., 2014). The outflow from the central part of a galaxy due to the AGN feedback mechanism can interact with the interstellar medium (ISM) effectively (Ostriker et al., 2010; Weinberger et al., 2017; Yuan et al., 2018). The feedback-driven outflow of gas enhances the star formation at larger radii from the core of the galaxy (Ishibashi et al., 2013; Ishibashi & Fabian, 2014). This outflow of gas can be responsible for enhancing the circumnuclear star formation rate. All these can affect measurements of both star formation rate and CIR, rendering a weak correlation between the two.

We employed CIR, to explore the presence of central features in Seyfert galaxies and their role in galaxy evolution. The analysis shows that CIR measured for Seyfert galaxies predicts the mass of central SMBHs even better than the estimates obtained by spectroscopic parameters like the central velocity dispersion. Being a photometric tool, this promises a cheap and fast technique to explore large galaxy samples, which has great potential in observations of new generation facilities like the James Webb Space Telescope.

Chapter 3

Connections between Central Intensity Ratio and hot gas properties of early-type galaxies

3.1 Introduction

The evolution scenario of galaxies is believed to be migrated from blue to red sequence via the quenching of star-formation. But, the driving mechanism behind this migration process is still unclear. Early-type galaxies (ETGs) possess a vast amount of hot gas at their interstellar medium (ISM) during this migration process, and this hot, diffuse gas is one of the prime sources of X-ray emission from early-type galaxies (O'Sullivan et al., 2003; Fabbiano, 2006). Most ETGs are known to be strong X-ray emitters. The contribution from various sources (like hot gas, active galactic nuclei (AGNs), supermassive black hole (SMBH) and X-ray binaries) to this X-ray emission of ETGs has been a hot topic (Kim & Fabbiano, 2003; Pellegrini, 2010; Boroson et al., 2011).

Hot gas that has been entrapped in the ISM of ETGs by the galaxy's gravitational potential is considered responsible for the X-ray emission (Canizares, 1999; Goulding et al., 2016). One of the most fundamental X-ray properties is the gas temperature (T_{GAS}), which is also a measure of the gravitational potential. Older galaxies contain vast amounts of hot diffuse gas the temperature of which is pro-

portional to its emission in X-rays (Kim & Fabbiano, 2015; Goulding et al., 2016; Gaspari et al., 2019). The studies using X-ray scaling relations on the role of hot ISM in the evolution scenario of ETGs suggested that the total galaxy mass is the regulating factor of the amount of hot gas (Mathews & Brighenti, 2003; Boroson et al., 2011; Kim & Fabbiano, 2013; Civano et al., 2014). Numerical simulations also used to reproduce the X-ray scaling relations and verified that X-ray gas luminosity ($L_{\mathrm{X,GAS}}$), and temperature of the hot gas are proportional to the galactic mass (Negri et al., 2014; Choi et al., 2015).

The mass of the central black hole, M_{BH}, of ETGs is well correlated with the X-ray gas luminosity and gas temperature of the host galaxy. In ETGs stars are moving with large velocities and the gas ejected from one star will collide with the gas expelled from other stars at a very high velocity, increasing the temperature of the interstellar gas. The hot gas is typically at a temperature of $T \sim 10^7$ K (Sarazin, 1997). Since ETGs possess large amounts of hot, diffuse interstellar gas, X-rays are produced by the thermal emission from this gas. Two of the most fundamental properties of the thermal ISM that emits X-rays are the gas temperature and the luminosity of the X-ray emission (Goulding et al., 2016; Gaspari et al., 2019). No optical variable, including stellar velocity dispersion (σ), appears to have stronger correlations than the X-ray gas luminosity when considering intrinsic scatter and correlation coefficient (Gaspari et al., 2019). The strong correlations $M_{\mathrm{BH}} - T_{\mathrm{GAS}}$ and $M_{\mathrm{BH}} - L_{\mathrm{X,GAS}}$ imply that X-ray properties are more fundamental than optical properties (Gaspari & Sadowski, 2017; Gaspari et al., 2019). Furthermore, the evolution of massive ETGs studied using a variety of scaling relations based on X-ray luminosity with K-band magnitude (M_{K}) reveals massive galaxies possess more stellar mass than the less massive systems (Su et al., 2015; Kim & Fabbiano, 2015; Goulding et al., 2016; Truong et al., 2020). The stellar mass loss in this systems may be the reason for the abundance of gas in the ISM, and $L_{\mathrm{X,GAS}} - \mathrm{Age}$ relation (Boroson et al., 2011) suggests that old galaxies are massive and harbour large amount of hot gas in their ISM.

ETGs have been classified into two categories: core and coreless galaxies, based on the nature of their central surface brightness profile (Kim & Fabbiano, 2015). The surface brightness profiles of the galaxies were fitted using the Nuker law in order to investigate the core region, and the slope of the profile (γ) was determined.

Core galaxies are classified to have a slope of $\gamma \leq 0.3$, while coreless galaxies are classified to have a slope of $\gamma > 0.3$ (Krajnović et al., 2013). Core galaxies are considered to evolve via 'dry mergers' with reducing star formation, while the coreless galaxies could be the outcome of gas-rich 'wet mergers' with ensuing star formation. The dry/wet merging scenario differentiates the formation mechanisms of core and coreless galaxies. Based on these merging events, different studies suggested that coreless galaxies are formed by the mergers of subsystems having large amounts of gas, commonly referred to as wet mergers. On the other hand, the formation of core galaxies is a process known as dry mergers, which involves the merger of systems with little or no gas. (Kormendy et al., 2009; Lauer, 2012; Gabor & Davé, 2015; Kim & Fabbiano, 2015). The hot gas that produces X-rays is more concentrated in core galaxies (Pellegrini, 2005; Kormendy et al., 2009; Lauer, 2012; Sarzi et al., 2013), also, they have large L_K with no evidence of recent star formation (Kormendy et al., 2009; Lauer, 2012). The galaxy properties of coreless galaxies are the exact reverse of those of core galaxies. While certain core galaxies may have low concentrations of hot gas, all coreless galaxies are hot gas poor (Pellegrini, 1999; Kim & Fabbiano, 2015).

The central intensity ratio, CIR, found to have strong correlations with features of ETGs (e.g. M_{BH}, σ, M_{bulge}, and M_{gal}; Aswathy & Ravikumar, 2018). Additionally, CIR provides important insights into the central star formation of host galaxies and exhibits substantial correlations with the structural parameters of late-type galaxies (Aswathy & Ravikumar, 2020). The outshining of spectral lines due to AGN activity does not seem to affect the estimation of CIR significantly and their use to determine the SMBH masses in Seyfert galaxies (Vinod et al., 2023). In this context, we investigate the connection between the CIR and hot gas properties of ETGs in the nearby Universe.

3.2 The sample and observations

The study involves analysis of a representative sample of nearby (D < 30 Mpc) ETGs. The sample consists of all ETGs with measurements of X-ray luminosity from hot gas ($L_{X,GAS}$) and Hubble Space Telescope (HST) observation using the filter F814W of Wide Field Planetary Camera 2 (WFPC2). The sample consists of

27 ellipticals and 9 lenticulars. In addition, we have included the Sombrero galaxy (NGC4594) which was classified earlier as spiral but later reported to have dual morphology (see, Gadotti & Sánchez-Janssen, 2012). We included this galaxy in our analysis as it is indistinguishable in all correlations exhibited by ellipticals in our sample. Further, we have avoided the completely edge-on lenticular galaxy NGC5866, with dust lanes along the major axis of its image, as the uncertainty in its CIR value could be high. Thus the final sample consists of 36 galaxies and are listed in Table 4.1.

3.2.1   The Central Intensity Ratio

Following Aswathy & Ravikumar (2018), we computed the CIR for sample galaxies using the aperture photometry tool MAG_APER provided in the Source Extractor (SExtractor, Bertin & Arnouts, 1996).

$$\text{CIR} = \frac{\text{I}_1}{\text{I}_2 - \text{I}_1} = \frac{10^{0.4(\text{m}_2 - \text{m}_1)}}{1 - 10^{0.4(\text{m}_2 - \text{m}_1)}} \tag{3.1}$$

where I_1 and I_2 are the intensities and m_1 and m_2 are the corresponding magnitudes of the light within the inner ($\text{r}_1 = 1.5$ arcsecs) and outer ($\text{r}_2 = 3$ arcsecs) apertures, respectively. The simple definition of CIR makes it independent of the central intensity, I(0), for galaxies with surface brightness at a radial distance r, I(r) = I(0)f(r), where f(r) is a function of r. Secondly, the definition boosts any addition to (or subtraction from) the central intensity I(0). Thirdly, CIR, being a ratio involving only surface brightness, shows remarkable stability over a range of radii (with $r_2 = 2r_1$) despite variations in distance and orientation of the systems, which can be validated using simple Monte Carlo simulations (Aswathy & Ravikumar, 2018, 2020).

Table 3.1: Properties of early-type galaxies. Name of the galaxy (column 1), Distance (2), Stellar mass (3), Morphology (4), CIR (5), uncertainty of CIR (6), X-ray gas luminosity in $0.3 - 8$ keV band from Forbes et al. (2017a) [except † = Lakhchaura et al. (2019)], $*$ = Goulding et al. (2016)] (7), Gas temperature from Kim & Fabbiano (2015) [except † = Lakhchaura et al. (2019)] (8), Age of the central stellar population from Alabi et al. (2017) [except a = Kim & Fabbiano (2015), b = Forbes et al. (2017c), c = Yamada et al. (2006), d = Barr et al. (2007)] (9), K-band magnitude from Cappellari et al. (2011) [except e = derived from the apparent magnitude K_T (2MASS keyword k_m_ext) using the method adopted by Cappellari et al. (2011) (10), Central light profile: $\cap$ = core, $\wedge$ = coreless from Krajnović et al. (2013) and Pellegrini (1999) (11).

Galaxy	Distance (Mpc)	$\log M_*$ ($M_\odot$)	Morphology	CIR	ΔCIR	$\log L_{\rm X,GAS}$ (erg s^{-1})	$T_{\rm GAS}$ (keV)	Age (Gyr)	$M_{\rm K}$ (mag)	Profile
(1)	(2)	(3)	(4)	(5)	(6)	(7)	(8)	(9)	(10)	(11)
NGC 0524	23.3	10.66	S0	0.82	0.03	40.04†	0.50	12.2[a]	-24.71	$\cap$
NGC 0821	23.4	11.00	E	1.23	0.06	38.40	0.09	11.0	-23.99	$\wedge$
NGC 1023	11.1	10.99	S0	1.03	0.02	38.79	0.30	12.3	-24.01	$\wedge$
NGC 1316	20.8	11.55	S0	1.11	0.01	40.70	-	4.7	-26.00[e]	$\cap$
NGC 1332	21.5	10.67	E	0.88	0.02	39.90†	0.62†	-	-24.61[e]	$\cap$
NGC 1374	18.1	10.52	E	1.27	0.03	38.60†	0.86†	-	-23.10[e]	-
NGC 1399	21.2	11.50	E	0.58	0.01	41.73	1.01†	11.0	-25.31[e]	$\cap$
NGC 1400	26.8	11.08	E/S0	1.08	0.02	39.67	-	9.57[d]	-24.31[e]	$\wedge$
NGC 2768	21.8	11.21	E/S0	1.01	0.02	39.88	0.31	12.3	-24.71	$\wedge$
NGC 2974	20.9	10.93	E	1.20	0.04	39.30	-	9.3	-23.62	$\wedge$

Table 3.1 continued.

Galaxy	Distance	$\log M_*$	Morphology	CIR	ΔCIR	$\log L_{\mathrm{X,GAS}}$	T_{GAS}	Age	M_{K}	Profile
	(Mpc)	$(M_\odot)$				(erg s^{-1})	(keV)	(Gyr)	(mag)	
(1)	(2)	(3)	(4)	(5)	(6)	(7)	(8)	(9)	(10)	(11)
NGC 3115	9.4	10.93	S0	0.82	0.01	40.40	-	9.0	-23.99^e	$<$
NGC 3377	10.9	10.50	E	1.41	0.04	38.00	0.19	7.0	-22.76	$<$
NGC 3585	17.3	10.71	E	0.97	0.02	39.36†	0.31†	-	-24.50^e	-
NGC 3607	22.2	11.39	S0	0.67	0.02	40.20	0.59	10.3	-24.74	$\cap$
NGC 3608	22.3	11.03	E	1.21	0.06	39.62	0.40	9.9	-23.65	$\cap$
NGC 4261	29.4	11.46	E	0.69	0.02	40.82*	0.76	16.3^a	-25.18	$\cap$
NGC 4278	15.6	10.95	E	0.89	0.03	39.39	0.30	11.8	-23.80	$\cap$
NGC 4365	23.3	11.51	E	0.69	0.02	39.66	0.46	13.4	-25.21	$\cap$
NGC 4374	18.5	11.51	E	0.60	0.01	40.82	0.73	13.7^b	-25.12	$\cap$
NGC 4382	17.9	10.90	S0-a	0.92	0.02	39.80*	0.39	1.6^a	-25.13	$\cap$
NGC 4406	16.8	11.60	E	0.85	0.02	41.01*	0.82	-	-25.04	$\cap$
NGC 4459	16.1	10.98	S0	1.26	0.04	39.39	0.40	7.0	-23.89	$<$
NGC 4472	17.1	11.78	E	0.53	0.02	41.36	0.95	10.5^c	-25.78	$\cap$
NGC 4473	15.3	10.96	E	0.86	0.01	39.09	0.31	13.1	-23.77	$\cap$
NGC 4486	17.2	11.62	E	0.53	0.02	42.93	1.50	12.7^b	-25.38	$\cap$
NGC 4494	16.6	11.02	E	1.14	0.03	39.11	0.34	8.0	-24.11	$<$

Table 3.1 continued.

Galaxy	Distance	log M_*	Morphology	CIR	ΔCIR	log $L_{X,GAS}$	T_{GAS}	Age	M_K	Profile
	(Mpc)	($M_\odot$)				(erg s^{-1})	(keV)	(Gyr)	(mag)	
(1)	(2)	(3)	(4)	(5)	(6)	(7)	(8)	(9)	(10)	(11)
NGC 4526	16.4	11.26	S0	0.98	0.03	39.45	0.31	11.0	-24.62	-
NGC 4552	15.8	10.87	E	0.91	0.02	40.30†	0.59	12.4^a	-24.29	$\cap$
NGC 4594	9.77	11.41	Sa	0.91	0.01	39.32	-	12.5^b	-24.99^e	$\cap$
NGC 4621	14.9	10.92	E	1.24	0.02	38.48†	0.27	10.6^c	-24.14	$<$
NGC 4636	14.3	11.17	E	0.57	0.02	41.50	0.73	13.4	-24.36	$\cap$
NGC 4649	17.3	11.60	E/S0	0.50	0.01	41.22	0.86	13.2^b	-25.46	$\cap$
NGC 5128	5.8	10.94	E/S0	0.48	0.03	40.20	-	-	-24.89^e	-
NGC 5576	24.8	11.04	E	1.13	0.05	38.95†	0.52	2.5^a	-24.15	$<$
NGC 5846	24.2	11.46	E/S0	0.66	0.02	41.70	0.72	12.7^b	-25.01	$\cap$
NGC 7457	12.9	10.13	S0	1.20	0.07	38.08	0.30	3.8	-22.38	$<$

3.3 Results

The estimated CIR of ETGs is well correlated with the properties of hot diffuse gas in the host galaxy. The scaling relations obtained between CIR and gas properties of galaxies shed light on the influence of hot gas in the evolution scenario of ETGs. The estimated CIR values and other properties of sample galaxies are listed in Table 4.1. As seen in Table 4.1 different parameters of galaxies are assembled from various authors. Estimations of X-ray luminosity from hot gas in the 0.3 - 8 keV band were taken in the preferred order from Forbes et al. (2017a), Lakhchaura et al. (2019), and Goulding et al. (2016). The temperature of the hot gas content was compiled from Kim & Fabbiano (2015) and Lakhchaura et al. (2019). K-band magnitude of the galaxies determined using 2MASS observations were taken from Cappellari et al. (2011) and we derived K-band magnitude for the sources which were not included by Cappellari et al. (2011). Core or coreless characterisation of the central light profile of the sample galaxies was taken from Krajnović et al. (2013) and Pellegrini (1999).

3.3.1   Correlation between the CIR and $L_{\mathrm{X,GAS}}$

We find a strong correlation between the CIR and X-ray gas luminosity of early-type galaxies. The observed correlation between CIR and $L_{\mathrm{X,GAS}}$ is shown in Fig. 3.2a. The linear correlation coefficient of this correlation is, $r = -0.79$ with a significance, $s > 99.99$ per cent (Press et al., 1992). Table 4.2 lists the linear correlation coefficients computed for the correlations with the best fitting parameters. ETGs follow a universal scaling relation such as $L_{\mathrm{X,GAS}} \propto T_{\mathrm{GAS}}$ (O'Sullivan et al., 2003; Boroson et al., 2011; Goulding et al., 2016). The observed negative correlation between CIR and $L_{\mathrm{X,GAS}}$ substantiates the latter relation so that the optical light is suppressed when X-ray luminosity is greater. Due to the high temperature of diffuse gas, the star formation might be quenched in the host galaxy, and this quenching of star formation may reduce the value of optical CIR.

The galaxy NGC4486 is an outlier in Fig. 3.2a. It is a massive elliptical galaxy that emits a synchrotron jet from its non-thermal core. The jet morphology of NGC4486 has been reported to be present at several wavelengths ranging from
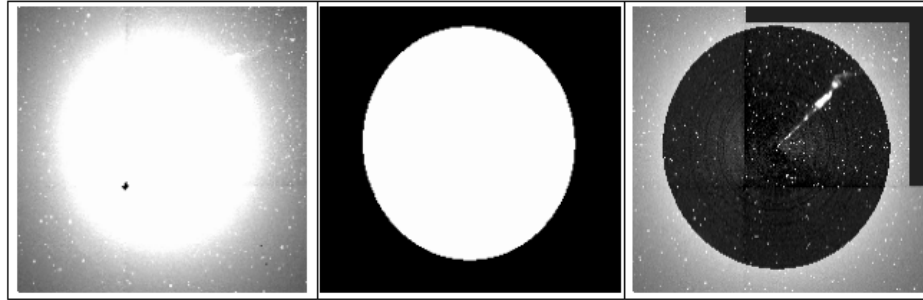
Figure 3.1: From left to right, galaxy image of NGC4486, the model of the galaxy obtained using *IRAF* and the residual image obtained after subtracting the model from galaxy image.

radio to X-ray (e.g., Marshall et al., 2002; Xilouris et al., 2004; Ferrarese et al., 2006). We also verified the jet morphology of NGC4486 with the help of *IRAF* task '*ellipse*'. The '*ellipse*' task returns a smooth image of the family of ellipses called the 2D model of the galaxy image. The residual image is obtained by subtracting this model image from the original image of the galaxy. We identified the jet feature of the galaxy NGC4486, by examining the residual image (see Fig. 3.1). The jet phenomenon emerging from the core of this galaxy can expel hot gas from the central region. The feedback mechanism from the central region of galaxies may suppress star formation and decrease the CIR value. The jet is, in fact, the major contributor to X-ray emission from the nucleus (Wilson & Yang, 2002). The nucleus and jet knots of NGC4486 have remarkably similar spectra, and the X-ray emission of the knots near the nucleus is very high (Yuan et al., 2009). So the synchrotron jet emission from the nucleus of NGC4486 might even contribute significantly to and boost the X-ray gas luminosity as well.

We identified that there is a distinction between core and coreless galaxies in the $CIR - L_{X,GAS}$ relation, with the core galaxies having larger $L_{X,GAS}$ and lower CIR values, while coreless galaxies exhibit the reverse (see Fig. 3.2a). The core galaxies are believed to be formed through dry mergers with suppressed star formation, while wet mergers coupled with enhanced star formation result in coreless galaxies (Kim & Fabbiano, 2015). So, the $CIR - L_{X,GAS}$ relation suggests that the star formation

process might have been quenched due to the lack of cold gas in core galaxies.

3.3.2   Correlation between the CIR and T_{GAS}

We observed a strong correlation between the CIR and temperature of the diffused gas inside the galaxy (within R_e) with a correlation coefficient, $r = -0.78$ and significance of $s > 99.99$ per cent (Fig. 3.2b). The connection between CIR and T_{GAS} is apparent, as the latter has a strong relationship with X-ray gas luminosity. It is commonly known that X-ray luminosity and gas temperature are positively correlated in massive galaxies (O'Sullivan et al., 2003; Mathews & Brighenti, 2003; Boroson et al., 2011; Negri et al., 2014). Our analysis further supported this argument, as we observed that the CIR is low when the gas temperature is high. The high temperature prevents star formation and lowers optical emission in the core areas of host galaxies.

At the same time, two galaxies, NGC4486 and NGC1374, deviated from the best fit CIR $- T_{\mathrm{GAS}}$ correlation. NGC4486 is also an outlier in the CIR $- L_{\mathrm{X,GAS}}$ relationship, with the peculiarities and reasons for their deviation from the fit described previously (see section 3.3.1). In addition, because it produces a large amount of X-rays, the NGC4486 has a high gas temperature (Kim & Fabbiano, 2015; Lakhchaura et al., 2019) at its core. The high temperature reduces the optical emission, lowering the CIR value. Simulations indicate that for gas-poor ETGs ($L_{\mathrm{X,GAS}} < 10^{40}\mathrm{erg\,s^{-1}}$), the outflow/wind condition of hot ISM results in higher T_{GAS} and lower $L_{\mathrm{X,GAS}}$ (Kim & Fabbiano, 2015). The $L_{\mathrm{X,GAS}}$ of NGC1374 is $< 10^{40}\mathrm{erg\,s^{-1}}$ and this galaxy may be a gas-poor ETG.

3.3.3   Correlation between the CIR and Age

The CIR of ETGs is correlated significantly ($r = -0.66$, $s > 99.99$ per cent) with the age of the central stellar population (Fig. 3.3a). X-ray gas luminosity of ETGs is positively correlated with their age, and the $L_{\mathrm{X,GAS}}$ reduction might be related to the recent star formation of the host galaxy induced by the merger events (Boroson et al., 2011). ETGs with a higher mass are older and have a lower CIR value (Aswathy & Ravikumar, 2018). Our observations also corroborated these claims, as CIR shows a lower value when $L_{\mathrm{X,GAS}}$ is higher. The CIR $-$ Age correlation
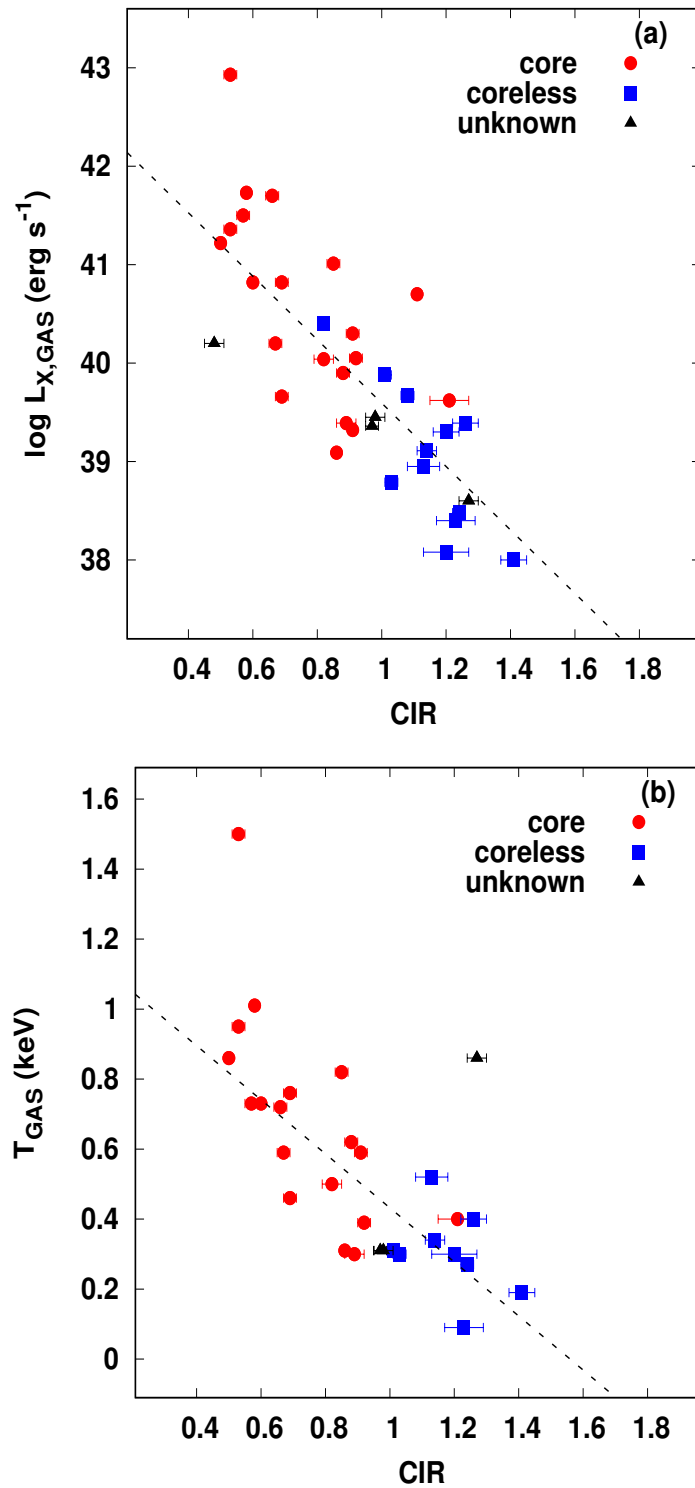
Figure 3.2: Correlation between the central intensity ratio and (a) X-ray gas luminosity ($L_{\mathrm{X,GAS}}$) and (b) Gas temperature (T_{GAS}) of the sample galaxies.
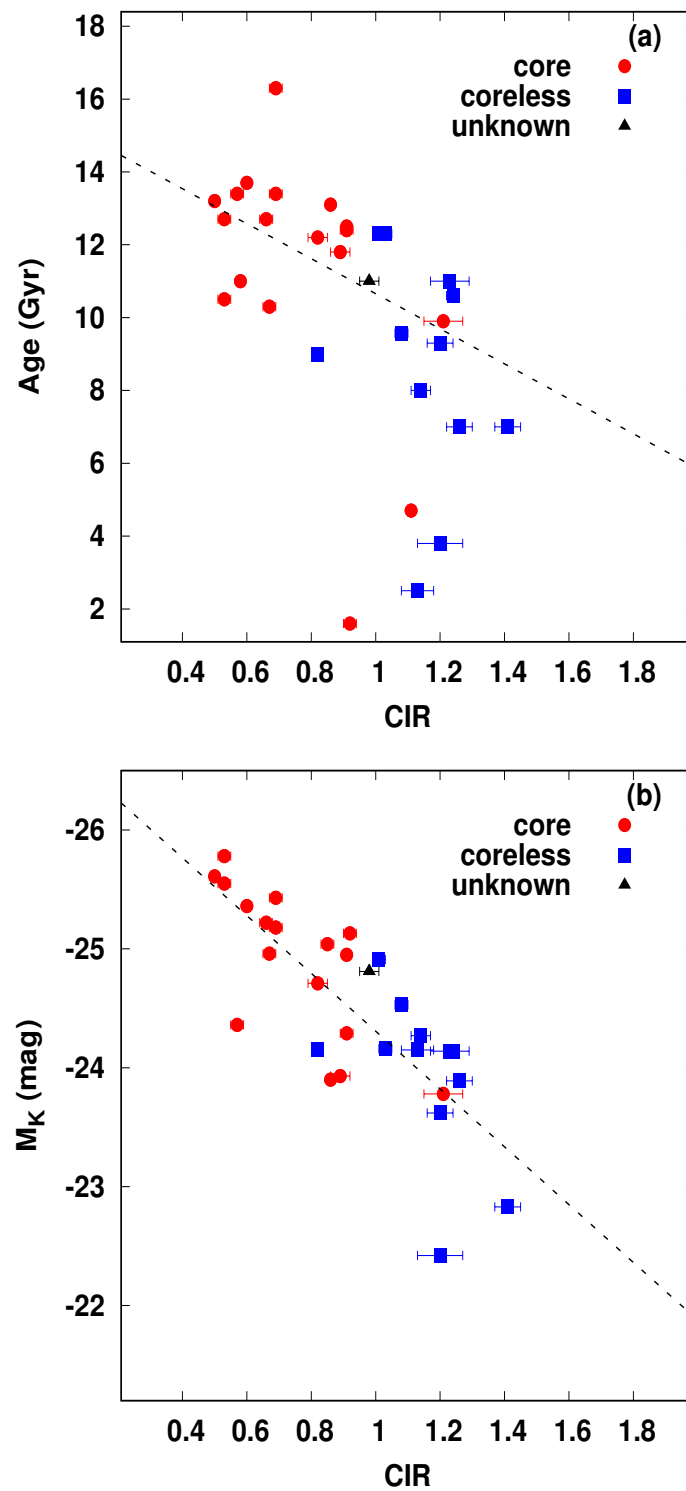
Figure 3.3: Correlation between the central intensity ratio and (a) Age of the central stellar population and (b) K-band magnitude (M_K) of the sample galaxies.

Table 3.2: The table lists the best-fitting parameters for the relation $x = \alpha \, \text{CIR} + \beta$ and linear correlation coefficient (r) for various relations. n denotes the number of galaxies.

x	α	β	r	s	n
$\log L_{\text{X,GAS}}$	-3.22±0.41	42.81±0.39	-0.79	> 99.99%	35
$\log T_{\text{GAS}}$	-0.77±0.11	1.20±0.10	-0.78	> 99.99%	28
Age	-4.81±1.09	15.46±1.02	-0.66	99.99%	26
M_{K}	2.34±0.31	-26.54±0.29	0.79	> 99.99%	35

thus implies that older ETGs have large amount of hot gas in their ISM and X-ray emission. Since the age of the ETGs is found to be positively correlated with $L_{\text{X,GAS}}$ (Boroson et al., 2011), the CIR − Age correlation suggests that older ETGs contain significant amounts of hot diffuse gas in their ISM.

Optical light mainly comes from the stellar components of a host galaxy. Stellar populations in ETGs are highly concentrated in the central regions of host galaxies. Since ETGs are evolved systems, they possess old stellar populations (age $\geq$ 5 Gyr) and relatively little star formation activity (Lacerna et al., 2020; Yoon et al., 2023). It is believed that the stellar mass loss resulting from the evolution process is the main source of hot gas in the core region of ETGs (Sarzi et al., 2013). This hot gas prevents star formation and/or suppresses the optical emission from the central region of ETGs. All stellar evolution models suggest that more massive galaxies tend to contain older stars more (Raichoor et al., 2011) and the age of the central stellar population of ETGs and their optical emission depends on the thermal effect of ISM of host galaxies. We observed that CIR appears to decrease as age increases, suggesting the suppression of optical emission at the central region of ETGs. Additionally, we noticed that the galaxies with ages less than 6 Gyr are deviating from the observed CIR − Age correlation.

3.3.4   Correlation between the CIR and $M_{\rm K}$

K-band absolute magnitude ($M_{\rm K}$) is treated as one of the proxies for stellar-mass since it strongly correlates with the stellar mass of galaxies (Cappellari et al., 2011; Ma et al., 2014). We find that the K-band magnitude of the galaxies is well correlated with their CIR (Fig. 3.3b). The correlation coefficient of CIR $-$ $M_{\rm K}$ relation is, $r = 0.79$ with a significance, $s > 99.99$ per cent. In both observational and simulated investigations, the $L_{\rm X,GAS}$ and $T_{\rm GAS}$ of nearby ETGs show strong correlations with $M_{\rm K}$. These correlations further imply that more massive ETGs ($M_{\rm K} < -24$) possess more hot gas than less massive galaxies. It is possible to explain the simulated and observed X-ray properties of ETGs as a linear function of $M_{\rm K}$ (Truong et al., 2020). The CIR $-$ $M_{\rm K}$ relation clearly shows that the massive ETGs have a large amount of stellar mass since they possess a high value of $M_{\rm K}$. Lower CIR values are found in older and more massive ETGs, indicating that star formation in the host galaxies has been quenched. However, the galaxy NGC1316 is an outlier in the observed CIR $-$ $M_{\rm K}$ correlation.

3.4   Discussion and conclusion

The central region of galaxies plays a major role in their evolution mechanism. ETGs have a thermal ISM that produces X-ray gas luminosity and temperature, which are perhaps the essential measurables in such systems and follow a universal scaling relation of $L_{\rm X,GAS} \propto T_{\rm GAS}$, enhancing understanding of the connection between gas temperature and galaxy potential (Goulding et al., 2016). In the study of groups and clusters of galaxies, the $L_{\rm X,GAS} - T_{\rm GAS}$ relationship has been widely used to perceive the evolution of host galaxies (O'Sullivan et al., 2003). In ETGs, a single power-law relationship between $L_{\rm X,GAS}$ and $T_{\rm GAS}$ explains the hot gas distribution within the core region of the host galaxies, where the gas temperature governs the observed X-ray gas luminosity.

For the first time, we identify significant correlations between CIR and X-ray properties of ETGs like, $L_{\rm X,GAS}$, and $T_{\rm GAS}$ (Figures 3.2a and 3.2b). The thermalization of the energy from stellar mass loss material caused by evolved stars often produces the X-ray luminosity in ETGs (Goulding et al., 2016). Optical CIR car-

ries information about the star formation in the central region of ETGs, and older galaxies possess lower CIR values (Aswathy & Ravikumar, 2018). The decrease in CIR indicates that star formation is much less near the centre of galaxies than in the outskirts. The hot diffuse gas in the ISM of ETGs may drive the stellar population and regulate the optical emission from the central region of the galaxies. Moreover, the flux ratio X-ray/optical seems to decrease systematically from the nuclear region (Marshall et al., 2002) of host galaxies. The amount of hot diffuse gas in older galaxies is higher (Boroson et al., 2011), and this hot environment may prevent star formation in the central region, lowering the CIR value.

The hot diffuse gas confined in the potential well of ETGs is believed to be emitted X-rays (Canizares, 1999) and core elliptical galaxies possess a greater abundance of hot gas (Kim & Fabbiano, 2015). It is quite natural that the gas temperature correlates well with the CIR since the latter shows a strong connection with $L_{\mathrm{X,GAS}}$ (Boroson et al., 2011; Kim & Fabbiano, 2015; Goulding et al., 2016). The common outlier in the CIR $-$ $L_{\mathrm{X,GAS}}$ and CIR $-$ T_{GAS} relations is NGC4486. NGC4486 possesses a high gas temperature (Lakhchaura et al., 2019) at its core, generates a vast amount of X-ray emission, and this extreme temperature can reduce the star formation and/or suppress the optical emission in the central region of the galaxy. Also, the synchrotron jet emanates from the nuclear region (Wilson & Yang, 2002; Yuan et al., 2009) might enhance the X-ray emission of this galaxy. NGC1374 is the second and remarkable outlier in the CIR $-$ T_{GAS} relation with a high temperature and low X-ray emission ($L_{\mathrm{X,GAS}} < 10^{40}\mathrm{erg\,s}^{-1}$) similar to gas-poor ETGs. The outflow process in the hot ISM of gas-poor ETGs causes T_{GAS} to rise and $L_{\mathrm{X,GAS}}$ to fall (Kim & Fabbiano, 2015) raises the possibility that NGC1374 may belong to gas-poor systems. In this view, the CIR $-$ T_{GAS} relation reveals the dependence of temperature on the star formation of ETGs.

The age of the central stellar population in the sample galaxies exhibits an anti-correlation with the CIR. According to an intriguing relationship between the $L_{\mathrm{X,GAS}}$ of ETGs and their age observed by Boroson et al. (2011), younger galaxies appear to have less hot gas than older galaxies. Similarly, the CIR $-$ Age correlation suggests that the older systems possess vast amounts of hot gas and produce extreme X-ray emissions. A further observation we made was that the CIR of the ETGs exhibits an anti-correlation with the absolute K-band magnitude, an often used surrogate for

the stellar mass (e.g. Cappellari et al., 2011; Ma et al., 2014; Truong et al., 2020) of the host galaxies. In more massive galaxies, the intense K-band luminosity may be triggered by the stellar mass (Kormendy & Ho, 2013a). We inferred from the $CIR - M_K$ relation that massive galaxies have large stellar masses but have weak optical emission from their centres. Observational studies (Kim & Fabbiano, 2015; Goulding et al., 2016) and simulations (Truong et al., 2020) have further highlighted the relationship between the measurables $L_{X,GAS}$, T_{GAS}, and M_K of ETGs since M_K displays a positive correlation with $L_{X,GAS}$ and T_{GAS}.

In contrast to coreless galaxies, which may be the result of gas-rich wet mergers with ensuing star formation, core galaxies are defined primarily by dry mergers with obstructing star formation (Kormendy et al., 2009; Lauer, 2012; Gabor & Davé, 2015). Due to a scarcity of cold gas in the atmosphere of core galaxies, the present study raises the possibility that the process of star formation may have been quenched in the host galaxy. Thus core galaxies possess lower CIR values in comparison with coreless galaxies. Also, there is an overlapping observed in all the correlations involving CIR manifesting an evolutionary path between core and coreless galaxies. Moreover, the simple photometric parameter, CIR, can be used to identify core and coreless galaxies without using any modeling of galaxies, at least in this X-ray emitting ETGs.

The above explanations are in agreement with our correlations involving CIR, since it shows strong connections with the hot gas properties of ETGs. The star formation process may have ceased in the central region of massive ETGs, resulting in a drop in CIR, as evidenced by the strong connections between CIR and galaxy properties such as M_{BH}, σ, M_{bulge}, and M_{gal} (Aswathy & Ravikumar, 2018). The hot gas trapped in the ISM due to the gravitational potential of galaxies (Canizares, 1999; Goulding et al., 2016) and the kinematics of stellar components in the core region might enhance the temperature of the gas, causes to the excessive emission of X-rays. The excess temperature reduces the star formation rate and the optical emission apparently. This hypothesis is further corroborated by the present study, where we observe low CIR values in massive galaxies that have extreme temperatures and X-ray emissions. To measure X-ray gas luminosity from ISM with greater accuracy, it is necessary to subtract various contributors to the X-ray emission in galaxies using rigorous spectroscopic modeling. In this context, the simple photometric pa-

rameter CIR can be used instead of employing spectroscopy for determining the $L_{\mathrm{X,GAS}}$ of ETGs. The aforementioned correlations obviate any doubt that CIR can be considered as a simple photometric parameter to study the properties of ETGs in the nearby Universe.

Chapter 4

Central Intensity Ratio in Mid-Infrared for early-type galaxies

4.1 Introduction

Recent photometric studies using high-resolution HST images show significant correlations between optical light concentration and host galaxy properties. Optical CIR is found to be significantly correlated with the SMBH mass, bulge stellar mass (Aswathy & Ravikumar, 2018; Sruthi & Ravikumar, 2021), stellar age, half-light radii, the total dynamical mass of the galaxy, central radio emission from low luminosity AGNs (Aswathy & Ravikumar, 2018), absolute B band magnitude and Mg_2 index (Sruthi & Ravikumar, 2021) in early-type galaxies. Aswathy & Ravikumar (2020) found significant correlations between properties of nuclear rings and CIR of their host galaxies using a sample of early-type spiral galaxies.

Galaxies are gravitationally bound systems of stars, stellar remnants, interstellar matter like gas and dust, and dark matter. Total stellar mass is a fundamental parameter in understanding the formation and evolution of galaxies. The stellar mass of galaxies is governed by mechanisms such as star formation, stellar feedback, gaseous feedback, and mergers (Marchesini et al., 2009).

Studying the spatial distribution of the stellar mass in nearby galaxies provides

an idea about the evolution in the concentration (quantity) and distribution of baryons over cosmic time (Meidt et al., 2011). The total stellar mass of a galaxy is one of the fundamental parameters that control its growth and evolution to a great extent as it shares a strong relation with star formation rates (SFRs) in galaxies (Daddi et al., 2007; Mobasher et al., 2009; Michalowski, M. J. et al., 2012). Reines & Volonteri (2015) reported a correlation between the BH mass and total stellar mass in early-type galaxies as well as in active galaxies.

The mid-infrared (MIR) wavelength observations of galaxies provide a window to trace old stellar populations that dominate the baryonic mass, where the extinction is lower than in the optical wavelengths (Rix & Rieke, 1993). Recent studies have shown Spitzer/IRAC 3.6 μm band is an excellent tracer of stellar mass (Buta et al., 2010; Sani et al., 2011; Meidt et al., 2011; Querejeta et al., 2015; Savorgnan & Graham, 2016; Forbes et al., 2017c). Even though the dust absorption is less in IR, the dust emission is significantly contributed to light detected in IRAC 3.6 channel along with the old stellar emission (Meidt et al., 2011; Querejeta et al., 2015). The prominent source of hot dust is the sites of massive star-forming regions, the dust surrounded by younger stars heated by the strong UV fluxes can re-radiate at IR wavelength and significantly contribute to the light at 3.6 μm. 3.3 μm poly-cyclic aromatic hydrocarbon (PAH) feature also contributed to the light at 3.6 μm, since the channel operating between $3.2 - 3.9$ μm (Meidt et al., 2011). Querejeta et al. (2015) has reported that about $10 - 30$ % of total 3.6 μm flux arises from the dust and can be higher values in disc galaxies.

Abraham et al. (1994) presented the parameter central concentration of light as one of the simple tools that can be used for morphological classification, that traces disk-to-bulge ratio and effective radius of bulge component and also traces the stellar population. Graham et al. (2001) has shown a correlation between galaxy stellar light concentration and supermassive black hole mass. Aswathy & Ravikumar (2018) introduced the idea of CIR and optical CIR found to be correlated with structural and dynamical parameters of the galaxy as discussed. Since ETGs are dominated by old stellar populations and possess very little dust content, the dust emission contribution towards 3.6 μm light is negligible. Therefore IRAC 3.6 μm light provides a good estimate of stellar mass which is not contaminated by dust emission, Forbes et al. (2017c) shows a good agreement between 3.6 μm stellar mass

and stellar mass derived 2MASS K-band (2.2 μm) data in early-type galaxies. In this light, we study the 3.6 μm CIR in early-type galaxies(ETGs), which may give an idea about the distribution/concentration of old stellar population at the centre of the galaxy since 3.6 μm light probes the stellar mass.

4.2   The Data and Data Reduction

Our sample consists of 27 galaxies, a representative of nearby early-type galaxies in the total stellar mass range of $10 < \log M_*/M_\odot < 11.7$ taken from Forbes et al. (2017c). We downloaded Spitzer/IRAC 3.6 μm band (channel 1) post-basic calibrated data (PBCD) images from the Spitzer Heritage Archive. The PBCD data of these galaxies are sufficient for our analysis since we could not find a significant change in CIR by performing photometry on images processed with the MOPEX software package. A number of spitzer/IRAC observations are available for most of the sample galaxies and there is no significant variation in the measurement of CIR from one observation to another. Also, we have excluded the observations having bad pixels in their central 10 arcsec region.

The CIR for the sample galaxies is determined using simple aperture photometry (MAG_APER) provided in source extractor (SExtractor, Bertin & Arnouts, 1996). Aswathy & Ravikumar (2018) defined the CIR as,

$$\text{CIR} = \frac{I_1}{I_2 - I_1} = \frac{10^{0.4(m_2 - m_1)}}{1 - 10^{0.4(m_2 - m_1)}} \tag{4.1}$$

I_1 and I_2 are the intensities of light within the inner and outer apertures at the centre of the galaxy image, m_1 and m_2 are the corresponding magnitudes. The Spitzer/IRAC image resolution is much lower than that of the HST, typical PSF FWHM ~ 2 arcsec. We used the magnitudes in the central 5 and 10 arcsecs of the host galaxy. The pixel scale of PBCD mosaic images is 0.6 arcsec/pixel, the inner radius is larger than the PSF in the Spitzer/IRAC images, and the outer radius is selected to be smaller than the half-light radii. The properties of the galaxies along with the calculated CIR are given in Table 4.1. Total stellar mass and 3.6 μm magnitude have been taken from Forbes et al. (2017c). Central velocity dispersion, absolute B band magnitude (M_B), and K band magnitude (M_K) were taken

from the HyperLEDA database (`http://leda.univ-lyon1.fr/`). HyperLEDA is a database with a collection of tools to study the physics of galaxies and cosmology, which compile measurements from recent surveys and published studies in order to establish a unique, homogenous description of celestial objects (Makarov et al., 2014).

4.3   Analysis

We find that CIR in the IR band is also closely related to the various properties of galaxies. 3.6 μm CIR shows anti-correlation with the mass of the central SMBH similar to that of optical CIR. CIR in IR shows a strong correlation with galaxy stellar mass and absolute B-band magnitude. The correlation coefficients of the linear correlations are given in Table 4.2 along with the values of the best-fitting parameters.

4.3.1   CIR and Stellar mass (M_*)

Studies of galaxy evolution depend on precise estimation of physical properties, especially mass metrics like stellar mass. Most of the stellar mass in an ETG is produced by the evolved stellar population. (Jarrett et al., 2023). The fundamental plane connecting stellar velocity dispersion (σ), luminosity (L), and size (R_e) has been revised by replacing L with M_* when precise stellar mass estimates are available (Auger et al., 2010; Zahid et al., 2016). The scaling relations involving M_* imply important insights into the evolution scenario of ETGs (Cannarozzo et al., 2020).

In the present study, CIR shows strong anti-correlation with the total stellar mass of the galaxy ($r = -0.86$, $s > 99.99\%$) as shown in Figure 4.1a. stellar mass is adopted from Forbes et al. (2017b), they calculated stellar mass by using 3.6 μm mass-to-light ratio from the latest stellar population model. The total stellar mass is a fundamental parameter of a galaxy that shares significant correlations with various parameters as discussed. The total luminosity of a galaxy at mid-infrared wavelengths is used to measure stellar mass for which the light mostly comes from old stars that dominate the mass and the effects of dust are much reduced compared to optical wavelengths. 3.6 μm light from galaxies is dominated by the light from old

stars and it is less affected by variations in the star formation history than shorter wavelengths (Forbes et al., 2017b).

The measured 3.6 μm CIR gives an idea about the variation of 3.6 μm light in the central two concentric apertures. The negative correlation between CIR and the total stellar mass of galaxies implies the decreasing of stellar content, mainly the old stellar population at the galaxy's centre along with the increase of total stellar mass. However, the galaxy NGC7457 shows significant deviation from the observed CIR $-M_*$ correlation.

4.3.2   CIR and Absolute B-band magnitude (M_B)

The optical B band is highly sensitive to star-forming components in nearby galaxies (Jahnke & Wisotzki, 2003). Absolute B band magnitude provides key information about the stellar population of galaxies, including their age, by analyzing the brightness of host galaxies (Kauffmann et al., 1993). Several host galaxy properties, including age, σ, M_{BH}, and M_* are correlated with the B band magnitude of ETGs (Forbes & Ponman, 1999; Haehnelt & Kauffmann, 2000; Graham & Driver, 2007; Wilman & Erwin, 2012). The less massive (comparatively young) galaxies in the sample possess sufficient dust in their ISM, which could boost infrared emission from their centres (da Cunha et al., 2010) and increase their CIR values.

It is seen that the CIR of the sample galaxies shows strong anti-correlation with the absolute B band magnitude of the host galaxy ($r = -0.86$, $s > 99.99\%$) as shown in Figure 4.1b. Sruthi & Ravikumar (2021) reported a significant anti-correlation between the absolute B band magnitude and optical CIR. Buta et al. (2010) reported a strong similarity between B-band and 3.6 μm wavelength, the 3.6 μm classifications are found to be well correlated with blue-light classifications, to an extent where the important features look identical in this two different wave-bands and dusty galaxies shows drastic differences.

Graham (2007) reported a positive correlation between M_{BH} and M_{B} for elliptical galaxies. So the relation between CIR and M_{B} is not surprising because the former is reported to be well correlated with M_{BH} (Aswathy & Ravikumar, 2018). The correlations involving M_{B} and M_* with the CIR suggest an intriguing relation between the galaxy's mass and their central light concentration/distribution.

Table 4.1: Properties of early-type galaxies. Name of the galaxy (column 1), Distance (2), Morphology (3), CIR (4), uncertainty of CIR (5), 3.6 μm apparent magnitude (6), Stellar mass (7), mass of the SMBH (8), and corresponding references (9), stellar velocity dispersion (10), absolute B-band magnitude (11), Mg$_2$ index (12), and Total K band magnitude (13) adopted from Hyperleda.

Galaxy	Distance	Morphology	CIR	ΔCIR	$m_{3.6}$	$\log M_*$	$\log M_{\mathrm{BH}}$	Ref	σ	M_{B}	Mg$_2$	M_{K}
	(Mpc)				(mag)	$(M_\odot)$	$(M_\odot)$		(km s^{-1})	(mag)	(mag)	(mag)
(1)	(2)	(3)	(4)	(5)	(6)	(7)	(8)	(9)	(10)	(11)	(12)	(13)
NGC 720	26.9	E5	0.54	0.01	6.92	11.27	8.56	2	239	-21.14	0.324	7.29
NGC 821	23.4	E6	1.02	0.01	7.57	11.00	7.59	1	197.7	-20.59	0.29	7.92
NGC 1023	11.1	S0	0.70	0.01	6.01	10.99	7.62	1	197.1	-20.61	0.289	6.26
NGC 1400	26.8	E1/S0	0.91	0.02	7.44	11.08	–	–	245.8	-20.44	0.303	7.85
NGC 1407	26.8	E0	0.55	0.01	6.16	11.6	9.65	1	265.6	-21.85	0.326	6.73
NGC 2768	21.8	E6/S0	0.69	0.02	6.68	11.21	–	1	185	-21.14	0.263	7.02
NGC 2974	20.9	E4/S0	0.72	0.01	7.47	10.93	8.23	1	232.2	-20.09	0.285	6.25
NGC 3115	9.4	S0	0.82	0.01	5.58	10.93	8.94	1	260.2	-20.05	0.29	5.89
NGC 3377	10.9	E5-6	1.12	0.02	7.09	10.50	7.89	1	136.1	-19.12	0.238	7.46
NGC 3607	22.2	S0	0.70	0.01	6.51	11.39	8.11	1	222.2	-20.94	0.291	7.02
NGC 3608	22.3	E1-2	0.82	0.02	7.41	11.03	8.30	1	194.2	-20.31	0.293	8.13
NGC 4111	14.6	S0	0.94	0.01	7.24	10.52	7.80	2	146.2	-19.26	0.224	7.56
NGC 4278	15.6	E1-2	0.78	0.01	6.84	10.95	8.53	2	237.3	-20.43	0.28	7.24

Table 4.1 continued.

Galaxy	Distance (Mpc)	Morphology	CIR	ΔCIR	$m_{3.6}$ (mag)	$\log M_*$ ($M_\odot$)	$\log M_{\rm BH}$ ($M_\odot$)	Ref	σ (km s^{-1})	$M_{\rm B}$ (mag)	Mg_2 (mag)	$M_{\rm K}$ (mag)
(1)	(2)	(3)	(4)	(5)	(6)	(7)	(8)	(9)	(10)	(11)	(12)	(13)
NGC 4365	23.1	E3	0.66	0.02	6.31	11.51	8.85	2	250.3	-21.42	0.308	6.66
NGC 4374	18.5	E1	0.63	0.01	5.81	11.51	8.95	1	277.6	-21.73	0.292	6.25
NGC 4459	16.0	S0	0.91	0.01	6.76	10.98	7.83	1	171.8	-19.92	0.241	7.18
NGC 4473	15.2	E5	0.78	0.01	6.74	10.96	8.08	1	178.6	-20.01	0.286	7.17
NGC 4486	16.7	E0/cD	0.53	0.02	5.30	11.62	9.81	1	323.0	-21.59	0.277	5.82
NGC 4494	16.6	E1-2	0.67	0.01	6.68	11.02	7.74	2	148.3	-20.54	0.255	7.02
NGC 4526	16.4	S0	0.72	0.01	6.17	11.26	8.67	1	224.6	-20.48	0.269	6.48
NGC 4564	15.9	E6	1.06	0.01	7.78	10.58	7.78	1	156.2	-19.19	0.309	7.98
NGC 4594	9.5	Sa	0.57	0.01	4.56	11.41	8.81	1	225.7	-20.97	0.296	4.98
NGC 4649	16.5	E2/S0	0.47	0.01	5.33	11.6	9.67	1	330.5	-21.50	0.328	5.75
NGC 4697	12.5	E6	0.81	0.01	5.85	11.15	8.26	1	165.2	-20.33	0.273	6.35
NGC 5846	24.2	E1/S0	0.60	0.01	6.50	11.46	9.04	3	237.2	-21.15	0.317	6.98
NGC 5866	14.9	S0	0.70	0.01	6.50	10.83	7.70	4	162.1	-20.13	0.195	6.88
NGC 7457	12.9	S0	0.88	0.02	7.94	10.13	7.00	1	68.0	-19.14	0.154	8.22

References: 1. Sahu et al. (2019), 2. Pellegrini (2010), 3. Savorgnan & Graham (2016), 4. Flohic et al. (2006)

Table 4.2: The table lists the best-fitting parameters for the relation x = α CIR + β and linear correlation coefficient (r) for various relations. n denotes the number of galaxies.

x	α	β	r	s	n
$\log M_\star$	-1.60 ± 0.22	12.32 ± 0.17	-0.86	> 99.99%	26
M_B	3.93 ± 0.53	-23.47 ± 0.41	0.87	> 99.99%	27
$\log M_{BH}$	-2.93 ± 0.63	10.57 ± 0.48	-0.70	99.97%	25
$\log \sigma$	-0.42 ± 0.09	2.63 ± 0.07	-0.70	> 99.98%	26

4.3.3 Variation of CIR with M_{BH} and σ

Central black holes are a crucial component of the formation and growth of galaxies, and they may have significant effects on the evolution of galaxies (Zhu et al., 2021). There has been a lot of interest in establishing empirical connections between M_{BH} and host galaxy properties, especially with σ (Tremaine et al., 2002; Gültekin et al., 2009; McConnell & Ma, 2013). The $M_{BH} - \sigma$ relation was considered to be the most fundamental relation in ETGs, because it exhibits the lowest scatter compared to other possible correlations (Ferrarese & Merritt, 2000; Gebhardt et al., 2000).

We find that CIR shows anti-correlation with the mass of SMBH residing at the centre of the galaxy, having linear correlation coefficient $r = -0.70$ with a significance, $s = 99.97\%$ (Figure 4.2a). Estimations of central black hole mass of the sample galaxies mainly involved stellar and/or gas dynamics (Sahu et al., 2019; Savorgnan & Graham, 2016; Pellegrini, 2010) and stellar velocity dispersion measurement is used for the galaxy NGC 5866 (Flohic et al., 2006). Optical CIR is reported to be well correlated with M_{BH} for both ETGs and the AGN host galaxies (Aswathy & Ravikumar, 2018; Vinod et al., 2023). We found a similar negative correlation between the mid-IR CIR and M_{BH}, which further suggests that star formation at the central region of ETGs has been suppressed. The central SMBH might expel the gas and dust from the central region of host galaxies (Werner et al., 2014), which may impede star formation. The lack of dust in the central region
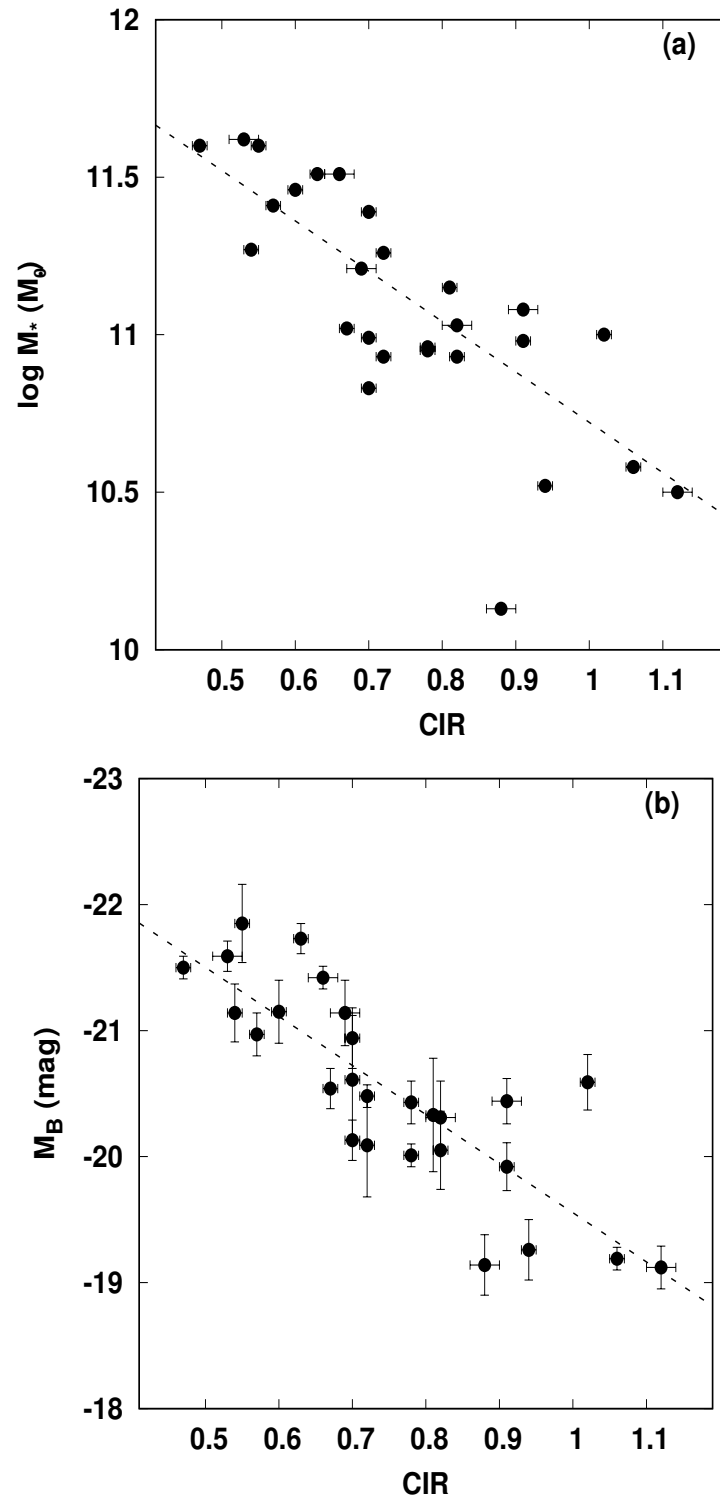
Figure 4.1: Correlation between the central intensity ratio and (a) Stellar mass ($M_\star$) and (b) B-band absolute magnitude (M_B) of the sample galaxies.
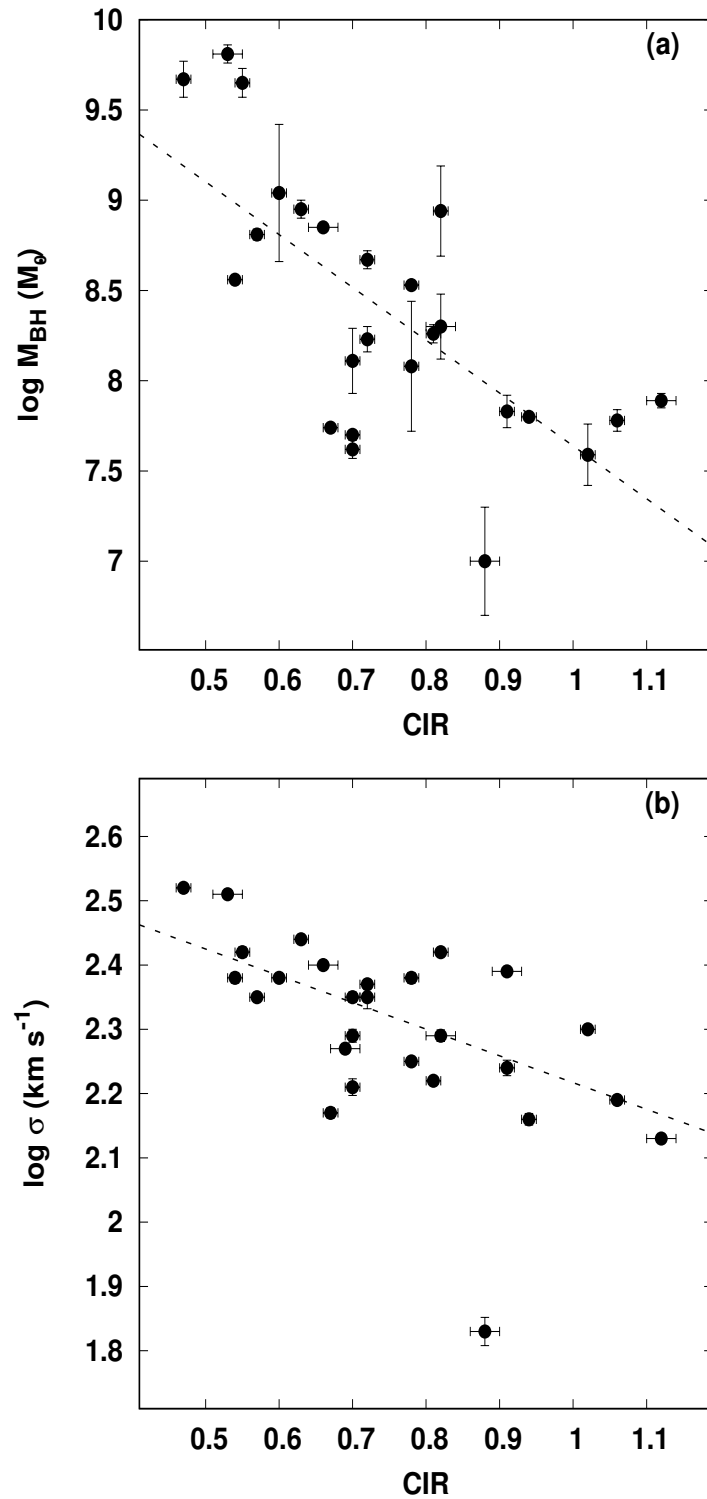
Figure 4.2: Correlation between the central intensity ratio and (a) mass of the SMBH (M_{BH}) and (b) Stellar velocity dispersion (σ) of the sample galaxies.

could also result in a reduction in infrared emission (da Cunha et al., 2010) and the CIR value.

Numerous studies have reported that the mass of central SMBH of the galaxy is well correlated with the central velocity dispersion (Ferrarese & Merritt, 2000; Gebhardt et al., 2000; Gültekin et al., 2009; Kormendy & Ho, 2013; Thomas et al., 2019). For ETGs, the strong correlation between optical CIR and central velocity dispersion is apparent since CIR is well correlated with M_{BH} (Aswathy & Ravikumar, 2018; Sruthi & Ravikumar, 2021). We could find a significant correlation between 3.6 μm CIR and central velocity dispersion of the host galaxies as well (Figure 4.2b). Here the galaxy NGC7457 shows a large deviation from the best fit of the CIR − M_{BH} and CIR − σ correlations. The galaxy NGC7457 was classified by Kormendy & Ho (2013a) as hosting a classical bulge, while they also raised the possibility that it might actually be a pseudobulge-dominant galaxy. This galaxy's black hole is relatively smaller than most others, and its stellar velocity dispersion is remarkably low (Kormendy & Ho, 2013a). Moreover, pseudo-bulge galaxies display significant deviations in the reported correlations involving CIR, which can be used as a simple photometric tool to distinguish between classical bulges and pseudo bulges (Aswathy & Ravikumar, 2018).

4.4   Discussion and conclusion

This study explores various relationships among well-known galaxy properties and the 3.6 μm CIR calculated by performing photometry on spitzer/IRAC images of galaxies. The optical CIR is reported to be well correlated with SMBH mass and other structural and dynamical properties. Galaxy morphology was found to be the same at the optical and 3.6 μm wavelengths (Buta et al., 2010). The optical central intensity ratio was reported to be well correlated with the mass of central SMBH and also correlated to structural and dynamical properties of galaxies (Aswathy & Ravikumar, 2018, 2020; Sruthi & Ravikumar, 2021). The CIR − M_{BH} relation implies that the massive black hole might be able to expel the gas and/or suppress the star formation in the central region of host galaxies. It is also noticed that the central light might be suppressed more by older galaxies than by younger galaxies (Aswathy & Ravikumar, 2018). The relative size of the nuclear ring and bar strength

of the galaxies, which are closely correlated with their CIR, demonstrate the coupled evolution of rings and bars connected to their star formation (Aswathy & Ravikumar, 2020). 3.6 μm CIR also found to be correlated with the mass of central SMBH, central velocity dispersion, total stellar mass of the galaxy, and absolute B-band magnitude.

CIR is very much responsive to any addition or removal of the light towards the centre of a galaxy. High star formation processes near the centre may be responsible for the addition of light while quenching of star formation can reduce the light at the centre and which reduces the CIR (Aswathy & Ravikumar, 2018; Sruthi & Ravikumar, 2021). Old stellar population, mainly K and M giants, contributes towards the 3.6 μm light while younger stars do not significantly contribute. However, the dust surrounding the young stars can be heated by strong UV fluxes and re-radiate in this wavelength. The star formation processes are expected to be not significant in early-type galaxies. We can not neglect star formation completely, since ultraviolet emissions from massive early-type galaxies have also been reported (eg., Schawinski et al., 2006). Schawinski et al. (2006) reported suppression of star formation caused by the outflows from the central black hole that expel the cold gas available for star formation. Borch (2006) has reported that lower massive galaxies are star-forming and the majority of massive galaxies ($\log M_*/M_\odot > 11$) are non-star-forming at redshift, $z < 1$. Mobasher et al. (2008) has reported mean SFR strongly depends on galactic stellar mass, less massive systems contributing high towards the total star formation rate density(SFRD) and high massive systems ($\log M_*/M_\odot > 10.5$) contributing less. SFRD of less massive systems increases with redshift from z=0 to z=1 implies that significant star formation activity of massive systems happens at earlier epochs than comparatively less massive systems.

The coevolution of SMBH and host galaxy is well established from a number of correlations including $M_{\mathrm{BH}} - \sigma$ (Ferrarese & Merritt, 2000; Hu, 2008; Gültekin et al., 2009; Saglia et al., 2016; Thomas et al., 2019), $M_{\mathrm{BH}} - M_{\mathrm{B}}$ (Graham, 2007), $M_{\mathrm{BH}}-$ absolute blue luminosity of elliptical galaxy (Kormendy & Richstone, 1995), $M_{\mathrm{BH}} - M_*$ or dynamical mass of galaxy (Schramm & Silverman, 2013; Kormendy & Ho, 2013; Reines & Volonteri, 2015), total gravitational mass of galaxy (Bandara et al., 2009). Bulge properties like luminosity (L_{bulge}) and mass (M_{bulge}) are strongly correlated to M_{BH} (Kormendy & Richstone, 1995; Marconi & Hunt, 2003;

Hring & Rix, 2004; Gültekin et al., 2009; Sani et al., 2011; Schramm & Silverman, 2013; Schutte et al., 2019). Since M_{BH} exhibits various correlations with different galaxy properties, the important implication is that every galaxy should contain a supermassive black hole and the evolution of central black holes and galactic bulges should be coupled by the co-evolution mechanism (Kormendy & Richstone, 1995; Jahnke & Macciò, 2011).

Sani et al. (2011) has reported significant correlations of M_{BH} with 3.6 μm bulge luminosity, bulge dynamical mass and stellar mass calculated by using IRAC 3.6 μm data. These correlations are also consistent with previous analyses performed at shorter wavelengths with $M_{\mathrm{BH}} - \sigma$ precision. In this work we reports correlations of 3.6 μm CIR with M_{BH}, σ, M_{B} and M_*. The optical CIR shares correlation with M_{BH}, σ, M_{B} also with the bulge stellar mass and dynamical mass of the galaxy (Aswathy & Ravikumar, 2018; Sruthi & Ravikumar, 2021). The CIR at different wavelengths, optical and 3.6 μm, shows the same trend with the fundamental parameters in ETGs.

The accurate measure of the stellar mass can be used as a crucial tool to understand the baryonic physics which is responsible for the current condition of galaxies (Querejeta et al., 2015). Stellar structural torques have been studied using stellar mass maps derived from near-IR imaging (Foyle et al., 2010). In order to comprehend the effects of gravitational potential on the distribution of gas and its dynamics, it is essential to know how the stellar mass is organized in the host galaxies (Knapen et al., 1995b; García-Burillo et al., 2005; Jogee et al., 2005; Hunt et al., 2008; Haan et al., 2009). Hence, stellar mass maps are considered a useful tool for figuring out how gas reacts to the driving gravitational potential of galaxies. In this context, $\mathrm{CIR} - M_*$ relation provides some useful information about the stellar mass and star formation of the host galaxies and CIR can be used as a fast and reliable method for estimating the M_* of ETGs.

Chapter 5

Summary and Future Prospects

Galaxies are considered the primary building blocks of our Universe and the studies on morphology and evolution of galaxies provide vital information about the evolution scenario of the Universe. The morphological and star-forming features of galaxies are crucial to the present knowledge of galaxy formation. Numerous studies proposed intriguing connections between morphology and the stellar distribution of galaxies. Most of the massive galaxies harbor SMBHs at their centres and this central region plays a vital role in the evolution of host galaxies. The relationship between the origin and evolution of SMBHs with their host galaxies is a hot topic. The accretion of matter towards the SMBH is the prime reason for the origin and growth of active galactic nuclei (AGNs) in the nuclear region of galaxies. The dynamics of gas in the interstellar medium (ISM) of galaxies also share significant information regarding the galaxy's evolution. In order to comprehend the evolution of these kinds of galaxies, it may be crucial to determine correlations between different parameters for a set of galaxies with comparable morphology. In this context, we investigate the central region of nearby galaxies by using simple photometry and exploring various correlations between galaxy properties.

Chapter 1 provides a brief overview of the work discussed in this thesis. Photometric analysis of the central region of galaxy images was carried out for the whole study. We explain about the telescopes which provided the photometric images that we used for our investigation. We also describe the software programs used to perform data analysis. A brief review of the literature is included here to emphasize

the importance of the subject discussed in this thesis in the present context. Lastly, we describe the motivation of our work as well as provide a quick overview of the thesis.

Chapter 2 deals with the study of the central intensity ratio of Seyfert galaxies in the nearby ($z < 0.02$) Universe. We took a complete sample of Seyfert galaxies brighter than $B_\mathrm{T} = 13.2$ with a median distance of 22 Mpc, consisting of 57 galaxies comprising 40 spirals, 9 lenticulars, and 8 elliptical galaxies. We find that CIR shows a strong correlation with the mass of the SMBH residing at the centre of the galaxy. The removal of cold gas by the active black hole might be suppressing the star formation near the central region of the galaxies, which can be held responsible for the decrease in CIR. We identified a large discrepancy that occurred in the estimation of central velocity dispersion (σ) due to the extra luminous feature of AGN. Thus, we propose that CIR can be utilized as a faster and more reliable tool to estimate the SMBH mass of AGNs than deriving from σ. The following list summarises the key findings of this study.

- We find a strong anti-correlation between the CIR and SMBH masses of Seyfert galaxies.

- The SMBH masses of ellipticals in the sample are systematically higher than those of lenticulars and spirals for a given CIR value.

- We find a weak correlation between CIR and central velocity dispersion of Seyfert galaxies.

- The extra luminous feature of AGN can outshine or dilute the stellar spectral lines and the measurement of stellar velocity dispersion is obtained with a significant discrepancy in AGNs (Riffel et al., 2013).

- We suggest this discrepancy may be responsible for the weak correlation between CIR and stellar velocity dispersion.

- In comparison to the CIR $-$ M_BH relation, we find that the scatter of the $\sigma - M_\mathrm{BH}$ relation is higher.

- As a result, we propose that CIR can be used as a fast and reliable tool for estimating the central SMBH mass of AGNs instead of stellar velocity dispersion.

The third chapter describes the correlations between CIR and X-ray gas properties of a sample of nearby (D < 30 Mpc) ETGs. For the first time, we identified significant correlations between CIR and the gas properties of ETGs. We find new scaling relations, CIR − $L_{\mathrm{X,GAS}}$ and CIR − T_{GAS}, that strongly suggest the role of central gas temperature on the star formation process and evolution scenario of early-type galaxies. The main conclusions of this study are summarized in the list given below.

- We find new key scalings, CIR − $L_{\mathrm{X,GAS}}$ and CIR − T_{GAS}, that strongly suggests that the central gas temperature depends on the star formation process and evolution scenario of early-type galaxies.

- We find that the CIR is well correlated with the absolute K-band magnitude and age of the central stellar population, suggesting that older galaxies are massive and possess more stellar mass.

- Core and coreless classification in ETGs can be possible through the correlations between CIR and host galaxy properties.

- To measure X-ray gas luminosity from ISM with greater accuracy, it is necessary to subtract various contributors to the X-ray emission in galaxies using rigorous spectroscopic modeling. In this context, we propose the simple photometric parameter CIR can be used instead of employing spectroscopy for determining the $L_{\mathrm{X,GAS}}$ of ETGs.

In the final part of the work which is discussed in Chapter 4, we estimated mid-infrared CIR for a representative sample of ETGs by using Spitzer/IRAC 3.6 μm data. Mid-IR CIR was found to be significantly correlated with the total stellar mass and absolute B band magnitude of the host galaxies. We observed mid-IR CIR also following significant correlations with M_{BH} and σ similar to optical CIR. Since mid-IR emission mainly comes from the old stars, CIR can be utilized as a better

tracer of stellar mass and used to study the variation of the old stellar population at the central region of galaxies. The results from this study are provided below.

- Mid-infrared CIR is found to be significantly anti-correlated with the total stellar mass and absolute B band magnitude of the host galaxies.

- Also shows a negative correlation with central supermassive black hole mass (SMBH) and central velocity dispersion similar to the relations exhibited by optical CIR.

- Negative correlation between CIR and total stellar mass of galaxy implies the decreasing of stellar content, mainly the old stellar population at the centre of the galaxy along with the increase of total stellar mass.

- Since mid-IR light is a better tracer of the stellar mass of ETGs, mid-IR CIR can be used to study the variation of old stellar population at the central region of galaxies and their evolution scenario.

5.0.1 Future scopes of the work

- We plan to extend the present study and estimation of CIR using high-resolution IR data observed by the James Webb Space Telescope (JWST).

- We also plan to estimate CIR using UV data observed by ASTROSAT subjected to the availability of archival data and explore various correlations between CIR and galaxy properties.

- The present study is carried out mainly with optical CIR. This can be extended to multi wavelengths to compare how the CIR varies with different wavelengths.

- With a representative sample of ETGs, we have observed a strong correlation between CIR and X-ray gas properties. So, we plan to extend this study to a larger sample once the data are available.

Chapter 6

Recommendations

- The central SMBH mass of AGNs is predicted by $CIR - M_{\mathrm{BH}}$ correlation even more accurately than by predictions from spectroscopic parameters like the central velocity dispersion. Being a photometric tool, this promises to be a quick and inexpensive method to explore large samples of galaxies.

- Instead of employing rigorous spectroscopic modeling, CIR can be used to predict the X-ray gas properties of similar kinds of early-type galaxies in the nearby Universe.

- Since mid-infrared light is an excellent tracer of stellar mass, CIR can be computed in this band and it is possible to infer stellar masses of nearby early-type galaxies in a fast and reliable way.

- CIR has great potential to be used to investigate the central region of more distant galaxies, by employing observations from next-generation facilities like the James Webb Space Telescope.

- To investigate the variation of the young stellar population at the central region of late-type galaxies, the high-resolution UV data observed by ASTROSAT can be used to compute CIR.

Appendix A

Appendix 1

1. IC2560 – (R')SB(r)b – S2
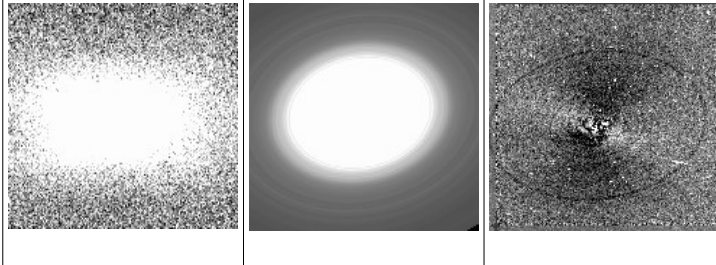
2. IC3639 – SB(rs)bc – S2

3. NGC0613 – SB(rs)bc – S?
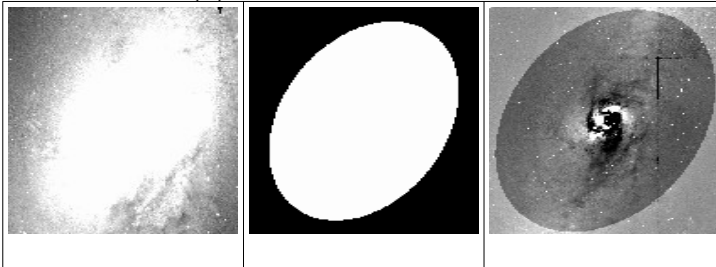
4. NGC0788 – SA(s)0/a – S2
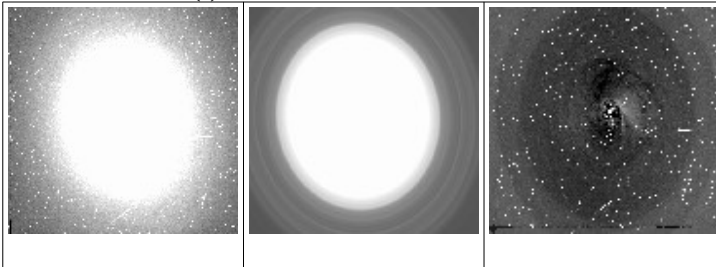
5. NGC1275 – E-cD - S2
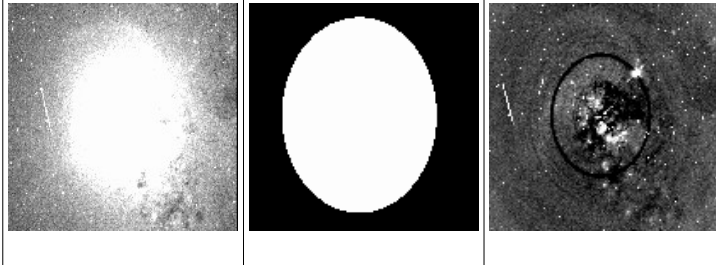
6. NGC1358 – SAB(r)0/a – S2
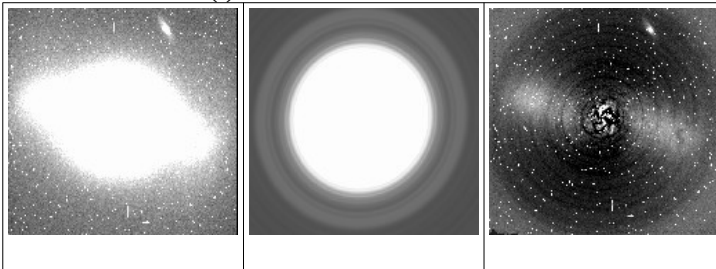
7. NGC1365 – SB(s)b – S1.8
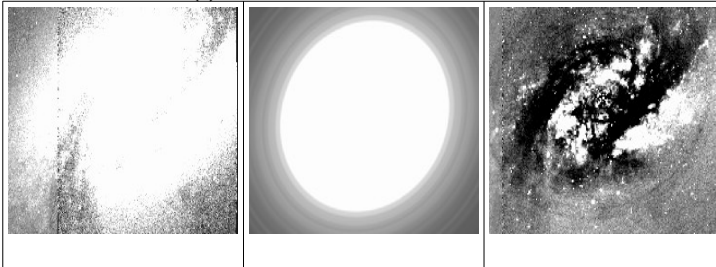
8. NGC1386 – SB0+(s) – S2
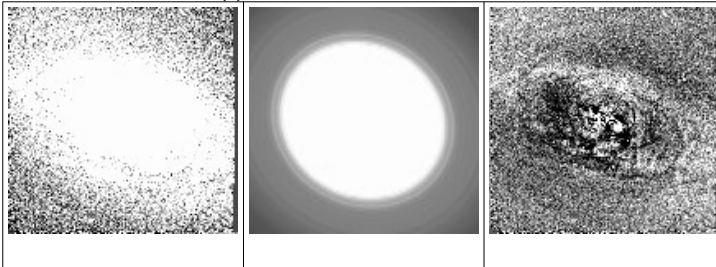
9. NGC1399 – E1 pec – S2
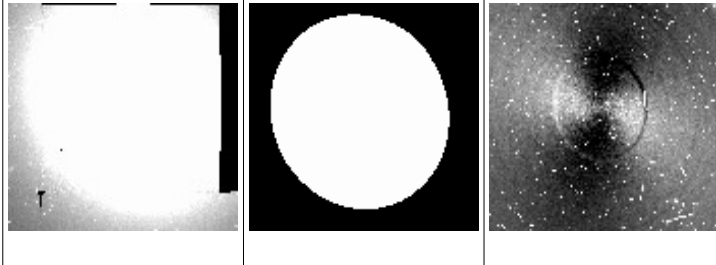
10. NGC1433 – (R')SB(r)ab – S2

11. NGC1566 – SAB(s)bc – S1.5
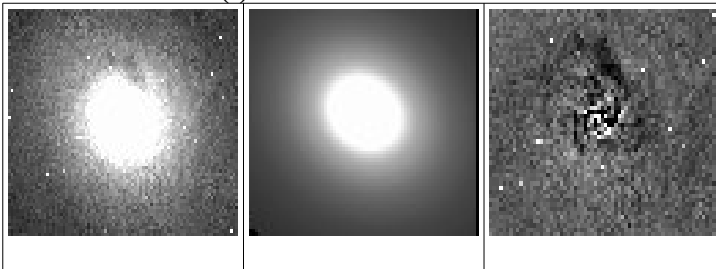
12. NGC1667 – SAB(r)c – S2
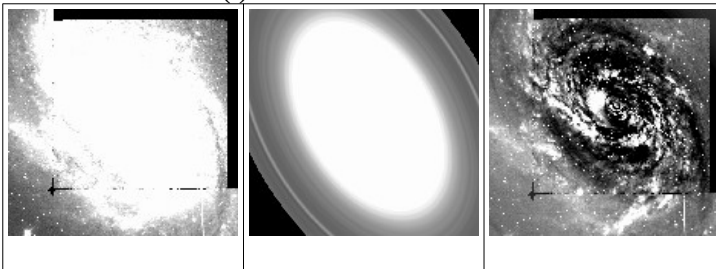
13. NGC1672 – SB(s)b – S2
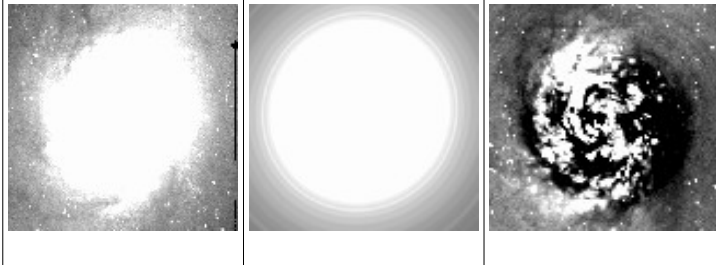
14. NGC1808 – (R)SAB(s)a – S2
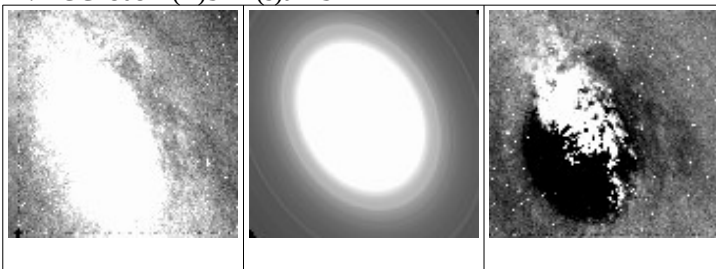
15. NGC2273 – SB(r)a – S2
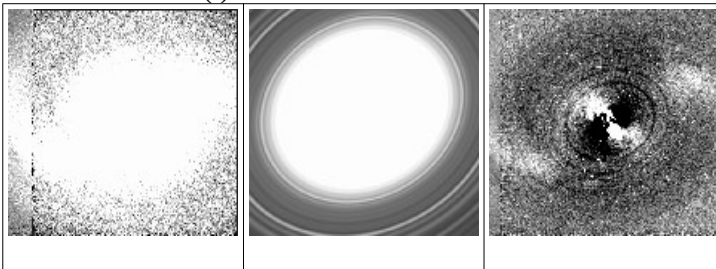
16. NGC2639 – (R)SA(r)a – S1.9
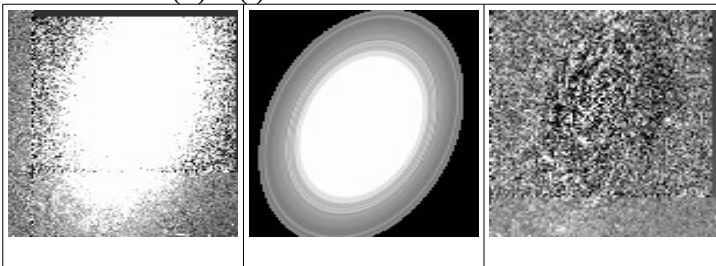
17. NGC2782 – SAB(rs)a pec – S2
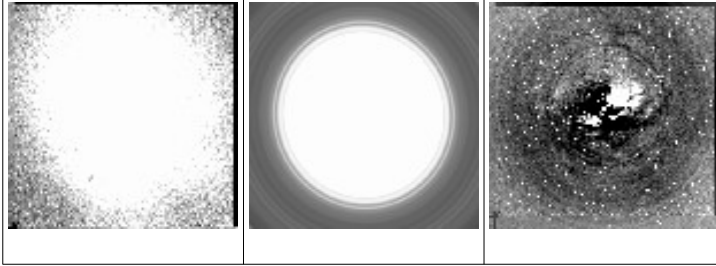
18.NGC2974 – E4 – S2
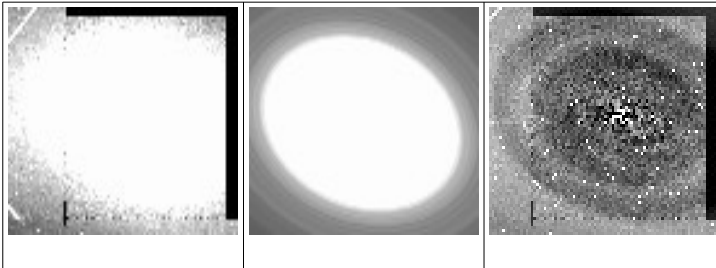
19. NGC3081 – (R)SAB(r)0/a – S2

20. NGC3169 – SA(s)a pec – S
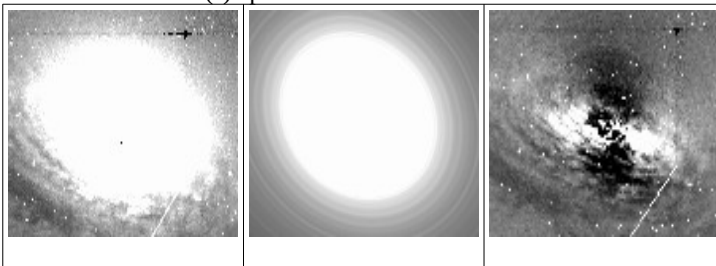
21. NGC3185 – (R)SB(r)a – S2
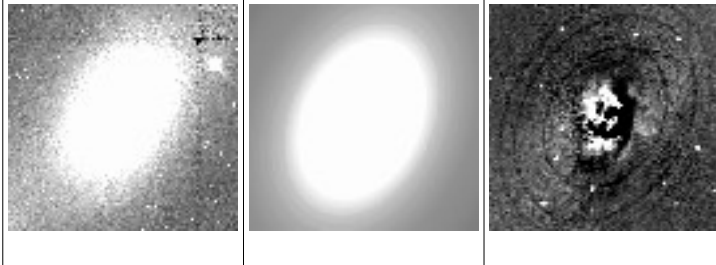
22. NGC3227 – SAB(s)a pec – S1.5
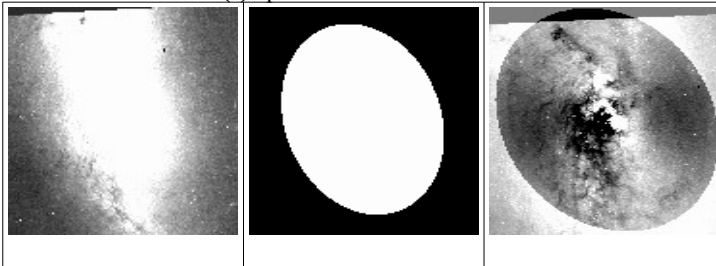
23. NGC3281 – SA(s)ab pec – S2
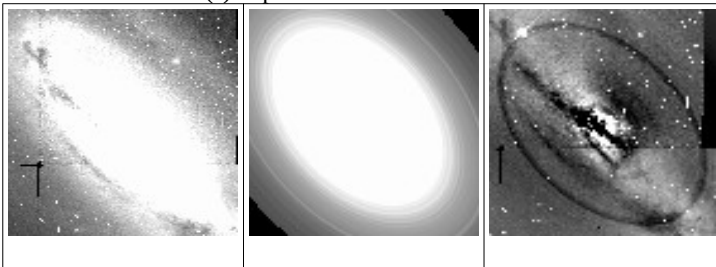
24. NGC3486 – SAB(r)c – S2
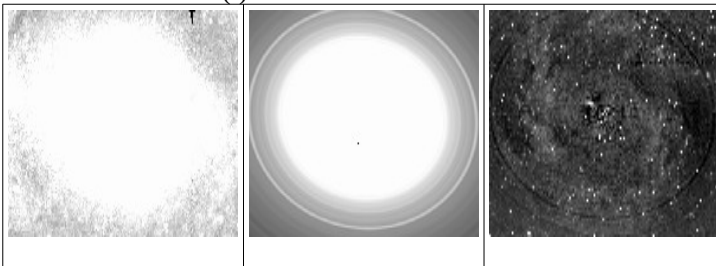
25. NGC3489 – SAB0+(rs) – S2
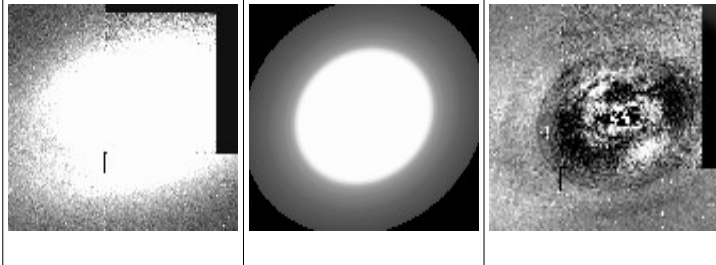
26. NGC3516 – (R)SB(s)0 – S1.2
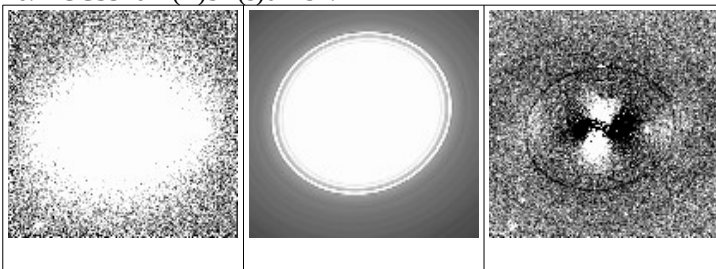
27. NGC3982 – SAB(r)b – S1.9
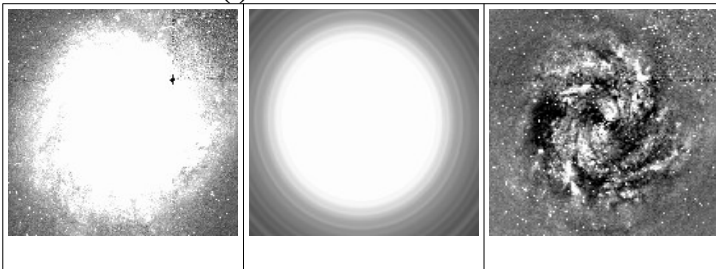
28. NGC4168 – E2 – S1.9

29. NGC4235 – SA(s)a – S1.2
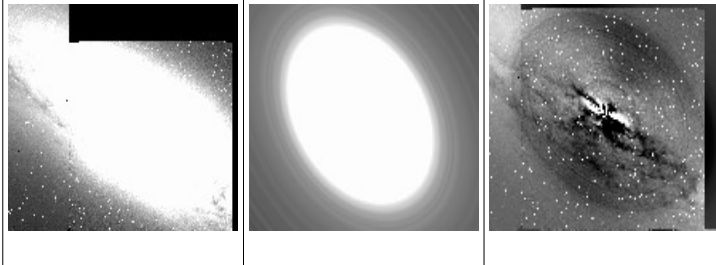
30. NGC4258 – SAB(s)bc – S1.9
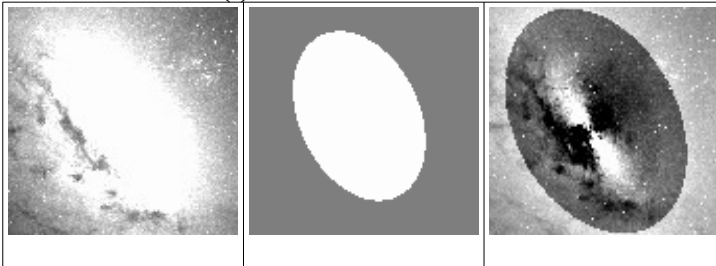
31. NGC4303 – SAB(rs)bc – S2
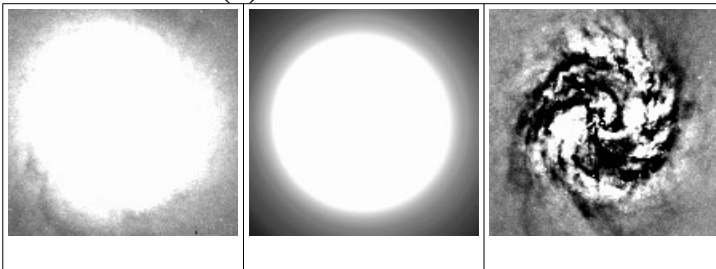
32. NGC4374 – E1 – S2
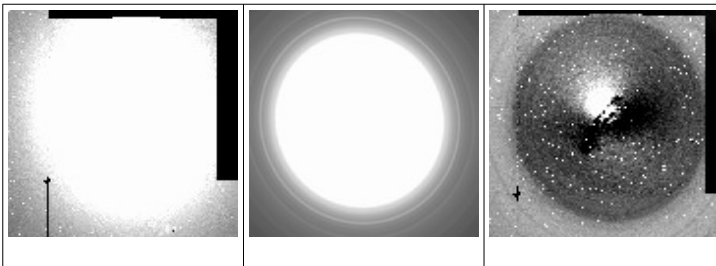
33. NGC4472 – E2 – S2
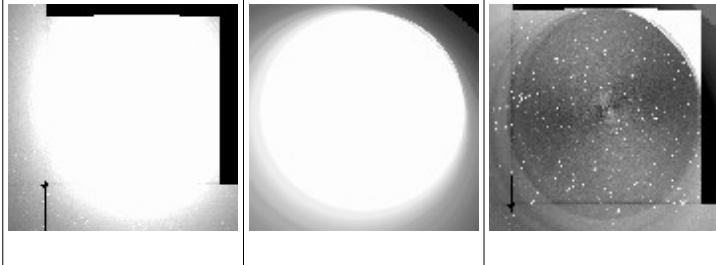
34. NGC4477 – SB0(s) – S2
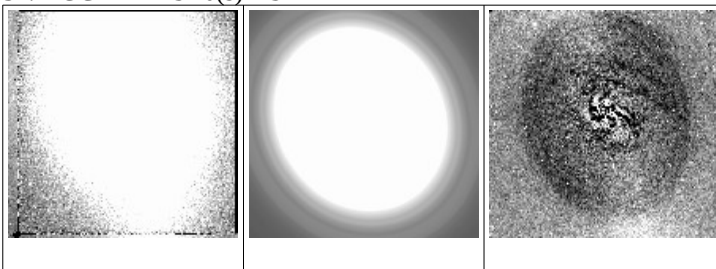
35. NGC4501 – SA(rs)b – S2
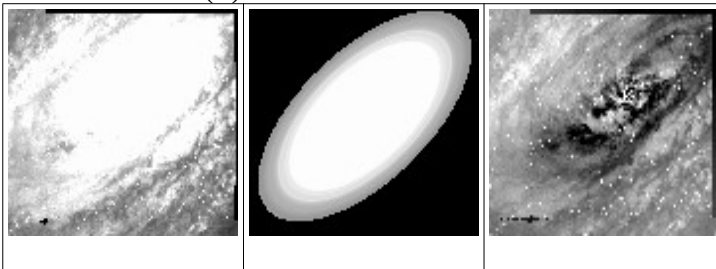
36. NGC4507 – (R')SAB(rs)b – S2

37. NGC4552 – E0-1 – S2
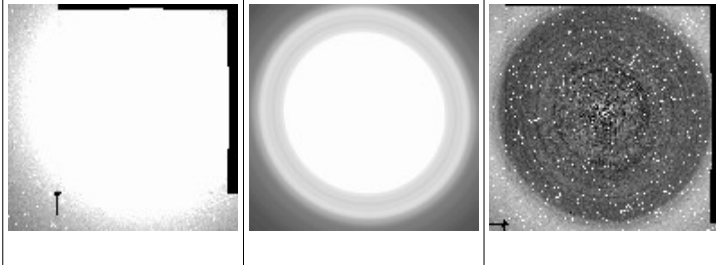
38. NGC4579 – SAB(rs)b – S1.9
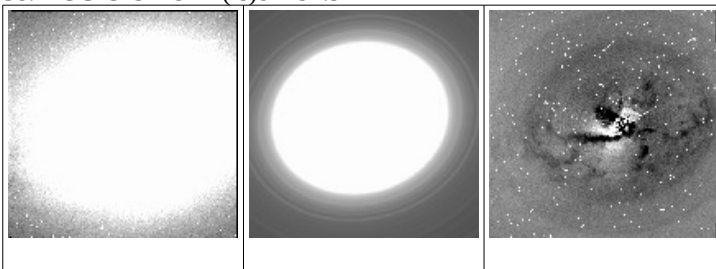
39. NGC4594 – SA(s)a – S1.9
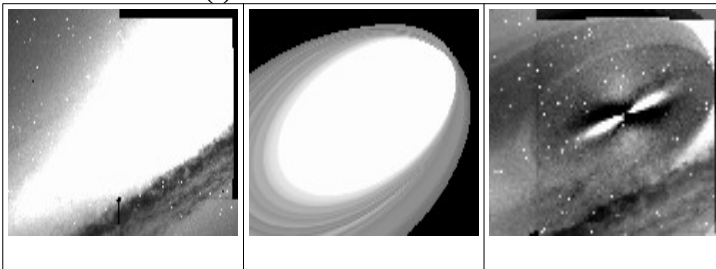
40. NGC4698 – SA(s)ab – S2
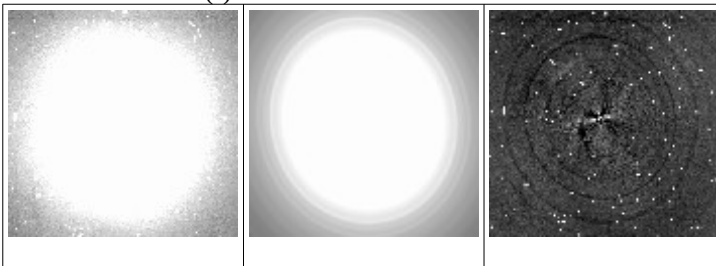
41. NGC4725 – SAB(r)ab pec – S2
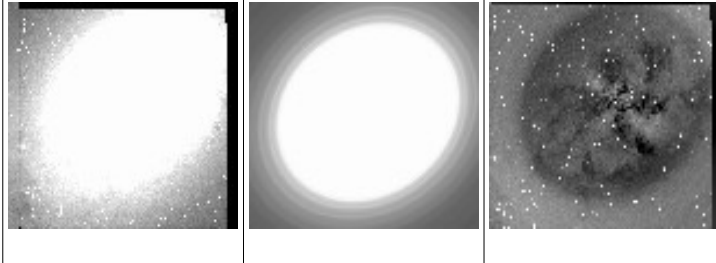
42. NGC5005 – SAB(rs)bc – S2

43. NGC5033 – SA(s)c – S1.9
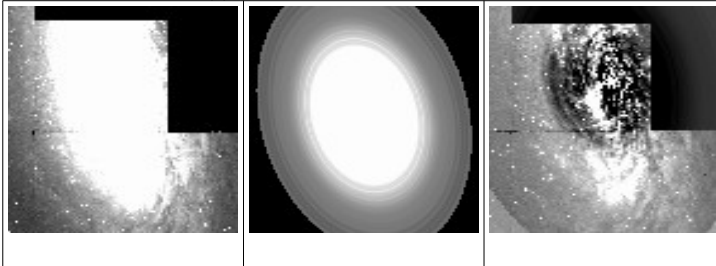
44. NGC5135 – SB(s)ab – S2
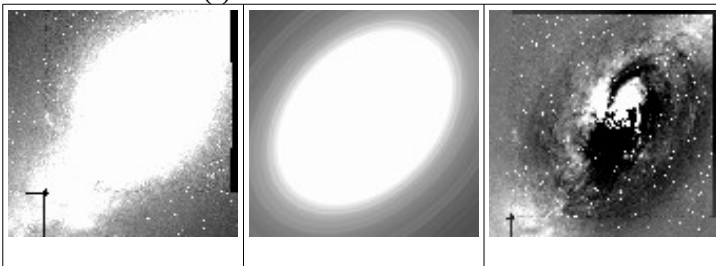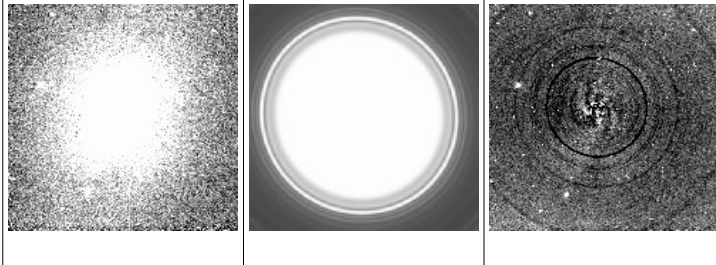
45. NGC5194 – SA(s)bc pec – S2
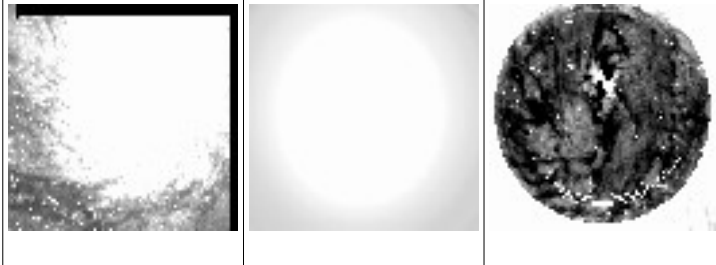
46. NGC5273 – SA0(s) – S1.5
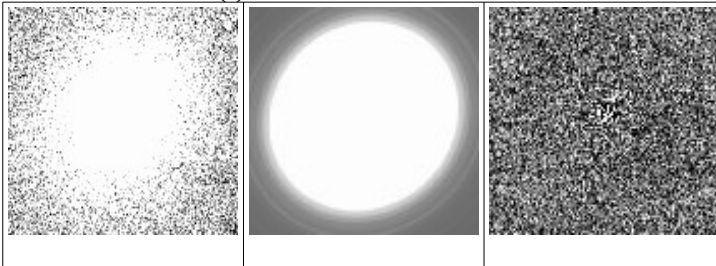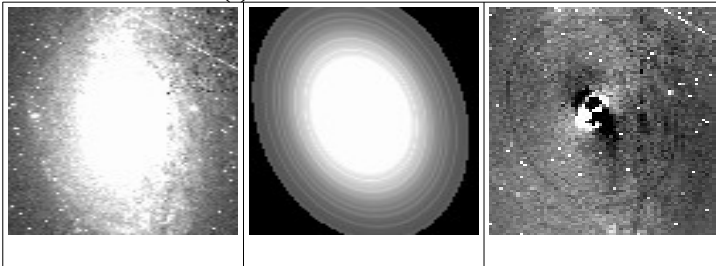

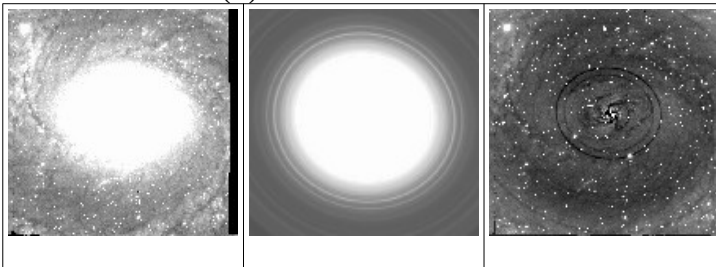47. NGC5322 – E3-4 – S
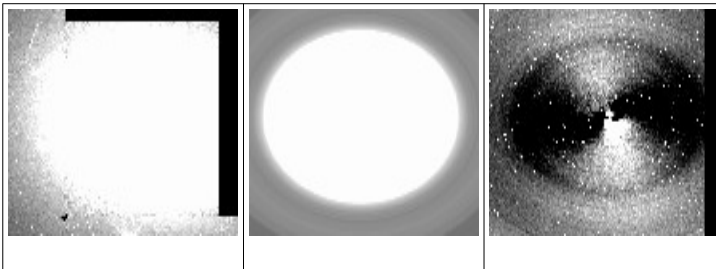
48. NGC5427 – SA(s)c pec – S2
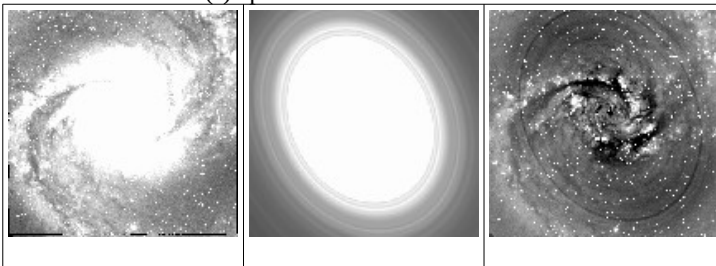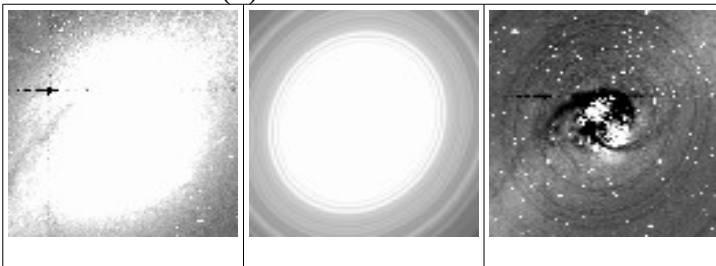
49. NGC5643 – SAB(rs)c – S2
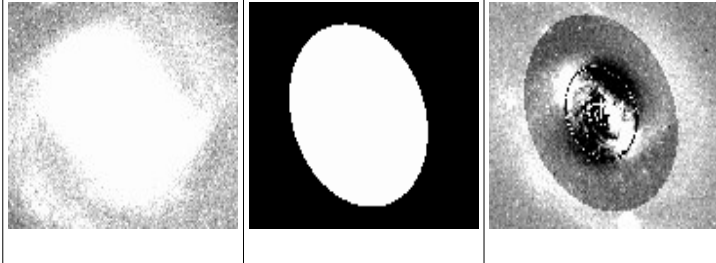

50. NGC5806 – SAB(s)b – S2

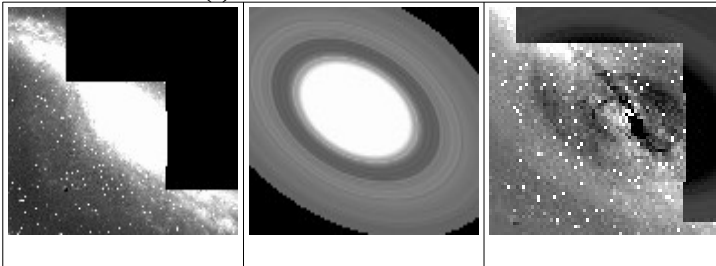51. NGC6814 – SAB(rs)bc – S1.5

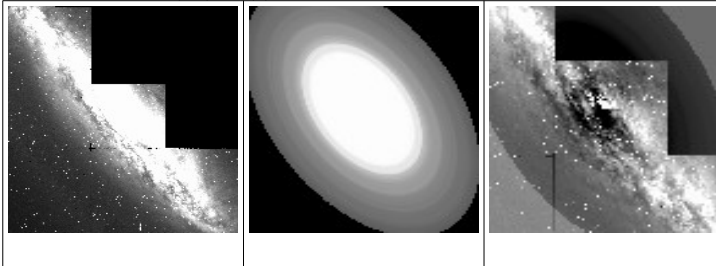52. NGC6951 – SAB(rs)bc – S2

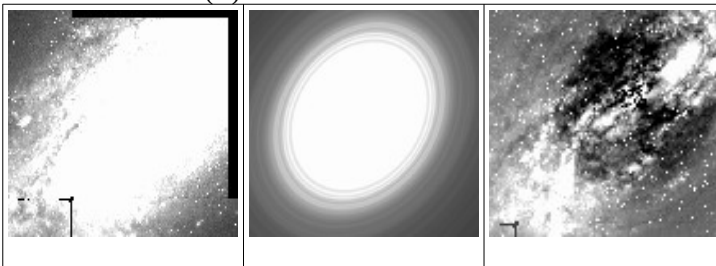53. NGC7469 – (R')SAB(rs)a – S1.2
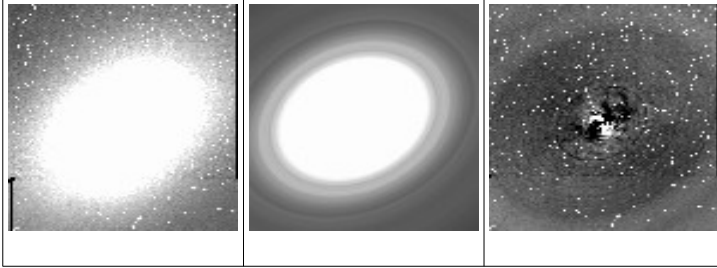

54. NGC7479 – SB(s)c – S1.9

55. NGC7582 – (R')SB(s)ab – S2

56. NGC7590 – SA(rs)bc – S2

57. NGC7743 – (R)SB0+(s) – S2

Bibliography

Abraham, R. G., Valdes, F., Yee, H. K. C., & van den Bergh, S. 1994, ApJ, 432, 75

Alabi, A. B., Forbes, D. A., Romanowsky, A. J., et al. 2017, MNRAS, 468, 3949

Alatalo, K., Lacy, M., Lanz, L., et al. 2015, ApJ, 798, 31

Alexander, D., & Hickox, R. 2012, New Astronomy Reviews, 56, 93

Allard, E. L., Knapen, J. H., Peletier, R. F., & Sarzi, M. 2006, MNRAS, 371, 1087

Alonso-Herrero, A., Pereira-Santaella, M., Rieke, G. H., et al. 2013, ApJ, 765, 78

Antonucci, R. 1993, ARA&A, 31, 473

Armus, L., Bernard-Salas, J., Spoon, H. W. W., et al. 2006, ApJ, 640, 204

Armus, L., Charmandaris, V., Bernard-Salas, J., et al. 2007, ApJ, 656, 148

Aswathy, S., & Ravikumar, C. D. 2018, MNRAS, 477, 2399

Aswathy, S., & Ravikumar, C. D. 2018, Monthly Notices of the Royal Astronomical
    Society, 477, 2399–2405

Aswathy, S., & Ravikumar, C. D. 2020, Research in Astronomy and Astrophysics,
    20, 015

Aswathy, S., & Ravikumar, C. D. 2020, Research in Astronomy and Astrophysics,
    20, 015

Auger, M. W., Treu, T., Bolton, A. S., et al. 2010, ApJ, 724, 511

Baldry, I. K. 2008, Astronomy and Geophysics, 49, 5.25

Bandara, K., Crampton, D., & Simard, L. 2009, The Astrophysical Journal, 704, 1135

Barr, J. M., Bedregal, A. G., Aragón-Salamanca, A., Merrifield, M. R., & Bamford, S. P. 2007, A&A, 470, 173

Barth, A. J., Ho, L. C., Filippenko, A. V., Rix, H.-W., & Sargent, W. L. W. 2001, ApJ, 546, 205

Barway, S., Saha, K., Vaghmare, K., & Kembhavi, A. K. 2016, MNRAS, 463, L41

Baum, S. A., & Heckman, T. 1989, ApJ, 336, 702

Begelman, M., & Rees, M. 1996, Gravity's fatal attraction. Black holes in the universe

Beifiori, A., Courteau, S., Corsini, E. M., & Zhu, Y. 2012, MNRAS, 419, 2497

Bertin, E., & Arnouts, S. 1996, A&AS, 117, 393

Bianchi, S., Chiaberge, M., Piconcelli, E., & Guainazzi, M. 2007, MNRAS, 374, 697

Bland-Hawthorn, J., Veilleux, S., & Cecil, G. 2007, Ap&SS, 311, 87

Boer, B., Schulz, H., & Keel, W. C. 1992, A&A, 260, 67

Boroson, B., Kim, D.-W., & Fabbiano, G. 2011, ApJ, 729, 12

Brinchmann, J., & Ellis, R. S. 2000, ApJ, 536, L77

Busch, G., Eckart, A., Valencia-S., M., et al. 2017, A&A, 598, A55

Buta, R. J., Sheth, K., Regan, M., et al. 2010, The Astrophysical Journal Supplement Series, 190, 147

Caglar, T., Burtscher, L., Brandl, B., et al. 2020, A&A, 634, A114

Canizares, C. 1999, The Detailed X-Ray Spectra of Elliptical Galaxies, Chandra Proposal ID 01600030

Cannarozzo, C., Sonnenfeld, A., & Nipoti, C. 2020, MNRAS, 498, 1101

Cappellari, M., Emsellem, E., Krajnović, D., et al. 2011, MNRAS, 413, 813

Choi, E., Ostriker, J. P., Naab, T., Oser, L., & Moster, B. P. 2015, MNRAS, 449, 4105

Christensen, L., Jahnke, K., Wisotzki, L., et al. 2006, A&A, 452, 869

Cid Fernandes, Roberto, J., & Terlevich, R. 1995, MNRAS, 272, 423

Cid Fernandes, R., Gu, Q., Melnick, J., et al. 2004, MNRAS, 355, 273

Cid Fernandes, R., Heckman, T., Schmitt, H., González Delgado, R. M., & Storchi-Bergmann, T. 2001, ApJ, 558, 81

Cid-Fernandes, R., Schmitt, H. R., & Storchi-Bergmann, T. 2001, in Revista Mexicana de Astronomia y Astrofisica Conference Series, Vol. 11, Revista Mexicana de Astronomia y Astrofisica Conference Series, 133

Civano, F., Fabbiano, G., Pellegrini, S., et al. 2014, ApJ, 790, 16

Cole, S., Lacey, C. G., Baugh, C. M., & Frenk, C. S. 2000, MNRAS, 319, 168

Combes, F., García-Burillo, S., Audibert, A., et al. 2019, A&A, 623, A79

Conselice, C. J. 2003, ApJS, 147, 1

Crenshaw, D. M., Fischer, T. C., Kraemer, S. B., Schmitt, H. R., & Turner, T. J. 2012, in Astronomical Society of the Pacific Conference Series, Vol. 460, AGN Winds in Charleston, ed. G. Chartas, F. Hamann, & K. M. Leighly, 261

Crenshaw, D. M., & Kraemer, S. B. 2007, in Astronomical Society of the Pacific Conference Series, Vol. 373, The Central Engine of Active Galactic Nuclei, ed. L. C. Ho & J. W. Wang, 319

Crenshaw, D. M., Kraemer, S. B., & George, I. M. 2003, ARA&A, 41, 117

Croton, D. J., Springel, V., White, S. D. M., et al. 2006, MNRAS, 365, 11

da Cunha, E., Eminian, C., Charlot, S., & Blaizot, J. 2010, MNRAS, 403, 1894

Daddi, E., Dickinson, M., Morrison, G., et al. 2007, The Astrophysical Journal, 670, 156

Davies, R. I., Müller Sánchez, F., Genzel, R., et al. 2007, ApJ, 671, 1388

Davis, B. L., Graham, A. W., & Cameron, E. 2018, ApJ, 869, 113

—. 2019, ApJ, 873, 85

Davis, B. L., Berrier, J. C., Johns, L., et al. 2014, ApJ, 789, 124

de Bruyn, A. G., & Wilson, A. S. 1978, A&A, 64, 433

De Lucia, G., Springel, V., White, S. D. M., Croton, D., & Kauffmann, G. 2006, MNRAS, 366, 499

de Vaucouleurs, G. 1948, Annales d'Astrophysique, 11, 247

—. 1959, Handbuch der Physik, 53, 275

de Vaucouleurs, G., de Vaucouleurs, A., Corwin, Herold G., J., et al. 1991, Third Reference Catalogue of Bright Galaxies

Devost, D. 2007, in American Astronomical Society Meeting Abstracts, Vol. 210, American Astronomical Society Meeting Abstracts #210, 112.09

Di Matteo, T., Springel, V., & Hernquist, L. 2005, Nature, 433, 604

Diamond-Stanic, A. M., & Rieke, G. H. 2012, ApJ, 746, 168

Diamond-Stanic, A. M., Rieke, G. H., & Rigby, J. R. 2009, ApJ, 698, 623

Doi, M., Fukugita, M., & Okamura, S. 1993, MNRAS, 264, 832

Dong, A.-J., & Wu, Q. 2015, MNRAS, 453, 3447

Dong, X. Y., & De Robertis, M. M. 2006, AJ, 131, 1236

Dressler, A. 1980, ApJ, 236, 351

Dullo, B. T., Knapen, J. H., Williams, D. R. A., et al. 2018, MNRAS, 475, 4670

Dumas, G., Mundell, C. G., Emsellem, E., & Nagar, N. M. 2007, MNRAS, 379, 1249

Edelson, R. A., Alexander, T., Crenshaw, D. M., et al. 1996, ApJ, 470, 364

Eliche-Moral, M. C., González-García, A. C., Balcells, M., et al. 2011, A&A, 533, A104

Ellison, S. L., Patton, D. R., Mendel, J. T., & Scudder, J. M. 2011, MNRAS, 418, 2043

Esquej, P., Alonso-Herrero, A., González-Martín, O., et al. 2014, ApJ, 780, 86

Evans, I. N., Koratkar, A. P., Storchi-Bergmann, T., et al. 1996, ApJS, 105, 93

Fabbiano, G. 2006, ARA&A, 44, 323

Fabian, A. C. 1999, Proceedings of the National Academy of Science, 96, 4749

Falcón-Barroso, J., Bacon, R., Bureau, M., et al. 2006, MNRAS, 369, 529

Fanaroff, B. L., & Riley, J. M. 1974, MNRAS, 167, 31P

Fazio, G. G., Hora, J. L., Allen, L. E., et al. 2004, ApJS, 154, 10

Ferrarese, L., & Merritt, D. 2000, ApJ, 539, L9

Ferrarese, L., & Merritt, D. 2000, The Astrophysical Journal, 539, L9

Ferrarese, L., Côté, P., Jordán, A., et al. 2006, ApJS, 164, 334

Fish, R. A. 1964, ApJ, 139, 284

Flohic, H. M. L. G., Eracleous, M., Chartas, G., Shields, J. C., & Moran, E. C. 2006, The Astrophysical Journal, 647, 140

Forbes, D. A., Alabi, A., Romanowsky, A. J., et al. 2017a, MNRAS, 464, L26

Forbes, D. A., & Ponman, T. J. 1999, MNRAS, 309, 623

Forbes, D. A., Sinpetru, L., Savorgnan, G., et al. 2017b, MNRAS, 464, 4611

—. 2017c, MNRAS, 464, 4611

Foyle, K., Rix, H.-W., & Zibetti, S. 2010, MNRAS, 407, 163

Fraser, C. W. 1972, The Observatory, 92, 51

Gabor, J. M., & Davé, R. 2015, MNRAS, 447, 374

Gadotti, D. A., & Sánchez-Janssen, R. 2012, MNRAS, 423, 877

Gan, Z., Yuan, F., Ostriker, J. P., Ciotti, L., & Novak, G. S. 2014, ApJ, 789, 150

García-Burillo, S., Combes, F., Schinnerer, E., Boone, F., & Hunt, L. K. 2005, A&A, 441, 1011

García-Burillo, S., Combes, F., Usero, A., et al. 2014, A&A, 567, A125

Gaspari, M., & Sadowski, A. 2017, ApJ, 837, 149

Gaspari, M., Eckert, D., Ettori, S., et al. 2019, ApJ, 884, 169

Gebhardt, K., Bender, R., Bower, G., et al. 2000, ApJ, 539, L13

Gebhardt, K., Bender, R., Bower, G., et al. 2000, The Astrophysical Journal, 539, L13

Gil de Paz, A., Madore, B. F., Boissier, S., et al. 2005, ApJ, 627, L29

—. 2007, ApJ, 661, 115

González, V., Labbé, I., Bouwens, R. J., et al. 2011, ApJ, 735, L34

González Delgado, R. M., Heckman, T., & Leitherer, C. 2001, ApJ, 546, 845

Goulding, A. D., Alexander, D. M., Lehmer, B. D., & Mullaney, J. R. 2010, MNRAS, 406, 597

Goulding, A. D., Greene, J. E., Ma, C.-P., et al. 2016, ApJ, 826, 167

Graham, A. W. 2007, Monthly Notices of the Royal Astronomical Society, 379, 711

Graham, A. W., & Driver, S. P. 2007, The Astrophysical Journal, 655, 77

Graham, A. W., Dullo, B. T., & Savorgnan, G. A. D. 2015, ApJ, 804, 32

Graham, A. W., Erwin, P., Caon, N., & Trujillo, I. 2001, The Astrophysical Journal, 563, L11

Graham, A. W., & Soria, R. 2019, MNRAS, 484, 794

Graham, A. W., Trujillo, I., & Caon, N. 2001, AJ, 122, 1707

Gültekin, K., Richstone, D. O., Gebhardt, K., et al. 2009, ApJ, 698, 198

Gültekin, K., Richstone, D. O., Gebhardt, K., et al. 2009, The Astrophysical Journal, 698, 198

Haan, S., Schinnerer, E., Emsellem, E., et al. 2009, ApJ, 692, 1623

Haehnelt, M. G., & Kauffmann, G. 2000, MNRAS, 318, L35

Häring, N., & Rix, H.-W. 2004, ApJ, 604, L89

Harrison, C. M. 2017, Nature Astronomy, 1, 0165

Heckman, T. M., & Best, P. N. 2014, ARA&A, 52, 589

Ho, L. C. 2008, ARA&A, 46, 475

Ho, L. C., Filippenko, A. V., & Sargent, W. L. 1995, ApJS, 98, 477

Hopkins, P. F., Hernquist, L., Cox, T. J., et al. 2006, ApJS, 163, 1

Hopkins, P. F., Torrey, P., Faucher-Giguère, C.-A., Quataert, E., & Murray, N. 2016, MNRAS, 458, 816

Hring, N., & Rix, H.-W. 2004, The Astrophysical Journal, 604, L89

Hu, J. 2008, Monthly Notices of the Royal Astronomical Society, 386, 2242

Hubble, E. P. 1936, Realm of the Nebulae

Hunt, L. K., Combes, F., García-Burillo, S., et al. 2008, A&A, 482, 133

Ishibashi, W., & Fabian, A. C. 2014, MNRAS, 441, 1474

Ishibashi, W., Fabian, A. C., & Canning, R. E. A. 2013, MNRAS, 431, 2350

Izumi, T., Kawakatu, N., & Kohno, K. 2016, ApJ, 827, 81

Jahnke, K., & Macciò, A. V. 2011, ApJ, 734, 92

Jahnke, K., & Wisotzki, L. 2003, MNRAS, 346, 304

Jarrett, T. H., Cluver, M. E., Taylor, E. N., et al. 2023, arXiv e-prints, arXiv:2301.05952

Jogee, S., Scoville, N., & Kenney, J. D. P. 2005, ApJ, 630, 837

Johansson, P. H., Naab, T., & Burkert, A. 2009, ApJ, 690, 802

Kang, W.-R., Woo, J.-H., Schulze, A., et al. 2013, ApJ, 767, 26

Kauffmann, G., & Haehnelt, M. 2000, MNRAS, 311, 576

Kauffmann, G., & Heckman, T. M. 2009, MNRAS, 397, 135

Kauffmann, G., White, S. D. M., & Guiderdoni, B. 1993, MNRAS, 264, 201

Kauffmann, G., Heckman, T. M., Tremonti, C., et al. 2003, MNRAS, 346, 1055

Kawakatu, N., Anabuki, N., Nagao, T., Umemura, M., & Nakagawa, T. 2006, ApJ, 637, 104

Kellermann, K. I., Sramek, R., Schmidt, M., Shaffer, D. B., & Green, R. 1989, AJ, 98, 1195

Khachikian, E. Y., & Weedman, D. W. 1974, ApJ, 192, 581

Kim, D.-W., & Fabbiano, G. 2003, ApJ, 586, 826

—. 2013, ApJ, 776, 116

—. 2015, ApJ, 812, 127

King, A., & Pounds, K. 2015, ARA&A, 53, 115

Knapen, J. H., Beckman, J. E., Heller, C. H., Shlosman, I., & de Jong, R. S. 1995a, ApJ, 454, 623

—. 1995b, ApJ, 454, 623

Koliopanos, F., Ciambur, B. C., Graham, A. W., et al. 2017, A&A, 601, A20

Koribalski, B. S., & López-Sánchez, Á. R. 2009, MNRAS, 400, 1749

Kormendy, J., Fisher, D. B., Cornell, M. E., & Bender, R. 2009, ApJS, 182, 216

Kormendy, J., & Gebhardt, K. 2001, in American Institute of Physics Conference Series, Vol. 586, 20th Texas Symposium on relativistic astrophysics, ed. J. C. Wheeler & H. Martel, 363–381

Kormendy, J., & Ho, L. C. 2013a, ARA&A, 51, 511

—. 2013b, ARA&A, 51, 511

Kormendy, J., & Ho, L. C. 2013, Annual Review of Astronomy and Astrophysics, 51, 511

Kormendy, J., & Kennicutt, Jr., R. C. 2004, ARA&A, 42, 603

Kormendy, J., & Richstone, D. 1995, ARA&A, 33, 581

Kormendy, J., & Richstone, D. 1995, Annual Review of Astronomy and Astrophysics, 33, 581

Krajnović, D., Karick, A. M., Davies, R. L., et al. 2013, MNRAS, 433, 2812

Krause, M., Fendt, C., & Neininger, N. 2007, A&A, 467, 1037

Lacerna, I., Ibarra-Medel, H., Avila-Reese, V., et al. 2020, A&A, 644, A117

Lakhchaura, K., Truong, N., & Werner, N. 2019, MNRAS, 488, L134

Lauer, T. R. 2012, ApJ, 759, 64

Lauer, T. R., Postman, M., Weaver, H. A., et al. 2021, ApJ, 906, 77

Laurikainen, E., Salo, H., Buta, R., Knapen, J. H., & Comerón, S. 2010, MNRAS, 405, 1089

López-Sánchez, Á. R. 2010, A&A, 521, A63

Lutz, D., Sturm, E., Genzel, R., et al. 2003, A&A, 409, 867

Lynden-Bell, D. 1969, Nature, 223, 690

Ma, C.-P., Greene, J. E., McConnell, N., et al. 2014, ApJ, 795, 158

Magorrian, J., Tremaine, S., Richstone, D., et al. 1998, AJ, 115, 2285

Maiolino, R., Krabbe, A., Thatte, N., & Genzel, R. 1998, ApJ, 493, 650

Makarov, D., Prugniel, P., Terekhova, N., Courtois, H., & Vauglin, I. 2014, A&A, 570, A13

Marchesini, D., van Dokkum, P. G., Schreiber, N. M. F., et al. 2009, The Astrophysical Journal, 701, 1765

Marconi, A., & Hunt, L. K. 2003, The Astrophysical Journal, 589, L21

Marconi, A., & Hunt, L. K. 2003, ApJ, 589, L21

Marshall, H. L., Miller, B. P., Davis, D. S., et al. 2002, ApJ, 564, 683

Martini, P., Regan, M. W., Mulchaey, J. S., & Pogge, R. W. 2003, ApJ, 589, 774

Masters, K. L., Lintott, C. J., Hart, R. E., et al. 2019, MNRAS, 487, 1808

Mathews, W. G., & Brighenti, F. 2003, ARA&A, 41, 191

McConnell, N. J., & Ma, C.-P. 2013, ApJ, 764, 184

Meidt, S. E., Schinnerer, E., Knapen, J. H., et al. 2011, The Astrophysical Journal, 744, 17

Meléndez, M., Kraemer, S. B., Schmitt, H. R., et al. 2008, ApJ, 689, 95

Melioli, C., & de Gouveia Dal Pino, E. M. 2015, ApJ, 812, 90

Michalowski, M. J., Dunlop, J. S., Cirasuolo, M., et al. 2012, A&A, 541, A85

Miller, P., Rawlings, S., & Saunders, R. 1993, MNRAS, 263, 425

Milvang-Jensen, B., & Jørgensen, I. 1999, Baltic Astronomy, 8, 535

Mobasher, B., Dahlen, T., Hopkins, A., et al. 2008, The Astrophysical Journal, 690, 1074

Mobasher, B., et al. 2009, Astrophys. J., 690, 1074

Moran, S. M., Loh, B. L., Ellis, R. S., et al. 2007, ApJ, 665, 1067

Morganti, R. 2017, Frontiers in Astronomy and Space Sciences, 4, 42

Morganti, R., Oosterloo, T., Oonk, J. B. R., Frieswijk, W., & Tadhunter, C. 2015, A&A, 580, A1

Muñoz Marín, V. M., González Delgado, R. M., Schmitt, H. R., et al. 2007, AJ, 134, 648

Negri, A., Posacki, S., Pellegrini, S., & Ciotti, L. 2014, MNRAS, 445, 1351

Noeske, K. G., Weiner, B. J., Faber, S. M., et al. 2007, The Astrophysical Journal, 660, L43

Norris, M. A., Meidt, S., de Ven, G. V., et al. 2014, The Astrophysical Journal, 797, 55

Nowak, N., Thomas, J., Erwin, P., et al. 2010, MNRAS, 403, 646

Okamura, S., Kodaira, K., & Watanabe, M. 1984, ApJ, 280, 7

Onken, C. A., Peterson, B. M., Dietrich, M., Robinson, A., & Salamanca, I. M. 2003, ApJ, 585, 121

Oohama, N., Okamura, S., Fukugita, M., Yasuda, N., & Nakamura, O. 2009, ApJ, 705, 245

Osterbrock, D. E. 1981, ApJ, 249, 462

Osterbrock, D. E., & Martel, A. 1993, ApJ, 414, 552

Osterbrock, D. E., & Pogge, R. W. 1985, ApJ, 297, 166

Ostriker, J. P., Choi, E., Ciotti, L., Novak, G. S., & Proga, D. 2010, ApJ, 722, 642

O'Sullivan, E., Ponman, T. J., & Collins, R. S. 2003, MNRAS, 340, 1375

Padovani, P. 1993, MNRAS, 263, 461

Pellegrini, S. 1999, A&A, 351, 487

—. 2005, MNRAS, 364, 169

—. 2010, ApJ, 717, 640

Pellegrini, S. 2010, The Astrophysical Journal, 717, 640–652

Pérez-Ramírez, D., Knapen, J. H., Peletier, R. F., et al. 2000, MNRAS, 317, 234

Pottasch, S. R., Beintema, D. A., Bernard Salas, J., & Feibelman, W. A. 2001, A&A, 380, 684

Pović, M., Sánchez-Portal, M., Pérez García, A. M., et al. 2009, ApJ, 706, 810

Press, W. H., Teukolsky, S. A., Vetterling, W. T., & Flannery, B. P. 1992, Numerical recipes in FORTRAN. The art of scientific computing

Querejeta, M., Meidt, S. E., Schinnerer, E., et al. 2015, The Astrophysical Journal Supplement Series, 219, 5

Querejeta, M., Schinnerer, E., García-Burillo, S., et al. 2016, A&A, 593, A118

Raichoor, A., Mei, S., Nakata, F., et al. 2011, ApJ, 732, 12

Ramos Almeida, C., Levenson, N. A., Rodríguez Espinosa, J. M., et al. 2009, ApJ, 702, 1127

Rashed, Y. E., Eckart, A., Valencia-S., M., et al. 2015, MNRAS, 454, 2918

Rees, M. J. 1984, ARA&A, 22, 471

Regan, M. W., & Elmegreen, D. M. 1997, AJ, 114, 965

Reines, A. E., & Volonteri, M. 2015, The Astrophysical Journal, 813, 82

Reynolds, J. H. 1913, MNRAS, 74, 132

Richstone, D., Ajhar, E. A., Bender, R., et al. 1998, Nature, 385, A14

Rieke, G. H. 2002, in Astronomical Society of the Pacific Conference Series, Vol.
    258, Issues in Unification of Active Galactic Nuclei, ed. R. Maiolino, A. Marconi,
    & N. Nagar, 113

Riffel, R. A., Storchi-Bergmann, T., Dors, O. L., & Winge, C. 2009, MNRAS, 393,
    783

Riffel, R. A., Storchi-Bergmann, T., Riffel, R., et al. 2013, MNRAS, 429, 2587

Rigby, J. R., Diamond-Stanic, A. M., & Aniano, G. 2009, ApJ, 700, 1878

Rix, H.-W., & Rieke, M. J. 1993, ApJ, 418, 123

Saglia, R. P., Opitsch, M., Erwin, P., et al. 2016, The Astrophysical Journal, 818,
    47

Saha, K., & Cortesi, A. 2018, ApJ, 862, L12

Sahu, N., Graham, A. W., & Davis, B. L. 2019, The Astrophysical Journal, 887, 10

Salim, S., Rich, R. M., Charlot, S., et al. 2007, ApJS, 173, 267

Salo, H., Laurikainen, E., Buta, R., & Knapen, J. H. 2010, ApJ, 715, L56

Sandage, A. 1961, The Hubble Atlas of Galaxies

Sandage, A., & Tammann, G. A. 1987, A Revised Shapley-Ames Catalog of Bright
    Galaxies

Sani, E., Marconi, A., Hunt, L. K., & Risaliti, G. 2011, Monthly Notices of the
    Royal Astronomical Society, 413, 1479

Sarazin, C. L. 1997, in Astronomical Society of the Pacific Conference Series, Vol. 116, The Nature of Elliptical Galaxies; 2nd Stromlo Symposium, ed. M. Arnaboldi, G. S. Da Costa, & P. Saha, 375

Sarzi, M., Allard, E. L., Knapen, J. H., & Mazzuca, L. M. 2007, MNRAS, 380, 949

Sarzi, M., Alatalo, K., Blitz, L., et al. 2013, MNRAS, 432, 1845

Savorgnan, G. A. D., & Graham, A. W. 2015, VizieR Online Data Catalog, J/MNRAS/446/2330

—. 2016, ApJS, 222, 10

Schawinski, K., Khochfar, S., Kaviraj, S., et al. 2006, Nature, 442, 888

Schaye, J., Crain, R. A., Bower, R. G., et al. 2015, MNRAS, 446, 521

Schramm, M., & Silverman, J. D. 2013, The Astrophysical Journal, 767, 13

Schutte, Z., Reines, A. E., & Greene, J. E. 2019, The Astrophysical Journal, 887, 245

Seyfert, C. K. 1943, ApJ, 97, 28

Shapley, H., & Ames, A. 1932, Annals of Harvard College Observatory, 88, 41

Sheth, K., Regan, M., Hinz, J. L., et al. 2010, PASP, 122, 1397

Sijacki, D., Springel, V., Di Matteo, T., & Hernquist, L. 2007, MNRAS, 380, 877

Sijacki, D., Vogelsberger, M., Genel, S., et al. 2015, MNRAS, 452, 575

Silverman, J. D., Kampczyk, P., Jahnke, K., et al. 2011, ApJ, 743, 2

Smajić, S., Moser, L., Eckart, A., et al. 2014, A&A, 567, A119

Smith, J. D. T., Dale, D. A., Armus, L., et al. 2004, ApJS, 154, 199

Soifer, B. T., & Neugebauer, G. 1991, AJ, 101, 354

Springel, V., Di Matteo, T., & Hernquist, L. 2005, MNRAS, 361, 776

Sruthi, K., & Ravikumar, C. D. 2021, MNRAS, 500, 1343

Storchi-Bergmann, T., Rodriguez-Ardila, A., Schmitt, H. R., Wilson, A. S., & Baldwin, J. A. 1996, ApJ, 472, 83

Su, Y., Irwin, J. A., White, Raymond E., I., & Cooper, M. C. 2015, ApJ, 806, 156

Tadhunter, C. 2008, Mem. Soc. Astron. Italiana, 79, 1205

Terlevich, R., & Melnick, J. 1985, MNRAS, 213, 841

Thilker, D. A., Bianchi, L., Boissier, S., et al. 2005, ApJ, 619, L79

Thomas, D., Maraston, C., Schawinski, K., Sarzi, M., & Silk, J. 2010, MNRAS, 404, 1775

Thomas, N., Davé, R., Anglés-Alcázar, D., & Jarvis, M. 2019, Monthly Notices of the Royal Astronomical Society, 487, 5764

Tody, D. 1986, in Society of Photo-Optical Instrumentation Engineers (SPIE) Conference Series, Vol. 627, Instrumentation in astronomy VI, ed. D. L. Crawford, 733

Tody, D. 1993, in Astronomical Society of the Pacific Conference Series, Vol. 52, Astronomical Data Analysis Software and Systems II, ed. R. J. Hanisch, R. J. V. Brissenden, & J. Barnes, 173

Tremaine, S., Gebhardt, K., Bender, R., et al. 2002, ApJ, 574, 740

Truong, N., Pillepich, A., Werner, N., et al. 2020, MNRAS, 494, 549

Urry, C. M., & Padovani, P. 1995, PASP, 107, 803

van den Bosch, R. C. E. 2016, ApJ, 831, 134

Veilleux, S., Cecil, G., & Bland-Hawthorn, J. 2005, ARA&A, 43, 769

Veilleux, S., Rupke, D. S. N., Kim, D. C., et al. 2009, ApJS, 182, 628

Villforth, C., Sarajedini, V., & Koekemoer, A. 2012, MNRAS, 426, 360

Vinod, K. T., Baheeja, C., Aswathy, S., & Ravikumar, C. D. 2023, Research in Astronomy and Astrophysics, 23, 045008

Wang, J., Fabbiano, G., Karovska, M., Elvis, M., & Risaliti, G. 2012, ApJ, 756, 180

Weedman, D. W. 1977, ARA&A, 15, 69

Weinberger, R., Springel, V., Hernquist, L., et al. 2017, MNRAS, 465, 3291

Werner, M. W., Roellig, T. L., Low, F. J., et al. 2004, ApJS, 154, 1

Werner, N., Oonk, J. B. R., Sun, M., et al. 2014, MNRAS, 439, 2291

Wilman, D. J., & Erwin, P. 2012, ApJ, 746, 160

Wilson, A. S., & Colbert, E. J. M. 1995, ApJ, 438, 62

Wilson, A. S., & Yang, Y. 2002, ApJ, 568, 133

Wolf, C., Meisenheimer, K., Rix, H. W., et al. 2003, A&A, 401, 73

Woo, J.-H., Schulze, A., Park, D., et al. 2013, ApJ, 772, 49

Woo, J.-H., Yoon, Y., Park, S., Park, D., & Kim, S. C. 2015, ApJ, 801, 38

Wylezalek, D., & Zakamska, N. L. 2016, MNRAS, 461, 3724

Xilouris, E. M., Madden, S. C., Galliano, F., Vigroux, L., & Sauvage, M. 2004, A&A, 416, 41

Yamada, Y., Arimoto, N., Vazdekis, A., & Peletier, R. F. 2006, ApJ, 637, 200

Yoon, Y., Ko, J., & Kim, J.-W. 2023, ApJ, 946, 41

Yuan, F., Yoon, D., Li, Y.-P., et al. 2018, ApJ, 857, 121

Yuan, F., Yu, Z., & Ho, L. C. 2009, ApJ, 703, 1034

Zahid, H. J., Geller, M. J., Fabricant, D. G., & Hwang, H. S. 2016, ApJ, 832, 203

Zhu, P., Ho, L. C., & Gao, H. 2021, ApJ, 907, 6